DEVELOPMENT OF SENSITIVE ELECTROCHEMICAL SENSOR FOR DETECTION OF GASEOUS H_2O_2

Jelena Isailović

Doctoral Dissertation
Jožef Stefan International Postgraduate School
Ljubljana, Slovenia

Supervisor: Dr. Samo B. Hočevar, Department of Analytical Chemistry, National Institute of Chemistry, Hajdrihova 19, Ljubljana, Slovenia

Evaluation Board:
Prof. Dr. Barbara Malič, Chair, Jožef Stefan International Postgraduate School, Ljubljana, Slovenia
Prof. Dr. Slobodan Gadžurić, Member, Faculty of Sciences, Novi Sad, Serbia
Prof. Dr. Mitja Kolar, Member, Faculty of Chemistry and Chemical Technology, Ljubljana, Slovenia
Dr. Nikola Tasić, Member, National Institute of Chemistry, Ljubljana, Slovenia

MEDNARODNA PODIPLOMSKA ŠOLA JOŽEFA STEFANA
JOŽEF STEFAN INTERNATIONAL POSTGRADUATE SCHOOL

Jelena Isailović

DEVELOPMENT OF SENSITIVE ELECTROCHEMICAL SENSOR FOR DETECTION OF GASEOUS H_2O_2

Doctoral Dissertation

RAZVOJ OBČUTLJIVEGA ELEKTROKEMIJSKEGA SENZORJA ZA DETEKCIJO PLINASTEGA H_2O_2

Doktorska disertacija

Supervisor: Dr. Samo B. Hočevar

Ljubljana, Slovenia, August 2023

"There is nothing more wonderful than being a scientist, nowhere I would rather be than in my lab, staining up my clothes and getting paid to play."

- *Marie Salomea Skłodowska–Curie*

Acknowledgments

Firstly, I would like to sincerely thank my mentor, Dr. Samo B. Hočevar, for his guidance, support, and patience throughout this study. I appreciate his commitment, continuous investment in my work, and his efforts and advice that helped me grow into the researcher I am today.

I would also like to thank the committee members, the chair, Prof. Dr. Barbara Malič, Prof. Dr. Slobodan Gadžurić, Prof. Dr. Mitja Kolar, and Dr. Nikola Tasić, for the comments and questions you shared that are beneficial in the completion of this study.

I appreciate all the continuous support and help that I received from my colleagues at the Department of Analytical Chemistry within the National Institute of Chemistry, Ljubljana. I would also like to express my gratitude to my esteemed colleague, Dr. Kristijan Vidović, without whose invaluable contributions I would not have successfully completed my first article.

My Ph.D. work was financially supported by the Slovenian Research Agency (P1-0034) and the Slovenian Research Agency's Young Researchers Programme (grant agreement No. 52020).

I have only heartfelt and ongoing thanks and love for my partner Rok, who, besides being there for me during the ordinary days, saw me and gave me strength, moral support, and wings throughout my scientific journey.

In addition, I would like to thank my parents and my sister, who supported me on my way on all conceivable levels. I can say with certainty that without you and your help, I would never have arrived at this point in life, both professionally and personally. You should know that you are the people who have made me what I am today.

Abstract

In recent decades, hydrogen peroxide (H_2O_2) has attracted considerable attention as an omnipresent analyte, finding applications in clinical studies/diagnosis, biology, environmental protection, atmospheric studies, homeland security, and various analytical methodologies. This dissertation provides valuable insights into three different types of electrochemical sensors specifically designed for the detection of low concentration levels of gaseous H_2O_2. Their stability, detection limits, sensitivity, repeatability, ability to analyze real samples, and challenges encountered in their practical application are examined.

In addition, the dissertation delves into a discussion of the advantages and disadvantages associated with the implementation of different sensing/modification/functional materials in the design of H_2O_2 sensors. These materials encompass a range of options, such as 2D materials (MXenes), polymeric substrates, metal oxides, and redox-active compounds such as ferrocyanide, all aiming to enhance electrochemical sensor performance.

Furthermore, considering their inherent advantages and limitations, the future prospects of these sensors are examined alongside potential scenarios for their application in indoor/outdoor H_2O_2 monitoring.

Doctoral dissertation provides comprehensive insights into the development and evaluation of sensitive electrochemical sensors for gaseous H_2O_2 detection, highlighting material selection, performance improvements, and future opportunities for their application in monitoring H_2O_2 in various environments.

Povzetek

V zadnjih desetletjih je vodikov peroksid (H_2O_2) privabil veliko pozornosti kot vseprisoten analit, ki je našel aplikacije v kliničnih študijah/diagnostiki, biologiji, varstvu okolja, atmosferskih študijah, domovinski varnosti in različnih analiznih metodologijah. Ta disertacija nudi dragocen vpogled v tri različne vrste elektrokemijskih senzorjev, posebej zasnovanih za zaznavanje nizkih koncentracij plinastega H_2O_2. Preučeni so njihova stabilnost, meje zaznave, občutljivost, ponovljivost, sposobnost analize realnih vzorcev in izzivi, s katerimi se srečujejo pri njihovi praktični uporabi.

Poleg tega se v disertaciji razpravlja o prednostih in slabostih, povezanih z implementacijo različnih senzorskih/modifikacijskih/funkcionalnih materialov pri načrtovanju senzorjev H_2O_2. Ti materiali obsegajo vrsto možnosti, kot so 2D materiali (MXenes), polimerni substrati, kovinski oksidi in redoks aktivni materiali, kot je ferocianid, katerih namen je izboljšava delovanja elektrokemijskih senzorjev.

Poleg tega so ob upoštevanju njihovih značilnih prednosti in omejitev preučeni prihodnji obeti teh senzorjev skupaj z možnimi scenariji za njihovo uporabo pri monitoringih H_2O_2 v zaprtih prostorih in/ali na prostem.

Doktorska disertacija nudi celovit vpogled v razvoj in vrednotenje občutljivih elektrokemijskih senzorjev za detekcijo plinastega H_2O_2, s poudarkom na izbiri materiala, izboljšavah delovanja in prihodnjih priložnostih za njihovo uporabo pri spremljanju H_2O_2 v različnih okoljih.

Contents

List of Figures

List of Tables

Abbreviations

AOP	... Advanced Oxidation Processing
HTP	... High-test peroxide
ABS	... Acrylonitrile butadiene styrene
ROS	... Reactive Oxygen Species
OS	... Oxidative stress
HSCs	... Hematopoietic stem cells
I/R	... Ischemia-reperfusion
UC	... Ulcerative colitis
ETC	... Electron transport chain
NADH	... Nicotine adenine dinucleotide
FADH2	... Flavin adenine dinucleotide
CMP	... Chemical mechanical pulping
TATP	... Triacetone triperoxide
DADP	... Diacetone diperoxide
HMTD	... Hexamethylenetriperoxidediamine
MEKP	... Methyl Ethyl Ketone Peroxide
TNT	... Trinitrotoluene
HMEs	... Homemade Explosives
WE	... Working Electrode
RE	... Reference Electrode
CE	... Counter Electrode
SPE	... Screen-Printed Electrodes
PAA	... Poly(acrylic acid)

Chapter 1

Introduction

1.1 Hydrogen Peroxide Importance and Its Occurrence

Hydrogen peroxide (H_2O_2) is the smallest and one of the most versatile oxidants. In addition to being an oxidizing agent, H_2O_2 can also be a reducing agent in both acidic and basic environments.

Reduction: $H_2O_2 + 2e^- \rightarrow 2OH^-$ (in basic medium) (1.1)
$H_2O_2 + 2H^+ + 2e^- \rightarrow 2H_2O$ (in acidic medium) (1.2)

Oxidation: $H_2O_2 + 2OH^- \rightarrow O_2 + H_2O + 2e^-$ (in basic medium) (1.3)
$H_2O_2 \rightarrow O_2 + 2H^+ + 2e^-$ (in acidic medium) (1.4)

H_2O_2 is a highly reactive natural metabolite in many living organisms, whereas its decomposition produces molecular oxygen (O_2) and water (H_2O). It is a ubiquitous compound that occurs in both the gas and aqueous phases and plays an important role in many fields. H_2O_2 is one of the end products of atmospheric oxidant chemistry in the gas phase, and its concentration in the gas phase and in liquid and solid precipitates can indicate the oxidizing power of the atmosphere. In addition, H_2O_2 plays an essential role in the chemistry of atmospheric aerosols and in one of the most important processes where it is involved as the oxidant of S(IV) to S(VI) that is closely related to the phenomenon of acid fog and acid rain [1].

The dissolution of gaseous H_2O_2 into atmospheric hydrometeors serves as a significant contributor to the presence of aqueous H_2O_2 [2]. This is also the main sink for gaseous H_2O_2, and precipitation consequently acts as a vital removal process for atmospheric peroxides [3, 4, 5]. However, other aqueous sources also exist; they include the dismutation of aqueous hydroperoxyl [6, 7], reduction of superoxide by organic compounds or hydrogen carbonate [8], photolysis of aqueous ozone [9], irradiation of aromatic carbonyls in the presence of phenols [10], and H_2O vapor photonucleation [11]. Studies have shown that the formation of H_2O_2 can be related to the presence of chemical species, such as SO_4^{2-}, NO^{3-}, and H^+, the level of rainfall, temperature, wind direction, the intensity of solar radiation, etc. It is also believed that electrical discharges (lightning) increase its concentration [12].

The first commercialization of H_2O_2 dates back to 1800, and its worldwide production increases yearly. It is believed that H_2O_2, in isolated or combined form (mainly), is one of the most used reagents with the most diverse applications. Undoubtedly, its usage must be conducted safely and responsibly to avoid risks of burning and explosions since H_2O_2 is known as a highly reactive compound.

H_2O_2 is used in specific treatment processes of effluents to remove organic impurities by using Advanced Oxidation Processing (AOP). These processes are based on the generation of the hydroxyl radical ($^{\bullet}OH$), which has high oxidizing power and can promote the degradation of several pollutants in a short time while reducing their scent [13, 14, 15]. Among the various processes for obtaining hydroxyl radicals are ozone, H_2O_2, their mixture (O_3/H_2O_2 or O_3/H_2O_2/UV), photocatalysis, and Fenton's reagent, i.e., the mixture of H_2O_2 and ferrous salts [16].

Aside from its role in pollution control, with a particular focus on environmental monitoring, H_2O_2 finds application in the textile, wood pulp, and paper industries as a crucial component in bleaching processes [17, 18]. In the next chapter of this thesis, we will address the critical role of monitoring the presence of H_2O_2 in the healthcare field. This process is of immense importance due to its indispensability and will be discussed in detail.

H_2O_2 can be utilized to sterilize numerous surfaces, including medicinal tools [19], and can be deployed as a vapor for room sterilization [20, 21]. It demonstrates broad-spectrum efficacy against viruses, bacteria, bacterial spores, and yeasts. Superior activity is seen against Gram-positive than Gram-negative bacteria. On the other hand, catalase(s) or other peroxidases in these microorganisms can increase tolerance in the presence of lower concentrations of H_2O_2 [22]. Lower concentration levels (3%) will work against most spores; higher concentrations (7-30%) and longer exposure times will improve sporicidal activity.

High-test peroxide (HTP), also known as high-concentration H_2O_2, can be used either as a monopropellant, i.e., only fuel, not mixed with other chemicals, or as an oxidizing component of a bipropellant rocket [23]. Functioning as a monopropellant, H_2O_2 takes benefit of its 70–98% decomposition to vapor and O_2. The propellant is driven into a reaction chamber, where a catalyst, usually an Ag or Pt screen, triggers decomposition, producing vapor expelled through a nozzle, generating momentum. H_2O_2 was the first important monopropellant adopted for use in rocket applications. It has been widely utilized for propulsion and power applications.

H_2O_2 is also important in the food industry [24, 25], the pharmaceutical industry, medical diagnostic, and process monitoring. It is present in numerous biological reactions as the product of various reactions involving oxidases and is an essential parameter in quantifying these bio-processes [26]. For instance, in diabetes, blood glucose levels can be measured using strip glucose tests. The enzyme glucose oxidase reacts with glucose, water, and oxygen to produce gluconic acid and H_2O_2. The generated H_2O_2 can then be utilized to oxidize a chromogen, or oxygen consumption is measured to estimate the glucose amount present. Similarly, for patients with asthma and chronic obstructive pulmonary disease (COPD), a chemiluminescence assay and a device to measure H_2O_2 in exhaled breath condensate are utilized in health diagnostics and the healthcare industry [27].

Other uses of H_2O_2 are in glow sticks – it reacts with certain di-esters to produce chemiluminescence [28], horticulture – weak H_2O_2 solution is used for watering because its natural decomposition releases O_2 that supplements plant's root growth and helps to treat root rot and prevents a variety of other pests from appearing [29], fishkeeping – it is used in aquaculture for decreasing mortality caused by various microbes [30], and removing yellow tones from aged plastics – in combination with a UV-light source, it is used to remove yellow tones from white or light grey acrylonitrile butadiene styrene (ABS) plastics to partly or fully restore the original color [31].

1.1.1 Reactive oxygen species and diseases

H_2O_2 in living organisms, in terms of redox signaling and regulation, is an endogenous oxidant [32]. As one of the most stable reactive oxygen species (ROS), H_2O_2 is involved in the regulation of protein function [33], and under certain circumstances, it is also a precursor of $^{\bullet}OH$ and hypochlorous acid (HOCl).

Due to its stability, short cellular half-life (~10^{-3} seconds), diffusivity, and specific reactivity, H_2O_2 is a pivotal redox signaling molecule in various biological processes [34]. It influences cell differentiation, proliferation, inflammation regulation, tissue repair, circadian rhythm modulation, and aging [35]. Conversely, H_2O_2 causes oxidative stress (OS), leading to biomolecular damage. OS arises from the complex interplay of cellular composition, localized H_2O_2 concentration, and the dynamics of its generation and elimination processes [36]. Under normal conditions, $^{\bullet}O^{2-}$ (superoxide anion) and H_2O_2 production and elimination are balanced, but excessive $^{\bullet}O^{2-}$ and H_2O_2 generation occurs during OS.

H_2O_2 is produced through monovalent reduction of superoxide or divalent reduction of O_2 [37]. Enzyme-catalyzed superoxide dismutation is the primary source, but oxidases like glucose oxidase, xanthine oxidase, urate oxidase, and amino acid oxidase can also produce H_2O_2. Due to its neutral pH and lack of charge (with a pKa≈10.8), H_2O_2 can readily traverse biological membranes. Despite being a strong oxidant, its slow reaction kinetics with biomolecules make it relatively unreactive, allowing it to accumulate at high concentrations in cells and tissues [38]. H_2O_2 can directly oxidize molecules and inactivate enzymes with thiol groups or methionine residues in their active sites [39].

Within mammalian cells, two distinct mechanisms contribute to the production of H_2O_2, i.e., enzymatic and non-enzymatic generation. The non-enzymatic one originates from the reduction by electrons and protons of the $^{\bullet}O_2^{-}$ anion, which consecutively comes from the reduction of O_2 in the mitochondrial respiration pathway and which takes place in the cellular mitochondrial matrix.

Elevated levels of H_2O_2 are intimately associated with inflamed tissues, inducing a critical mechanism that significantly contributes to the host's defense against microbial threats [40]. During inflammation, H_2O_2 by-products interact with proteins, lipids, nucleic acids, and other metabolites, causing related molecular damage that can be significant and lead to cell apoptosis (cell death) [41]. Inflammation is a contributing factor to some chronic diseases, such as Alzheimer's disease [42, 43].

Neoplastic cells with heightened metabolic activity often exhibit elevated H_2O_2 levels, playing a role in tumor development and progression. These cells induce antioxidant proteins to counteract H_2O_2's impact, maintaining a delicate balance between H_2O_2 generation and antioxidants [38]. Specific doses of H_2O_2 and $^{\bullet}O^{2-}$ stimulate cell proliferation in various cancer types [44]. Human cancer cell types generally have low glutathione peroxidase levels and catalase, the enzyme responsible for H_2O_2 breakdown [45].

In healthy hematopoietic stem cells, primitive cells that can develop into all types of blood cells (HSCs), when OS pathways become excessively activated, it increases the production and accumulation of $^{\bullet}O^{2-}$ and H_2O_2 within the cells. This disruption severely impairs the normal biological functions of HSCs and plays a crucial role in the progression of leukemia [46].

Among other ROS-related conditions, ischemia-reperfusion (I/R) injury is among the most studied, along with myocardial infarction, stroke, and other thrombotic events. Reperfusion occurs when blood circulation is restored to tissues after ischemia, as the restoration of circulation after the absence of nutrients and oxygen triggers inflammation and the subsequent OS damage affected tissues [47]. Researchers investigating the link

between H_2O_2 and I/R injury have noted increased H_2O_2 production in postischemic tissues. This heightened generation results from enzymes that reduce molecular O_2 to $^{\bullet}O^{2-}$, leading to the release of H_2O_2 in both extracellular and intracellular spaces [48].

Ulcerative colitis (UC) is an inflammatory bowel disease that follows late adolescence and early adulthood and causes a chronic relapsing and remitting course characterized by abdominal pain, bloody diarrhea, and tenesmus, all related to inflammation of the large intestine [49]. An immune abnormality is a possible mechanism that may cause this disease, although significantly elevated levels of H_2O_2 have been documented in the colonic epithelium immediately before the onset of UC, suggesting an underlying role in its development [50].

Sepsis is a life-threatening response to infection that can result in multiorgan failure and fatal hemodynamic shock. In sepsis, cytotoxic H_2O_2 levels in the blood can be up to 18 times higher than normal [51]. Hypermetabolism during sepsis increases ATP production through oxidative phosphorylation, leading to H_2O_2 generation via the electron transport chain (ETC). Heightened bioenergetic reactions cause H_2O_2 overproduction, which, if not properly removed, can lead to cell death, severe bioenergetic dysfunction, and cellular damage. Prolonged exposure disrupts redox equilibrium, contributing to organ failure, microvascular dysfunction, and fatal septic shock [52].

H_2O_2 inhibits Krebs cycle enzymes, reducing NADH and FADH2 production involved in cellular redox reactions. This damages the mitochondrial proton gradient and proton motive force needed for pyruvate translocase, hindering pyruvate transport into the mitochondria. Consequently, cytosolic pyruvate increases, converting to lactate, leading to hyperlactatemia [53].

Pancreatic β-cells, responsible for insulin production, are vulnerable to OS due to lower antioxidant enzyme expression compared to the liver and kidneys. H_2O_2 is implicated in the dysfunction of β-cells in both type 1 and type 2 diabetes mellitus, conditions marked by hyperglycemia and related health complications [54]. In type 2 diabetes, chronically elevated blood glucose levels increase oxidative phosphorylation, leading to higher H_2O_2 production in β-cells [55]. Enhanced expression of antioxidant enzymes like superoxide dismutase (SOD1 and SOD2), catalase, GSH peroxidase, and thioredoxin protects β-cells from oxidative damage induced by various agents [56]. Peroxiredoxins, antioxidant enzymes in β-cells, have shown promise in mitigating the effects of H_2O_2 and other reactive species, providing protective effects against OS [57].

Cells have numerous sources of H_2O_2 and scavenger molecules that tightly control H_2O_2 concentration in different subcellular compartments. To better understand the molecules and objectives involved in this delicate equilibrium (physiological/pathological H_2O_2 concentration), it is vital to know the molecular mechanisms operating at the cellular level in detail.

1.1.2 H_2O_2 in bleaching agents

Bleaching agents whiten or lighten a substrate by degrading dyed components or changing their absorbance properties. Their application extends across multiple industries, including the wood (pulp and paper), textile, as well as commercial and household cleaning sectors, where they find wide utilization. Typically, during the bleaching process, the aim is to eliminate chromophoric sites that enable the substrate to effectively absorb visible light by virtue of electron delocalization over conjugated double bonds. The whitening agent will initiate an irreversible reaction by either breaking or adding across these double bonds.

Interestingly, more than half of the world's H_2O_2 production is used in the wood industry for pulp and paper bleaching to whiten and brighten paper and other cellulose-based products [58]. It is used in chemical and mechanical pulping processes to remove lignin, the natural polymer that gives wood its brown color. In chemical pulping, H_2O_2 is combined with other chemicals, such as NaOH, to remove lignin from wood chips. The resulting pulp is then bleached with H_2O_2 to produce a bright white color [59]. H_2O_2 also plays a crucial role in the mechanical pulping process by effectively bleaching the pulp subsequent to its mechanical separation from the wood fibers. This process, known as chemical mechanical pulping (CMP), produces pulp with bright white color and improved strength properties [60]. In addition, H_2O_2 is used to bleach recycled paper and to remove contaminants, such as inks and dyes, from the pulp. In the realm of the paper and pulp industry, H_2O_2 has a vital role as a bleaching agent due to its exceptional capacity to generate brilliant white hues and enhance the strength and overall quality of the end product [61].

For a complete bleaching process, H_2O_2 is used before dyeing and to oxidize reductive dyes in dyeing. Combined bleaching is sometimes used to achieve an extremely white cloth/yarn: hypochlorite in pre-bleaching and H_2O_2 for anti-chlorination, yellowing, and bleaching. In most textile industries, completely white fabric is achieved only by an alkaline boil-out procedure, hot peroxide bleaching, repeated if necessary, and the addition of optical whiteners [62, 63]. Usually, whitened textiles are yarn, knitwear, and textile cloths primarily from cotton, wool, and silk, less so from viscose, and some from cotton/polyester mixtures. The utilization of both hypochlorite and peroxide, in combination for whitening, is diminishing. The shift towards exclusive peroxide-based bleaching necessitates a careful selection of suitable optical whiteners and organic stabilizers. In place of hypochlorite, certain companies have introduced a blended bleaching approach utilizing per-acetic acid and H_2O_2 [64].

Another significant industrial presence of H_2O_2 involves the production of sodium percarbonate and sodium perborate, which serve as gentle bleaching agents in laundry detergents. Sodium percarbonate, an adduct of sodium carbonate and H_2O_2, is the active ingredient in such laundry products. Once dissolved in H_2O, it produces H_2O_2 and sodium carbonate. These bleaching agents are only effective at certain wash temperatures (60 °C) and are often used with bleach activators, which facilitate cleaning at lower temperatures [65].

Tooth whitening or tooth bleaching techniques primarily rely on the use of H_2O_2 or one of its precursors, such as carbamide peroxide [66]. They bleach the chromogens within the dense, inner bony structure of the teeth (dentine), thus reducing the body color of the tooth, and are often used in combination with an activating agent such as heat and light. These agents can be administered in different ways for tooth-bleaching purposes. There are two primary approaches for utilizing H_2O_2 in dental procedures. One is the external application of H_2O_2 to the teeth, known as vital bleaching, while the other involves internal use within the pulp chamber, commonly referred to as non-vital bleaching [67, 68, 69]. Tooth whitening can be accomplished using a 10% carbamide peroxide gel in a bleaching tray at night, H_2O_2 strips [70], and 35% H_2O_2 with or without light or heat activation [71]. It can also be found in most whitening toothpastes.

H_2O_2 has various other domestic and professional uses. Diluted H_2O_2 (2-12%) mixed with aqueous NH_3 has been used to bleach human hair. It can react with blood as a bleaching agent if a blood stain is fresh or not too old. A generous application of H_2O_2, if necessary in more than a single application, will bleach the stain fully out.

1.1.3 H_2O_2 and national/homeland security

Concentrated H_2O_2 has unique properties that make it increasingly sought-after by research and development institutions and relevant industries involved in rocket propulsion. Its ease of handling, exceptional performance, and remarkable versatility as both a potent oxidizer (in explosives) and monopropellant contribute to its rising popularity in these domains. Its other remarkable properties include high density, low vapor pressure, and low toxicity [72].

The discovery of H_2O_2 dates back almost two centuries, yet it was only in the period preceding World War II that German researchers began to explore and exploit the exceptional qualities of concentrated solutions. During this time, they also stumbled upon the explosive properties characteristic of concentrated H_2O_2 solutions [73, 74]. The initial breakthrough came with the combination of an 89% solution of H_2O_2, cotton, and petroleum jelly, which yielded successful results [75]. Subsequently, in the post-World War II era, researchers further explored concentrated H_2O_2 formulas blended with glycerol, investigating the detonation ranges of these mixtures [76]. It became evident that numerous substances such as methanol, ethanol, isopropanol, ethylene glycol, mannitol, ethyl acetate, cane sugar, diethylene glycol, diethyl ether, acetone, dioxane, aniline, and several others proved to be excessively sensitive when combined with concentrated H_2O_2, making their use in this context impractical.

Nonetheless, it is important to note that pure H_2O_2 (100%) or its concentrated solutions do not fall under the classification of high explosives in their liquid form. This distinction arises from the understanding that the detonation of H_2O_2 should be examined within the framework of three distinct categories: liquids, gases, and two-phase occurrence [77].

The first patent on H_2O_2/glycerol high explosive showed that H_2O_2 was sufficient to oxidize the glycerol during detonation [78]. As research progressed, scientists successfully formulated other explosive mixtures, many of which exhibited considerable practical potential. By employing H_2O_2 as an oxidizer alongside diverse organic substances, they were able to create a range of explosives and propellants that surpassed the energy content achieved through the detonation of pure H_2O_2. Numerous patents show the innovation in this field, illustrating the blending of H_2O_2 with materials such as flour, sawdust, H_2O, glycerol, ammonium nitrate, gelling agents, and various other components to yield explosive mixtures with enhanced properties [79]. Usually, these mixtures are H_2O_2 in concentrations of 60- 90%, combined with ingredients such as sawdust, resin, and a gelling agent such as starch or agar. There are also suggestions for mixtures that use higher concentrations of H_2O_2, along with hydrazine (or ammonium nitrate) and H_2O. These formulations aim to produce explosive compositions rich in gaseous detonation products. It is also noteworthy that certain "exotic" explosives can be produced with lower concentrations of H_2O_2, e.g., a 30% solution known as perhydrol [80]. A notable example of such an explosive is triacetone triperoxide (TATP), an organic peroxide that has recently attracted considerable attention because of its rapid and relatively simple synthesis from inexpensive chemicals [81]. Other organic peroxide explosives used by terrorist groups include diacetone diperoxide (DADP) and hexamethylenetriperoxidediamine (HMTD), as well as methyl ethyl ketone peroxide (MEKP) [81]. TATP has a high content of active O_2 and is considered a primary explosive due to its shock sensitivity, easily leading to explosive decomposition [81]. While TATP possesses notable detonation power akin to trinitrotoluene (TNT), it exhibits a highly sensitive nature and stability issues, thus being categorized as a powerful secondary explosive [81].

Terrorists often use substances such as TATP, DADP, and HMTD as homemade explosives (HMEs) in their improvised explosive devices. These substances are not necessarily selected for their exceptional explosive power or long-term stability, which are priorities in military applications, but for other critical factors [81]. Ease of synthesis with readily available reagents is an important consideration, as terrorists seek to produce these explosives from common starting materials. Additionally, they prioritize ease of initiation and a desire to minimize traceability, making it challenging for authorities to track their origins.

One of the most important strategies for the detection of peroxide-based explosives is to test for gaseous H_2O_2, which is invariably used as a precursor in the synthesis of peroxide-based explosives and is often a decomposition product of peroxide-based explosives.

1.2 Detection of H_2O_2

H_2O_2 analysis is conducted across a range of sample matrices encompassing environmental samples, such as H_2O and soil, and human fluids like sweat, blood, and cell and tissue cultures. This broad array of sample types necessitates diverse measurement strategies and quantification approaches to assess H_2O_2 levels accurately and precisely. H_2O_2 is measured using a diverse range of methods such as optical, including colorimetry [82, 83], chemiluminescence [84, 85], and fluorescence [86, 87, 88]; electrochemical, including potentiometry [89, 90], voltammetry [91, 92], and amperometry [93, 94, 95]; titrimetry [96]; chromatographic [97, 98] and spectroscopic [99, 100] methods. Most of these methods are connected to relatively high costs, complex testing processes, sophisticated and bulky instrumentation requirements, the need for trained personnel to operate, and interference from sample matrices. Electrochemical techniques demonstrate, on the other hand, promising prospects in measuring H_2O_2 due to their low cost, high sensitivity, high selectivity, miniaturization capabilities, simple instrumentation, and short response time [93].

Over the past three decades, a plethora of electrochemical techniques, including voltammetry, chronoamperometry, potentiometry, coulometry, and electrochemical impedance spectroscopy, have emerged as suitable tools for measuring H_2O_2 in diverse in-vitro and in-vivo applications [101, 102, 103]. Despite numerous endeavors to develop electrochemical sensors to determine H_2O_2 accurately, several challenges persist in achieving ease of handling and applicability, along with high sensitivity, selectivity, reproducibility, and a short response time. These characteristics collectively contribute to developing electrochemical sensors that meet the stringent requirements of reliable H_2O_2 detection, and efforts continue to refine and enhance the sensors' performances.

Notably, while the detection of H_2O_2 in liquid samples is a relatively well-established process [104, 105, 106], its detection in the gaseous samples remains a significant challenge due to the aforementioned reasons encompassing, particularly the usual low concentrations and the inherent instability of H_2O_2. The unique properties and behavior of H_2O_2 in its gaseous state introduce complexities that complicate accurate and reliable detection methods. As a result, researchers continue to face obstacles in developing effective techniques for detecting and measuring H_2O_2 in the gas phase. The pursuit of robust and sensitive detection methods for gaseous H_2O_2 remains an active area of research and development in the scientific community.

This dissertation addresses and emphasizes the study, development, and optimization of sensing principles for the sensitive detection and quantification of gaseous H_2O_2. The upcoming chapter will provide a comprehensive and detailed explanation of various

electrochemical methods, including cycling voltammetry, that were mostly used in this research. It will delve into the underlying principles, methodologies, and application of these techniques, offering a thorough understanding of their potential in accurately measuring gaseous H_2O_2.

1.3 Electrochemical Detection

Various electroanalytical methods can be differentiated from each other by the type of analytical signal they produce and excitation waveforms. In this sense, there are three main types of generated signals: *potential*, *current*, and *charge*. In addition, other electrochemical quantities can be calculated in a facile and automated manner, including *capacitance*, *impedance*, *resistance*, etc. On the other hand, there are two principal types of electroanalytical techniques: interfacial and bulk. In the bulk techniques, a property of the solution in the electrochemical cell is measured, while in the interfacial techniques, a potential, current, or charge depends on the species present in the interface between the electrode and the electrolyte solution. The most known bulk technique used in electrochemistry is conductometry, mainly used to measure the ionic conductivity of the solution. Conductometric sensors work based on the principle of changes in electrical conductivity when exposed to specific target analytes. These sensors are designed to detect and quantify the presence of various substances, including gases, ions, and volatile organic compounds (VOCs), by measuring changes in conductance. [107]. There are many examples of its electroanalytical usage in the detection of CO_2 [108], alpha-fetoprotein [109], glucose [110], or H_2O_2 [111, 112]. As for the interfacial techniques, the main differentiation is into *static* (zero-current) and *dynamic* techniques. In potentiometry, which is the most known and typically utilized zero-current technique, the response from the sample is obtained through the potential established between ion-selective and reference electrodes. Different membrane materials, with ion recognition capability, have been developed to convey the relatively high selectivity of this technique. The potentiometric probes have been widely used for several decades to indirectly monitor different ionic species in less or more complex samples, such as the potentiometric determination of pH. With the availability of inexpensive glass pH electrodes and pH meters, determining pH is one of the most frequent quantitative analytical measurements and one of the most simple potentiostatic-based techniques [113].

Dynamic techniques are divided into controlled-potential and constant-current techniques. Controlled-potential techniques are based on dynamic current conditions, such as in the cases of voltammetry and amperometry. The electrode potential is used to direct an electron-transfer reaction, and the resulting current is measured. The detected current is a direct reflection of the electron transfer rate occurring at the interface between the electrode and the solution/electrolyte. These techniques can measure any electroactive chemical species prone to oxidation or reduction reactions. Their advantages include high sensitivity (also in combination with several pre-concentration approaches, such as stripping anodic or cathodic voltammetry), portable and low-cost instrumentation, and a wide range of electrodes suited for different environments and applications [113]. Finally, the constant-current techniques include techniques such as coulometry and electrogravimetry, being rarely used in contemporary research. In addition, electrochemical impedance spectroscopy (EIS) is a powerful technique used for interfacial analysis on the electrode/electrolyte interface that measures the current signal resulting from the AC-induced perturbation of the system. The current signal is then transformed into signals which are more appealing for analytical purposes, such as the

impedance, or the impedance-derived parameters, such as the charge-transfer resistance (R_{ct}) or the double-layer capacitance (C_{dl}), depending on the measurement mode, i.e., in the presence or the absence of the redox-active probe, respectively [114, 115]. Despite lower selectivity, such measurements enable excellent sensitivity.

1.3.1 Controlled-potential techniques

The base of all controlled-potential techniques is the ability to measure the current response to an applied (excitation) potential. Voltammetry is viewed as one of the starting points in electrochemistry regarding controlled-potential methods, which can be presented in different forms. In the present chapter, some of these techniques will be reviewed.

In voltammetry, a time-dependent potential is applied to an electrochemical cell (usually consisting of working, reference, and counter electrodes) between the working and reference electrode, and the resulting current is measured between the working and counter electrode. A resulting voltammogram is a graphical representation that shows the relationship between the resulting current and the applied potential. It is a valuable tool for obtaining quantitative and qualitative information on the species participating in the oxidation and/or reduction reactions [113], Figure 1.2.

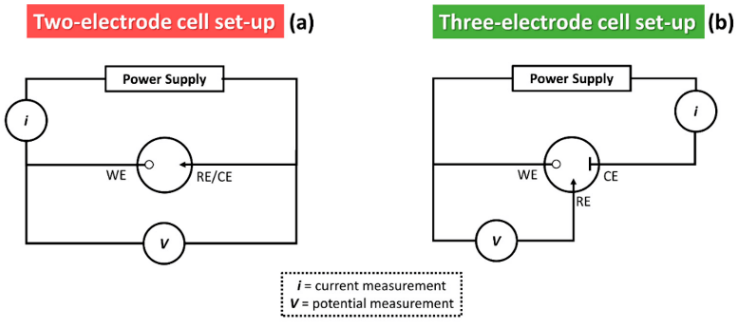

Figure 1.1: Graphical representation of a) two and b) three-electrode cell set-up [116].

Early voltammetric techniques used a two-electrode system for measurements, where one electrode was the working electrode (WE), and the other one represented both the reference (RE) and counter (CE) electrode, Figure 1.1 a); however, modern techniques usually use three-electrode systems like those mentioned in the previous chapter, Figure 1.1 b). A time-dependent potential excitation signal is applied to the WE, changing its potential relative to the fixed potential of the RE and measuring the current that flows between the WE and CE.

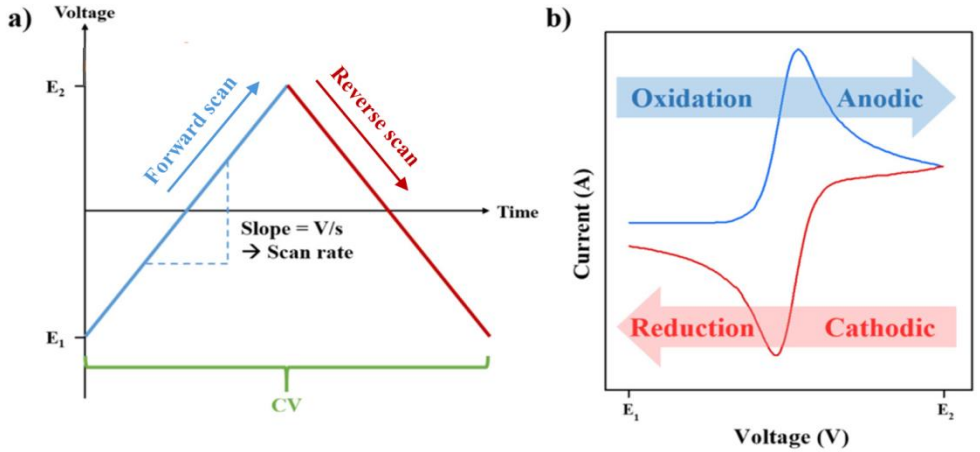

Figure 1.2: a) Voltage vs. time profile of cyclic voltammetry. b) Typical (reversible) cyclic voltammogram showing cathodic and anodic signals [117].

1.3.2 Voltammetric techniques in electroanalysis

Voltammetric techniques involve the potential scan in a selected potential window and the corresponding measurement of the current response produced from electron transfer events between the electroactive species and the WE. Since the phenomenon involves the oxidation or reduction reactions of the electroactive species present in the system, the measured current can be considered proportional to the analyte(s) concentration(s), and the peak potential gives the techniques its selective feature.

Over the years, various (sub)techniques have been developed to enhance the speed, selectivity, and sensitivity of voltammetric measurements. Instead of relying solely on a straightforward staircase ramp, alternative forms of potential modulation have been introduced. Additionally, while the focus remains on the widely employed classic voltammetric techniques, this chapter will also tackle several pulse techniques that have been mentioned for comprehensive coverage.

1) *Stripping voltammetry*

Stripping voltammetry, as another representative of the voltammetric techniques, can consist of three related methods, depending on the analyte of interest: anodic stripping voltammetry, cathodic stripping voltammetry, and adsorptive stripping voltammetry. These techniques are by far mostly used for trace metals analysis in water-based media.

Anodic stripping voltammetry consists of two steps; the first step is a controlled potential electrolysis/pre-concentration in which the WE is held at a cathodic potential sufficient to pre-concentrate the metal ion on/in the electrode surface. A WE is usually a hanging mercury drop or a mercury film electrode; however, over the years, other environmentally friendly solutions have emerged, such as the bismuth-film, antimony-film, and copper-film electrodes [118, 119, 120]. The pre-concentration step provides an increase in the analyte concentration by transferring it from the bulk solution with a larger volume to the electrode with a lower volume. During the pre-concentration step, the solution is typically stirred to increase the deposition rate. At the end of the deposition/pre-concentration step, the stirring is stopped, and the solution becomes quiescent. The deposition/accumulation/pre-concentration step typically ranges from less than 1 to 30 minutes, whereas analytes at lower concentrations may require longer accumulation times. After the equilibration step of usually 10-15 s, i.e., without stirring to make the solution quiescent, and applying the same pre-concentration potential, the potential is incrementally scanned in an anodic direction, i.e., towards more positive

potentials. Once the WE reaches a sufficient potential, the analyte is re-oxidized and stripped from the electrode, returning back to the solution in its oxidized/ionic form. Because the analyte is concentrated on/in the electrode, detection limits are significantly lower compared to other electrochemical techniques. The detection limits obtained with anodic stripping voltammetry can go down to the ng L^{-1} concentration range [113].

Cathodic stripping voltammetry shares similarities with anodic stripping voltammetry but with two key distinctions. Firstly, the electrode is oxidized during the electrochemical pre-concentration step, reacting with the analyte to create an insoluble film at the electrode surface. Secondly, the stripping process involves scanning the potential cathodically towards more negative potential values. The reduction process reverts the already oxidized electrode to its original state, effectively releasing the analyte into the solution.

The pre-concentration step in the adsorptive (cathodic) stripping voltammetry usually occurs, e.g., for trace metal detection, in the presence of a chelating agent (ligand) at the selected negative potential. The complex metal ion is adsorbed at the electrode surface. During the pre-concentration step, the electrode is maintained at a potential that enhances adsorption. Following the pre-concentration step, the potential can be scanned either in an anodic or cathodic direction, depending on the analyte, i.e., either oxidizing or reducing the analyte, respectively. The adsorptive cathodic stripping voltammetry is typically used for metal analytes that cannot form amalgams, alloys, or intermetallic compounds in/at the electrode surface.

2) *Cycling Voltammetry*

In cyclic voltammetry, the potential is scanned in both directions, i.e., in anodic and cathodic directions. This technique is usually the first one used when investigating the selected electrochemical process/system and gives important information about the redox properties of the analyte(s) (reversibility/kinetics), electrochemical characteristics of the electrode material, electrolyte, etc. [113]. In general, cyclic voltammetry holds a great electrochemical diagnostic potential.

In the example below, the potential is first scanned to more positive values, resulting in the oxidation reaction for the reduced species (R) $R \rightleftarrows O+ne^-$. Once the potential attains a predefined switching potential, the voltammetric scan proceeds towards increasingly negative potentials. Because the oxidation species (O) were generated on the forward scan, during the reverse scan, they are reduced back to $O+ne^- \rightleftarrows R$. The resulting voltammogram exhibits distinct signals representing the oxidation and reduction processes. Each peak is characterized by its peak potential and peak current, as shown in Figure 1.3.

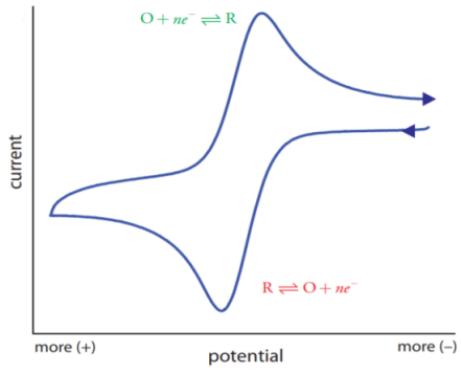

Figure 1.3: Cyclic voltammogram with typical oxidation-reduction curves [121].

3) *Normal Pulse Voltammetry*

This technique uses a series of potential pulses of increasing amplitude. The current measurement is made near the end of each pulse, allowing enough time for the charging current to decay (faster decay than the decay of Faradaic current). Typically, pulse voltammetry is performed in a solution without active stirring. The potential is applied in a pulsed manner, starting from an initial potential. The pulse duration is usually 1 to 100 ms, and the interval between pulses is typically 0,1 to 5 s.

4) *Square-wave Voltammetry*

In this case, the excitation signals involve consecutive and symmetrical positive and negative going square-wave potential pulses overlapping with a staircase waveform, where the forward pulse of the square-wave coincides with the staircase step. The current is sampled, similarly as in other pulse techniques, a few ms before the end of the voltammetric pulse (in both directions). The net current is obtained by taking the difference between the forward and reverse currents. The height of the net signal exhibits a direct proportionality to the concentration of the electroactive species, thereby serving as a reliable quantitative measure. Notably, the technique offers the advantage of achieving very low detection limits, reaching as low as 10^{-8} M; usually, it is combined with the electrochemical stripping protocols. Moreover, a deeper look into the square-wave voltammetry reveals its powerful electrochemical diagnostic character.

1.4 Screen-Printed Electrodes

Until a few decades ago, the most commonly used electrochemical cells were conventional glass cells with a separate two or three-electrode system. Because of the progress in technology and material science, various supporting electrodes (and electrochemical sensors) have developed rapidly. They have changed shape and size, become simple to use, and can be manufactured at large scales [122, 123, 124, 125].

The development of screen-printed electrodes (SPEs) has made the field of electrochemistry simpler and more accessible. At the same time, it has also brought some challenges in tuning the sensitivity and complexity of the electrochemical systems. The overall technological process for fabricating SPEs allowed us to acquire a wide range of new electrode setups and to modify electrodes with ease using various commercially available inks for RE, CE, and WE, which can be developed and optimized for specific target analytes. For example, boron-doped diamond electrodes, hexacyanoferrate-modified screen-printed carbon, gold nanoparticle-decorated carbon nanotubes, screen-printed carbon, screen-printed carbon electrodes modified with silver nanoparticles, Prussian Blue/carbon electrodes, etc. [126, 127, 128, 129]. The emergence of novel nano and other advanced materials opens countless possibilities for bulk and/or surface modifications to tailor numerous electrode architectures suiting specific needs.

In both potential-controlled experiments and current-controlled experiments, the widely employed three-electrode system plays a crucial role. The WE serves as the site where an electrochemical reaction takes place [113, 130, 131]. Given the limitations of using unmodified supporting WE alone, achieving optimal sensitivity, selectivity, and reproducibility in electroanalysis often requires employing various surface and/or bulk modification approaches [113].

Over time, SPEs are becoming more sophisticated and versatile while their size, and weight are shrinking as well, and they can be used both for the detection in the solutions and in the gas phase. The usage of SPEs in the solutions offers the opportunity to work in a more controlled, stable, sensitive, selective, and reproducible environment. The system can be optimized as robust and might provide a shorter analysis time for the

detection. The advantages of SPE-based sensors for measuring in the gas phase include the possibility of miniaturization and portability, adjustable sensitivity and selectivity, a wide linear range, minimal space, and power requirements, and cost-effective instrumentation. Compared to the same design in the solution, the application of SPE in the gas phase could lack stability, reproducibility, selectivity, and sensitivity; all these challenges pose a need for further investigation of these electrochemical systems [132, 133].

The SPE consists of a chemically inert ceramic substrate onto which three electrodes, i.e., WE, RE, and CE, are screen-printed (see Figure 1.4). The WE is the most important part of the SPE at which electrochemical reactions occur, while the RE and CE serve to complete the circuit.

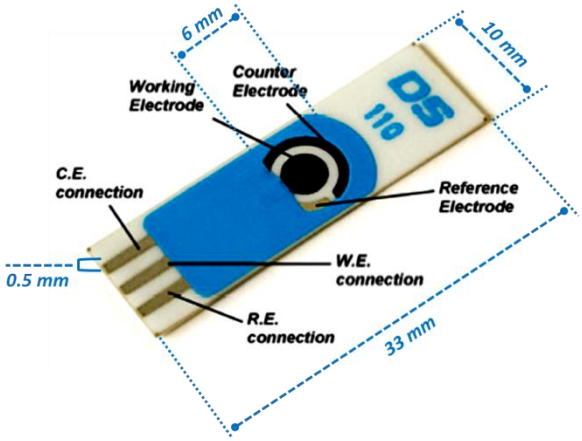

Figure 1.4: Model of SPCE with all the essential parts [134].

SPE fabrication involves the utilization of inks comprising particles, a polymeric binder, and additional additives to enhance dispersion, printing, and adhesion [135, 136, 137]. The composition of the ink, including the types, sizes, and loading of particles, plays an important role in influencing the electron transfer process and ultimately affects the overall electroanalytical performance of the screen-printed electrode/sensor. The variation of ink composition provides an avenue for further tailoring the sensor's characteristics to meet specific requirements.

To address these requirements, the electrode surfaces are modified with a great selection of inorganic and organic (nano) materials which gives them the sensitivity and/or selectivity features together with enhanced reproducibility, durability, interference-free operation, etc., allowing for improved sensing functionality and performance in diverse applications [138, 139].

1.5 Electrochemical Gas Sensors

Electrochemical gas sensors, Figure 1.5, exploit (electro)chemical reactions to measure the concentration of a particular gas in an environment.

They are equipped with two or three, occasionally even four electrodes in contact with an electrolyte. The electrodes are usually made by introducing a high-surface-area material onto a porous membrane. The WE establishes contact with the electrolyte and the ambient air to be monitored, typically through a permeable membrane. Sensors, along with the sensor housing, are often enclosed within a plastic or glass casing that includes a gas entry point for the gas or volatile solution to be analyzed and electrical contacts.

As the gas permeates to the sensor placed in the glass cell, it diffuses through the electrolyte toward the WE. The gaseous analyte can come from the external gas flow into the glass cell, or it can be placed as a solution under the sensor, where it will succumb to the decomposition and/or evaporation into the gas molecules, which accumulate in the electrolyte. The gas undergoes oxidation or reduction at the WE through an electrochemical reaction [140, 141]. This reaction produces an electric current that flows through the external circuit, which is connected to a measuring device such as a potentiostat, galvanostat, or electrochemical impedance analyzer. The measuring device amplifies and processes the signal further.

Chemiresistive sensors are chemical sensors that operate based on changes in electrical resistance when exposed to specific target analytes. These sensors are designed to detect and quantify the presence of various substances, including gases, volatile organic compounds (VOCs), and other chemicals, by measuring alterations in electrical resistance. While chemiresistive gas sensors have applications in measuring gaseous H_2O_2 concentrations [142], they may not necessarily outperform voltammetric or amperometric gas sensors. One of the limitations of chemiresistive sensors is their lack of high selectivity, especially when using certain sensing materials. Some sensors can respond to multiple gases, resulting in cross-sensitivity, difficulties distinguishing specific gases in complex environments, and compromising accuracy and selectivity. Additionally, these sensors are sensitive to environmental conditions, such as high temperatures and humidity, which can affect their response and lead to reading inaccuracies [143]. On the other hand, electrochemical gas sensors offer distinct advantages and simpler operating systems mentioned in this chapter.

In the case of voltammetric or amperometric gas sensors, the magnitude of the electric current can be determined by the extent of oxidation or reduction of the gas and, in addition, by the redox modifier present at the WE. Electrochemical gas sensors are usually designed in a way to limit the gas supply through diffusion, resulting in a linear relationship between the output of the sensor and the gas concentration [144]. This linear output is advantageous compared to other sensor technologies that require linearization of their output. It allows for more accurate and precise measurement of low concentrations and simplifies calibration, which typically requires only a baseline measurement and five to eight calibration points. The control of diffusion offers an additional benefit. The sensor can be tailored to target specific gas concentration ranges by adjusting the diffusion barrier [144].

Electrochemical gas sensor technology has been used in the industry for many years. The increasing demand for small and powerful sensors with low power consumption and user-friendly characteristics has been a driving force behind the continuous advancements in sensing technology.

The sensitivity and selectivity of the sensor towards specific gaseous analytes can be finely tuned through various modification techniques applied to the SPEs; however, there are very scarce reports tackling the optimization and detection of very low levels (ppbv) of gaseous H_2O_2. In general, these modifications allow for the precise detection of desired gaseous analytes while reducing sensitivity to potential interferences. By adjusting the composition of the electrolyte, density, and pH, the analytical performance of the sensor can be optimized to target particular analytes.

Furthermore, the surface of the WE can be modified through the introduction of different components such as metals, metal oxides, polymers, anumerous nanostructured materials, and their combinations. These modifications improve sensitivity, selectivity, chemical and/or electrochemical stability, and expand the usable potential window of the sensor.

In summary, the versatility of SPEs, together with various modifiers, sensing schemes, and their combinations, allows precise control of gas sensing performance considering the sensitivity and selectivity of the sensor towards specific gaseous analytes.

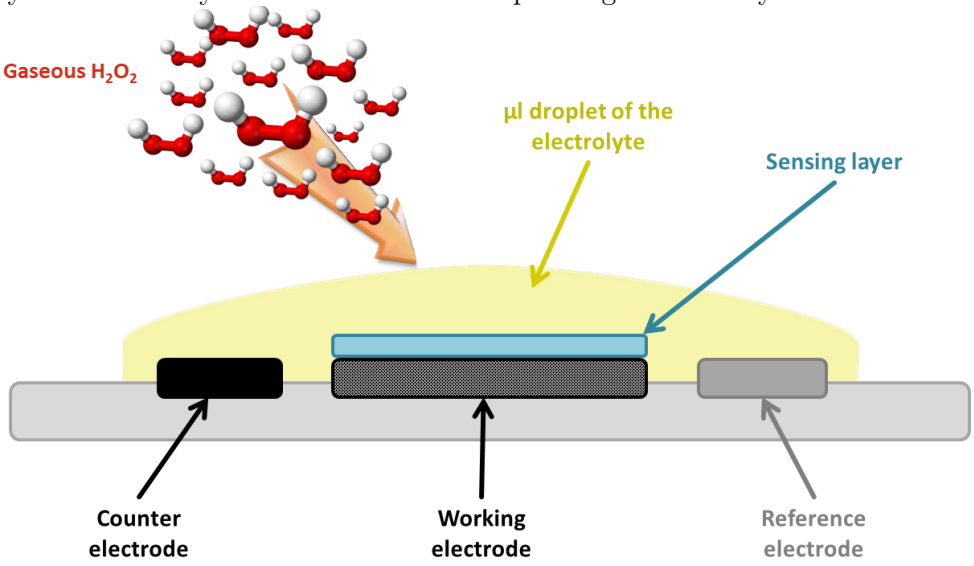

Figure 1.5: Cross-section scheme of the electrochemical gas sensor.

1.5.1 Electrode modifications

A modified electrode refers to a conducting or semiconducting material that has undergone surface modification by being coated with a thin or thick film. This film can take various forms, including monomolecular, multi-molecular, ionic, or polymeric compositions, and it plays a crucial role in altering the properties of the electrode surface [145, 146]. By modifying the electrochemical, optical, and other surface characteristics, these coatings broaden and enhance the capabilities of electrochemical techniques.

The primary objective of modifying an electrode surface is to impart its predictable function through the properties of the adlayer. This predictability enables precise control and manipulation of electrochemical processes, resulting in desired outcomes and tailored responses.

Recent advancements in surface characterization techniques have revolutionized the ability to understand modified interfaces at a molecular or even atomic level. Combining these sophisticated characterization techniques with electrochemical approaches makes it possible to verify the intended functionality of the modification and set the groundwork for continuous refinement of the modification strategies.

The selected substrate serves as the supporting electrode upon which the adlayer is deposited. It can be either a commercially available or custom-fabricated supporting electrode. While conventional electrode material can be used as a supporting substrate, certain materials are more suitable for modification. In the case of detecting H_2O_2, three generations of sensors and corresponding materials have been used to modify the WE [147]. These modifications are both used in the detection of gaseous analytes and liquids.

The 1st-generation electrochemical H_2O_2 sensors consider the thermodynamics of H_2O_2 reactions, which predict its direct reduction or oxidation at various electrode materials; however, the slow electron transfer kinetics result in high overpotentials for H_2O_2 oxidation/reduction [148, 149]. Overpotential refers to the voltage difference between the redox potentials measured under ideal thermodynamic conditions and the actual experimental conditions. To overcome this challenge, certain materials have

demonstrated the ability to accelerate redox transformations of H_2O_2. Noble metals such as gold (Au) [150, 151], silver (Ag) [106], and platinum (Pt) [152] have shown promising results in facilitating the desired redox reactions. Similarly, other metals like copper (Cu) [153, 154] and metal oxides such as CuO [153, 155] have exhibited catalytic properties that aid in accelerating H_2O_2 redox processes. Additionally, non-metal catalysts, including various types of carbon-based materials [156], have also been explored to enhance the kinetics of H_2O_2 electrochemical reactions. Previously mentioned redox systems involving H_2O_2 are predominantly utilized in bulk solutions due to the relative ease of detecting H_2O_2 in aqueous solutions compared to gas phase detection. Indeed, the electrochemical detection of H_2O_2 in the gas phase has been regarded as both intriguing and challenging. As a result, there is a relatively low number of articles focusing on the detection of gaseous H_2O_2 compared to its detection in solutions. The unique challenges and complexities associated with gas-phase electrochemical detection of H_2O_2 have sparked interest, led to ongoing investigations in this area, and strongly motivated this doctoral thesis. In addition to the modification of the WE, the preconditioning of the electrode surface can significantly impact the overall analytical performance of the gas sensor. One such preconditioning technique is electrochemical cleaning/treatment, which involves subjecting the electrode to constant potential polarization, cyclic voltammetric pretreatment in H_2SO_4 and H_2O_2, heat treatment [157] or O_2 plasma treatment [138, 158]. This process helps optimize the electrode surface, removing contaminants or interfering species that could affect the measurements, enlarge the electrode surface and/or introduce additional functional groups.

The 2nd generation of electrochemical H_2O_2 sensors represents a significant advancement, specifically aimed at addressing the sluggish electrode kinetics observed with bare electrodes. These sensors utilize surface-modified electrodes incorporating electroconductive and electrocatalytic materials. Among the commonly employed modifications are noble metal nanoparticles, such as Au, Au-Pt [159], Ag, Pt, and palladium (Pd) [160]. Additionally, combinations of different metals or composites, metal oxides, carbon derivatives, and conducting polymers have been explored to reduce the overpotential associated with H_2O_2 electrode reactions [161, 162, 163].

One approach involves the use of inorganic or organic polymers, as well as polyelectrolytes, to coat carbon or metallic electrode surfaces [164, 165]. These modifications have demonstrated the ability to achieve lower detection limits for H_2O_2 in the micro- to nanomolar concentration range. Furthermore, various substances like amino acid derivatives [166], pyrrole, aniline, pyridine, and diverse heterocyclic compounds [167] have been successfully employed as electrode modifiers.

A significant breakthrough in surface modification has been achieved by utilizing nanocomposite materials that incorporate nano-sized noble metal particles with strong electrocatalytic properties. Carbon nanomaterials, including single-layer sheets and single-walled [168] or multi-walled [169] carbon nanotubes, offer numerous binding sites for a wide range of organic and inorganic compounds. This enables improved selectivity and sensitivity in H_2O_2 measurements, with detection limits reaching the nanomolar range. The combination of particles from two different metals, known as "bi-metallic" configurations [170, 171], has also been explored for electrochemical H_2O_2 detection.

An intriguing class of materials that have emerged in recent years are MXenes, specifically 2D transition-metal carbides/nitrides. These materials are characterized by their general formula $M_{n+1}X_nT_X$, where n can be 1, 2, or 3, representing three common structures. Symbol M denotes an early transition metal, such as Ti, Mo, or V, while X refers to carbon or nitrogen. Designation T encompasses various surface terminations, including fluorine (−F), hydroxyl (−OH), and/or oxygen (=O) [172, 173, 174]. MXenes exhibit exceptional physicochemical properties that make them highly attractive for

numerous applications. They possess impressive mechanical strength, facilitating their use in structural applications. Additionally, they demonstrate good thermal conductivity, enabling efficient heat transfer. One of the notable features of MXenes is their tunable bandgap, which can span from semiconducting to metallic character, offering flexibility for different electronic applications. Furthermore, MXenes exhibit hydrophilic surfaces with numerous functional groups, allowing for post-modification and solution processing. This characteristic opens up possibilities for tailoring their unique properties to specific needs and integrating them into various sensing devices and systems [174].

The incorporation of redox mediators represents another crucial improvement in electrochemical sensors, facilitating electron exchange between the electrode and H_2O_2. Commonly used redox mediators include metal complexes, particularly iron complexes, known for their reliable electrochemical reversibility. Some of these mediators are sparingly water-soluble compounds, such as ferrocene derivatives [175], Prussian Blue [176], iron oxides [177], and other metal derivatives. They are immobilized on the electrode surface mostly through adsorption, exhibiting highly sensitive mediation properties.

By incorporating these advanced modifications, the second-generation electrochemical H_2O_2 sensors offer enhanced performance in terms of sensitivity and selectivity. They enable precise measurements of H_2O_2 with lower detection limits, providing a valuable tool for various applications requiring accurate detection and quantification of this analyte.

The advancement of electrochemical H_2O_2 sensors has led to the development of *3rd-generation sensors*, which involve the modification of electrodes using proteins and redox enzymes. These sophisticated systems aim to mimic the intricate redox processes observed in living organisms, offering enhanced efficiency and specificity for H_2O_2. These approaches involve the immobilization of carefully selected enzymes or non-enzymatic proteins on the electrode surface. These biomolecules possess specific reactivity towards H_2O_2, facilitating the mediation of electron transfer between H_2O_2 and the electrode. Frequently utilized enzymes include horseradish peroxidase [178, 179], catalase [180], heme, hemoglobin [181], myoglobin [182], and cytochromes [183]. The redox couple Fe^{2+}/Fe^{3+} within the prosthetic group of these proteins plays a crucial role in mediating the electron transfer process. Soluble or surface-immobilized redox mediators are often introduced into the electrolyte solution to enhance the performance of protein-based electrochemical sensors. These mediators, such as hexacyanoferrates, ferrocene derivatives, methylene blue, or quinones, facilitate and optimize the electron transfer between the biomolecules and the electrode [184].

While protein-modified electrodes offer several advantages, such as their ability to catalyze specific reactions and mimic biological processes, they do come with certain limitations. The preparation of these electrodes can be time-consuming, requiring frequent fresh preparation. Additionally, the cost of high-priced proteins poses a significant financial challenge. The enzyme's activity can also be susceptible to rapid decrease due to denaturation, and incorrect orientation of the enzyme at the electrode surface can impair its catalytic activity. Furthermore, the presence of electrolytes in the measuring buffer can potentially influence the activity of redox enzymes.

1.5.2 Electrolytes

Every electrochemical process occurs within a specific ionically conductive medium, typically a solvent containing dissolved ions. This medium, often referred to as the supporting electrolyte or simply the electrolyte, plays an important role in every electrochemical experiment and sensing scheme.

The presence of medium comprising mobile ions is essential in an electrochemical cell as it allows for the control and measurement of electrode potential/current, a key parameter in virtually all electrochemical investigations. A suitable medium should possess a solvating power to dissolve reactants and products involved in the electrode reactions, low reactivity, and should exhibit stability in a wide potential window. Additionally, it is desirable for the medium to have relatively low viscosity, enabling efficient transport of reactants and products to and from the electrodes. Thus, the selection of an appropriate solvent-electrolyte combination is a critical decision in electrochemistry. Researchers strive to identify mediums that fulfill these requirements while considering factors such as stability, availability, safety, and environmental impact. By carefully choosing the solvent-electrolyte combination, optimized experimental conditions can be reached, enabling advancements from fundamental research to practical applications related to energy storage, corrosion prevention, chemical synthesis, electrochemical sensing, diagnostics, and beyond.

Electrolytes can be generally categorized into two groups: strong electrolytes and weak electrolytes. Strong electrolytes are substances that, when dissolved, undergo complete dissociation into ions. An illustrative example is sodium chloride (NaCl) in H_2O, where the compound dissociates fully into sodium and chloride ions. In contrast, weak electrolytes exist in a partially dissociated state, with a significant portion of the dissolved electrolyte remaining in its uncharged form, typically as neutral molecules. Acetic acid (CH_3COOH) in H_2O serves as a prime example of a weak electrolyte. In a 0.1 M CH_3COOH solution, only about 1% of the acid dissociates into protons and acetate ions, while the remaining approximately 99% remains neutral CH_3COOH molecules.

When selecting electrolytes, the impact of ion size on conductivity is an important factor to be considered. At first glance, large ions might seem less favorable due to their lower mobility. However, there are instances where large ions offer advantages in terms of solvation. In low-polarity solvents, where the solvation energies for ions are typically low, large ions can be more readily solvated compared to small ions. In these cases, salts containing small, highly charged ions often become insoluble. Furthermore, large ions are less susceptible to ion-pairing interactions within such solvents.

Alternatively, electrolytes can be categorized into two main types: aqueous electrolytes and solid electrolytes. For example, aqueous electrolytes have historically been at the forefront of battery research and commercialization [185]. For instance, the first Leclanché cell (zinc-carbon battery) utilized an ammonium chloride (NH_4Cl) aqueous solution as its electrolyte. This laid the foundation for the development of the neutral Zn-MnO_2 battery in its dry cell form.

Solid electrolytes, on the other hand, can be further divided into four groups.

a) Gel electrolytes closely resemble liquid electrolytes as they consist of liquids within a flexible lattice framework [186].
b) Dry polymer electrolytes differ from liquid and gel electrolytes in that the salt is directly dissolved into a solid medium, often a polymer with a relatively high dielectric constant, such as polyethylene oxide or polyacrylonitrile. To enhance mechanical strength and conductivity, composites with inert ceramic phases are often employed, resulting in two major classes: polymer-in-ceramic and ceramic-in-polymer electrolytes [187, 188].
c) Solid ceramic electrolytes enable ion migration through vacancies or interstitials within the ceramic lattice. There are also glassy-ceramic electrolytes.
d) Organic ionic plastic crystals represent organic salts that exhibit mesophases, showing characteristics between liquids and solids [189]. In these materials, the mobile ions exhibit a fascinating characteristic where their orientations or

rotations lack a definite order, while their central positions maintain a structured arrangement within the crystal lattice.

Additionally, there are "exotic" electrolytes, such as Nafion, ionic liquids, poly(acrylic acid) (PAA), etc. Nafion, a proton-conducting fluorosulfonic acid ionomer material, finds applications in fuel-cell technology as well as electrochemical sensors. PAA, renowned for its remarkable H_2O retention properties, has exhibited significant potential as a gel electrolyte material. These gel electrolytes possess ionic conductivity comparable to that of aqueous electrolytes, making them suitable for a wide range of devices. Additionally, the flexibility of PAA enables its utilization in various applications [190, 191]. Furthermore, its capability to absorb gaseous molecules allows it to function as an accumulation (and derivatization) medium, enhancing its versatility and usefulness in diverse settings.

The unique properties of these electrolytes make them suitable for specific applications. For instance, the semi-solid nature and low volatility of solid-polymer electrolytes, combined with their resistance to solvent loss by evaporation, make them convenient for high-vacuum conditions. Room-temperature ionic liquids, composed solely of ions without volatile or uncharged components, have gained popularity due to their low volatility, low reactivity, low H_2O solubility, and relatively high ionic conductivity [192]. Although their conductivity may seem low considering their ion content, factors such as ion size, viscosity, and ion association contribute to their performances.

Chapter 2

Goals and Hypothesis

This dissertation aims to tackle the most critical aspects concerning the still challenging sensing of low concentration levels of gaseous H_2O_2 and to suggest novel and effective sensor architectures for its sensitive, selective, and point-of-need detection. The purpose of this dissertation is to provide a thorough and systematic study and selection of an appropriate supporting (and disposable) electrode system and suitable modifications enabling efficient H_2O_2 accumulation, redox transformation, signal amplification, and efficient detection using materials such as metal/metal oxides, 2D laminated materials (MXenes), polymeric materials, etc., together with specific electrochemical sensing schemes. Furthermore, this doctoral thesis aims to provide relevant discussion and understanding of the physical and electrochemical phenomena involved in the detection processes occurring at the sensing interfaces.

Goals of the dissertation:

- Study and improvement of the electrochemical properties of disposable screen-printed electrodes (conductivity, reproducibility, signal-to-noise ratio) by chemical and electrochemical methodologies/treatments;
- Selection of suitable sensing redox/catalytic modification materials, e.g., state-of-the-art 2D and 3D nanomaterials, metal-oxide, and metal ions.
- Development of new sensing/accumulation/protective membranes for improved detection of gaseous H_2O_2;
- Development of quantification methods for measuring gaseous H_2O_2 (amperometry, voltammetry, etc.);
- Real environmental detection of gaseous H_2O_2.

Hypotheses:

- (Electro)chemical pretreatment and modification of the working electrode will enhance the electroanalytical properties and performance of the gas sensor, considering sensitivity, selectivity, and reproducibility;
- 2D laminated MXenes will increase and/or stabilize the analytical signal when integrated into the sensing architecture;
- Electrochemically deposited MnO_2 can serve as the redox mediator for sensitive detection of H_2O_2 via chemical-electrochemical sensing pathway;
- Gel-like electrolyte with favorable characteristics, such as pH, viscosity, conductivity, and H_2O_2 accumulation, will lead to highly sensitive and selective detection of gaseous H_2O_2;

- The chitosan-based membrane can serve as the protective/stabilization layer against unwanted oxidations of MXenes, leading to their improved electrocatalytic effect;
- Fine-tuning of the operational parameters will result in lower limits of detection.

Chapter 3

Scientific Publications

The dissertation comprises two distinguished manuscripts, each published in highly esteemed scientific journals. In Manuscript 1 (3.1), we explored several hypotheses, namely the enhancement of electroanalytical properties and performance of the newly developed gas sensors through (electro)chemical pretreatment and modification of the working electrodes. Our pretreatment protocol was carried out in a 0.1 M H_2SO_4 solution, employing cyclic voltammetry and two distinct modifiers for the working electrode surface. Additionally, we demonstrated that the electrochemically deposited MnO_2 serves as a convenient redox mediator for the sensitive detection of H_2O_2 via the chemical-electrochemical sensing pathway. We also showed that the gel-like electrolyte composed of poly(acrylic acid) (PAA) possesses favorable gas sensing characteristics such as pH, viscosity, conductivity, and H_2O_2 accumulation properties, thus enabling highly sensitive and selective detection of gaseous H_2O_2 while simultaneously acting as an electrolyte and accumulation medium for H_2O_2. We demonstrated that both gas sensors, i.e., the one with included MnO_2 and the other one without MnO_2, exhibited excellent electroanalytical performances for the detection of very low concentration levels of H_2O_2. Interestingly, the one without MnO_2 revealed a slightly lower limit of detection. The optimization of experimental parameters was shown as an important part of the sensor preparation protocol resulting in improved sensing performance. The effectiveness and applicability of such sensing architecture were demonstrated by measuring a released H_2O_2 during the disinfection process.

Moving on to Manuscript 2 (3.2), we addressed the remaining hypotheses: the second and fifth. Here, we explored the integration of 2D layered MXenes into the sensing architecture of the sensor on the top of the ferrocyanide layer, which resulted in increased and reliable electroanalytical signals. This integration successfully fulfilled the first and second hypotheses. We introduced a chitosan-based membrane to stabilize the MXenes as an immobilization layer and effectively prevent their unwanted oxidation. Experimental data and Supplementary Information support the improved electrocatalytic effect of MXenes and the beneficial properties of chitosan. Also, in this case, the practical applicability of the developed gas sensor was successfully demonstrated through the measurement of released H_2O_2 during real hair bleaching.

In summary, these two manuscripts, published in scientific journals with relatively high impact factors, represent significant contributions to the field of sensitive electrochemical gas sensing at room temperature, showing innovative approaches, successful experimental demonstrations, and the validation of multiple hypotheses. This dissertation's comprehensive body of research reinforces our commitment to advancing scientific knowledge and pushing the boundaries of very challenging electrochemical gas sensing.

3.1 Manuscript 1: "Simple Electrochemical Sensors for Highly Sensitive Detection of Gaseous Hydrogen Peroxide Using Polyacrylic-acid-based Sensing Membrane"

Published – Sensors and Actuators B: Chemical

As emphasized in the introduction of this dissertation, the existing methods for detecting gaseous H_2O_2 typically rely on complex, bulky, and relatively expensive instrumentation. This necessitates highly skilled personnel, together with limiting the feasibility of on-site, fast, direct, and reliable detection protocols for measuring particularly low concentrations of gaseous H_2O_2 using portable and user-friendly analytical equipment. On the other hand, electrochemistry, in combination with a great selection of modification (nano) materials, supporting electrodes, and advanced electrochemical techniques, offers unsurpassable possibilities for tailoring powerful sensors for gaseous H_2O_2. While there are many reports on the H_2O_2 sensors for their deployment in liquid samples, there are very few reports on the sensitive and selective detection in the gaseous phase. Recognizing such needs and opportunities, this research focused on utilizing electrochemical methods, specifically cyclic voltammetry, to enable the development of sensitive sensors that meet these requirements.

Simplicity was a guiding principle in the development of point-of-interest and disposable sensors for gaseous H_2O_2, pursuing the goal of creating devices that are relatively easy to fabricate and operate. To achieve this, we explored various materials for supporting electrodes, guided by thorough electrochemical studies of (electro)chemically pretreated electrodes. The chosen approach further involved modifying screen-printed carbon electrodes as the platform for developing sensitive gas sensors. Through a series of rigorous investigations, we successfully demonstrated that these sensors, when modified with MnO_2 and/or polyacrylic acid-based membrane/electrolyte and in combination with cyclic voltammetry, exhibited remarkable features such as extremely low limits of detection, excellent reproducibility, selectivity, and the ability to detect H_2O_2 in real samples.

Furthermore, to establish the reliability and suitability of these sensors for their intended purpose, we conducted validation studies comparing their performance against a standardized spectrophotometric method.

Sensors & Actuators: B. Chemical 352 (2022) 131053

Contents lists available at ScienceDirect

Sensors and Actuators: B. Chemical

journal homepage: www.elsevier.com/locate/snb

Simple electrochemical sensors for highly sensitive detection of gaseous hydrogen peroxide using polyacrylic-acid-based sensing membrane

Jelena Isailović [a,b], Kristijan Vidović [a], Samo B. Hočevar [a,*]

[a] Department of Analytical Chemistry, National Institute of Chemistry, Hajdrihova 19, Ljubljana, Slovenia
[b] Jožef Stefan International Postgraduate School, Jamova cesta 39, Ljubljana, Slovenia

ARTICLE INFO

Keywords:
Gaseous H_2O_2
Voltammetric gas sensors
Screen-printed electrode
Polyacrylic-acid-based sensing membrane
MnO_2 redox modifier

ABSTRACT

In this study, we present a simple electrochemical sensing platform for the detection of low concentration levels of gaseous hydrogen peroxide (H_2O_2). The sensors were designed using a supporting screen-printed electrode system modified with a polyacrylic-acid-based (PAA) sensing membrane that serves simultaneously as an electrolyte and accumulation medium. We prepared and compared two types of sensors, i.e., (i) PAA sensor and (ii) MnO_2/PAA sensor with a MnO_2 pre-modified working electrode surface. Both sensors exhibited good electroanalytical performances for detecting trace levels of gaseous H_2O_2 with the limits of detection of 3 μg m^{-3} (MnO_2/PAA sensor) and 2 μg m^{-3} (PAA sensor), a linear response in the examined concentration range of 15–121 mg m^{-3}, and repeatability with RSDs of 10.4% (MnO_2/PAA sensor) and 4.7% (PAA sensor). The practical applicability of both sensors was successfully demonstrated by detecting gaseous H_2O_2 in the real environment, i.e., in a room that was disinfected with 10% H_2O_2 solution.

1. Introduction

Hydrogen peroxide (H_2O_2) is undoubtedly one of the most omnipresent compounds, which plays an essential role in many fields, such as inorganic and organic synthesis, textile and wood industry, pharmacy, cosmetics, food production, biomedicine, clinical diagnostics, biology, material science, etc. [1,2]. Its significance in living organisms is obvious; H_2O_2 is present as a key molecule in combination with numerous enzymes (oxidases and peroxidases) [3]. It has a vital role as a signaling molecule regulating various processes connected to the immune system, apoptosis, root growth and is documented as an important biomarker related to oxidative stress [4,5], infections, and, as a gaseous molecule, to several diseases, such as lung cancer, asthma, chronic obstructive pulmonary disease (COPD), acute respiratory distress syndrome (ARDS), and cystic fibrosis (CF) [6–11]. Gaseous H_2O_2 has also been recognized as one of the key molecules in different atmospheric processes. There are several reports on its occurrence in combination with UV radiation, the existence of free radicals, and chemical transformations of primary and secondary organic aerosols [12]. Unfortunately, the role of H_2O_2 is also known in connection with homeland security issues; it is one of the main decomposition products of peroxo-explosives [13–18]. These explosives are relatively inexpensive and straightforward to prepare, whereas the essential components for their preparation can be bought in the nearest supermarket. The peroxo-explosives are relatively unstable under humid conditions; one of the decomposition products is H_2O_2, which can be exploited as a key gaseous marker for electrochemical detection to combat terroristic activities [14–16].

H_2O_2 can be detected with numerous techniques such as high-performance liquid chromatography [19], colorimetry [20], chemiluminescence [21], fluorescence [22], and electrochemistry [23–25]. Among these techniques, electrochemistry offers unique advantages due to its inherent characteristics such as high sensitivity [26–29], a possibility for almost unlimited use of different modifiers, membranes, and their combinations, and unsurpassed suitability for the miniaturization of electrode systems. Numerous sensors are based on the integration of, e.g., various enzymes [30,31], redox modifiers, metals [25,26], metal-oxides [32] non-metallic nanoparticles [33,34], and polymeric compounds into sensing membranes [35,36], which enable sensitive and selective detection of H_2O_2. However, there are many reports on electrochemical sensors for detecting H_2O_2 in liquid samples, but only a few of them tackle its detection in the gas phase [37,38].

In this work, we present a simple preparation and study of two sensitive electrochemical gas sensors for H_2O_2, encompassing a

* Corresponding author.
E-mail address: samo.hocevar@ki.si (S.B. Hočevar).

https://doi.org/10.1016/j.snb.2021.131053
Received 8 July 2021; Received in revised form 29 October 2021; Accepted 1 November 2021
Available online 5 November 2021

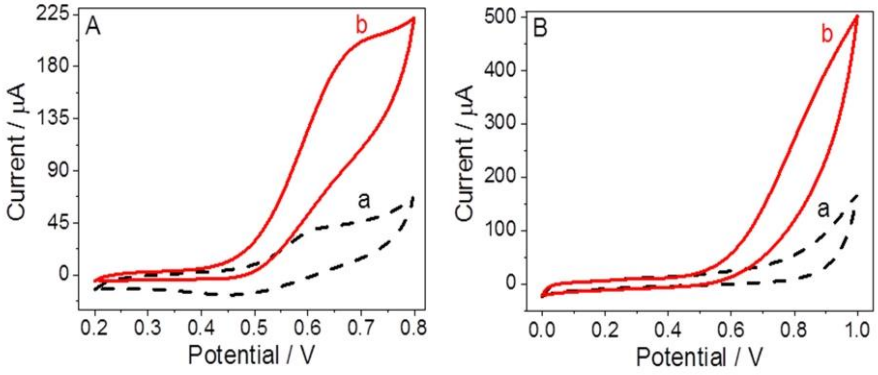

Fig. 1. Cyclic voltammograms obtained at the MnO_2/PAA (A) and PAA (B) gas sensors for background (a) and 90 mg m^{-3} H_2O_2 (b) using an accumulation time of 12 min. Scan rate: 100 mV s^{-1}.

polyacrylic-acid-based sensing membrane alone and in combination with MnO_2 underlayer predeposited on the supporting screen-printed electrode. Both sensors exhibited favorable detection of gaseous H_2O_2 in the low mg m^{-3} range under ambient conditions and excellent insensitivity toward several potentially present interfering gaseous compounds. Moreover, the sensors showed superior or competitive sensitivity compared to other electrochemical analogs.

2. Experimental

2.1. Apparatus

Electrochemical studies were carried out using a portable electrochemical workstation PalmSens4 potentiostat/galvanostat analyzer (PalmSens BV) in combination with a cable connector for screen-printed electrodes (DRP-CAC 71606, Metrohm DropSens), and the PSTrace 5.8 software (PalmSens BV). The supporting screen-printed electrode system consisted of a carbon working electrode (d = 4 mm), a silver quasi-reference electrode, and a carbon counter electrode (DRP-110, Metrohm DropSens), designed for working with microvolume samples.

2.2. Reagents and solutions

Methanol (VWR International), ethanol (Carlo Erba Reagents), H_2O_2 (30%), ammonia, formaldehyde (all from Merck), and phenol (Sigma-Aldrich) were of the analytical grade purity. Test solutions yielding the desired gaseous-phase analyte concentrations above the solution were prepared in 100 mL glass flasks according to the Henry's law [39] in the presence of the ambient atmosphere, i.e., no pre-purging was applied. In all experiments, 3.0 mL of the solution with an adequate analyte concentration was used. Afterward, the gas sensor attached to the electrode holder was tightly inserted into the horizontally-positioned flask in the area above the solution. The corresponding Henry's constants were obtained from the list in the Ref. [39]. All solutions used in this work were prepared using water purified with the Elix 10/Milli-Q Gradient unit (Millipore, Bedford, MA, USA).

2.3. Modification of screen-printed electrodes with gas sensing membranes

Before modification, the supporting screen-printed working electrode was electrochemically activated in a 0.1 M H_2SO_4 solution using cycling voltammetry, in the potential range of − 2.5 to 2.5 V, with a scan rate of 100 mV s^{-1} (3 cycles) to improve electrode-to-electrode reproducibility and particularly sensor's sensitivity, as shown in Fig. S1. This was followed by drying the activated screen-printed electrode system in a stream of gaseous N_2. In the case of MnO_2/polyacrylic-acid-based sensor (MnO_2/PAA sensor), the working electrode was first electrochemically modified with MnO_2. The modification was carried out in a solution (in a 20 mL electrochemical cell) composed of 1.0 mL of 0.4 M manganese dichloride (Sigma-Aldrich) and 14.0 mL of 1.5 M sodium hydroxide (Merck), with the pH of 14, using cyclic voltammetric scans in a range of − 0.5–0.4 V, with a scan rate of 100 mV s^{-1} (180 cycles). During the modification with MnO_2, only the working electrode of the screen-printed electrode system was connected to the potentiostat, whereas a conventional reference Ag/AgCl/(KCl satd.) electrode (Metrohm) and counter platinum wire electrode (Metrohm) were used. Finally, the screen-printed electrode system was modified via drop-casting 50 µL of viscous sensing membrane mixture consisting of 1.0 g of polyacrylic acid (450.000 g mol^{-1}; Sigma-Aldrich) and 10.0 mL of 0.1 M phosphate buffer solution (pH = 7.2), resulting in a polyacrylic acid/phosphate buffer molar ratio of ca. 0.002:1. In the case of PAA sensor, the screen-printed electrode system was modified only with a 50 µL sensing membrane mixture with a thickness of ca. 1.5 mm.

2.4. Electrochemical measurements

Cyclic voltammetric measurements were carried out in a potential range of 0.0 V up to + 1.0 V (if not stated otherwise) in combination with a scan rate of 100 mV s^{-1}. All measurements were performed at room temperature (22–23 °C) in a model atmosphere above the corresponding hydrogen peroxide solution, in the presence of atmospheric gases.

3. Results and discussion

3.1. Electrochemical sensing

Fig. 1 shows cyclic voltammograms (CVs) obtained at the MnO_2/PAA sensor (A) and PAA sensor (B) in the absence (a) and presence (b) of gaseous H_2O_2. Based on preliminary experiments, a potential window between 0.2 and 0.8 V was used for measuring with the MnO_2/PAA sensor and between 0.0 and 1.0 V for measuring with the PAA sensor. In the absence of H_2O_2, the MnO_2/PAA sensor revealed two redox signals corresponding to the oxidation of Mn(II,III) to Mn(IV) and the reduction of Mn(IV) to Mn(II,III) at around 0.60 V and 0.45 V, respectively (Fig. 1A, curve a). The peak-to-peak separation was approximately 170 mV, indicating that the Mn(II,III)/Mn(IV) redox system is quasi-reversible, also consistent with previous reports [40,41]. It is evident that the increase of the oxidation signal (Fig. 1A, curve b) directly correlates with the presence of 90 mg m^{-3} gaseous H_2O_2 in the model atmosphere above the sensor's surface. The reaction mechanism, also

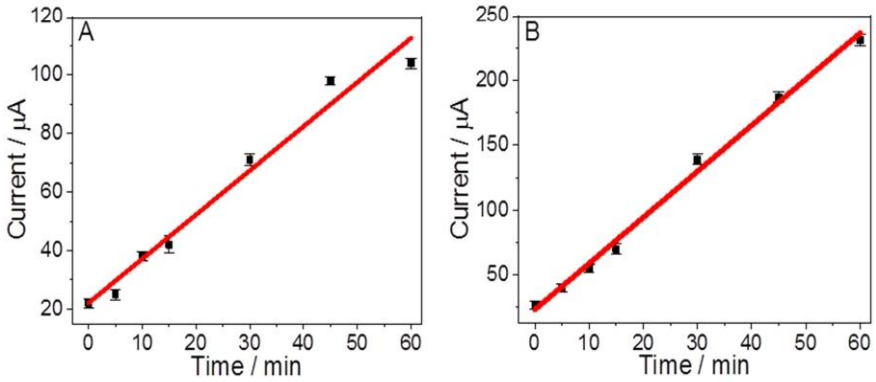

Fig. 2. Effect of the accumulation time upon the signal of 15 mg m^{-3} H_2O_2 in the range of 0–60 min obtained at the MnO_2/PAA (A) and PAA (B) sensor (seven different sensors were used per time point). Other conditions are as in Fig. 1.

proposed by other studies of MnO_2 species [40,41], can be explained as: in the presence of H_2O_2, the MnO_2 is chemically (in addition to electrochemical reduction) reduced from Mn(IV) to Mn(II,III) (Eq. (1)); thus, the following electrochemical re-oxidation exhibits an increased signal during the potential scan in anodic direction, according to Eq. (2):

Chemical reaction: $MnO_2(IV) + H_2O_2 \rightarrow MnO(II)$ or $Mn_2O_3(III) + H_2O + O_2$ (1)

Electrochemical re-oxidation reaction: $MnO(II)$ or Mn_2O_3 $(III) \rightarrow MnO_2(IV) + 2e^-$ (2)

On the other hand, the PAA sensor, i.e., the one without deposited MnO_2, does not exhibit any visible redox signals in the absence of H_2O_2, except an increased current due to commencement of water oxidation reaction at more positive potentials, similarly as in the case of the MnO_2/PAA sensor. However, in the presence of 90 mg m^{-3} H_2O_2, a substantial increase of the anodic current (starting at ca. + 0.5 V) was recorded, which corresponds to the oxidation of H_2O_2, as demonstrated in Fig. 1B (curve b). It is evident that the viscous polyacrylic-acid-based sensing membrane enables an efficient accumulation of gaseous H_2O_2, and at the same time, acts as a suitable electrolyte for electrochemical measurements.

The following study involved transferring the sensor after a 12-minute accumulation period from the H_2O_2-containing atmosphere (15 mg m^{-3}) to the H_2O_2-free atmosphere, followed by continuous cycling voltammetric measurements (100 cycles). It was shown that both sensors maintained constant cyclic voltammetric signals after ca. first 20 cycles, and then the signal started to gradually attenuate during further potential scans; however, the shape of the voltammetric signals was not affected considerably. Moreover, the PAA sensor exhibited somewhat better stability with practically unchanged responses during the first twenty cycles (Fig. S2). This signal diminution is expected and can be attributed to the decomposition of H_2O_2 at the ambient conditions and/or decrease of its concentration with successive measurement cycles due to a very confined cell volume of 50 μL (vs. relatively large electrode surface of 12.6 mm^2). Nevertheless, even after 100 cycles, the sensor still exhibited a weak signal of H_2O_2, thus corroborating the suitability of the polyacrylic-acid-based sensing membrane as an electrolyte and H_2O_2 accumulation medium. At the same time, it is apparent that the sensor enables even longer exposures/accumulation times under ambient conditions, thus assuring a further increase in sensitivity, if necessary. However, after exposing the sensor to ambient air for more than ca. 60 min, the sensor started to exhibit poorer performance that might be attributed to the drying of the sensor surface.

3.2. Electroanalytical performance

Aimed at obtaining more insights into the electroanalytical characteristics of both gas sensor types, we studied the effect of the

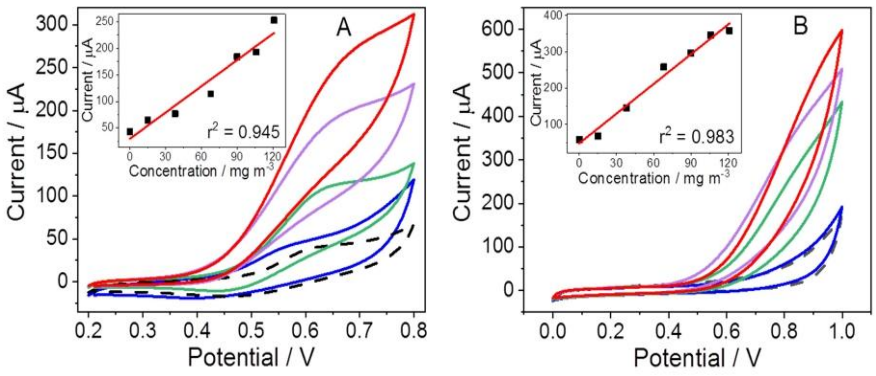

Fig. 3. Cyclic voltammograms obtained at the MnO_2/PAA (A) and PAA (B) sensors for successive increments of gaseous H_2O_2 concentrations in the range of 15–121 mg m^{-3} (voltammograms for 15, 68, 106, and 121 mg m^{-3} are shown) together with a background response (dashed line). Each measurement was carried out with a newly prepared sensor. The insets show the corresponding calibration plots. Other conditions are as in Fig. 1.

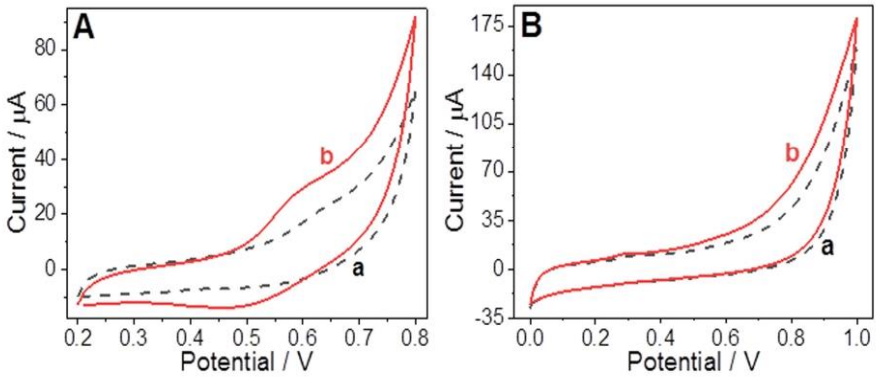

Fig. 4. Cyclic voltammograms obtained at the (A) MnO_2/PAA sensor for background (a) and 20 µg m^{-3} gaseous H_2O_2 (b), and (B) PAA sensor for background (a) and 10 µg m^{-3} gaseous H_2O_2 (b), using an accumulation time of 40 min. Scan rate: 100 mV s^{-1}.

accumulation time upon the sensors' voltammetric responses. This study was carried out using an H_2O_2 concentration of 15 mg m^{-3} (Fig. 2).

The current signal increased linearly with increasing accumulation time in the examined range of 0–60 min for both gas sensors. As can be seen, the signals obtained at the MnO_2/PAA sensor exhibited somewhat lower linearity vs. the PAA sensor, i.e., 0.974 vs. 0.995, respectively, and the response of the MnO_2/PAA sensor started to level off at accumulation times of around 60 min. On the other hand, the PAA sensor showed improved linear time-dependence without any saturation effect, i.e., signal leveling off, observed in the investigated accumulation time range.

We followed the current responses of both gas sensors when increasing the scan rate of cyclic voltammetric measurements, as demonstrated in Fig. S3. In the case of MnO_2/PAA sensor, the current signal exhibited a highly linear dependence on the square-root of the scan rate ($r^2 = 0.999$), implying the diffusion-controlled process. When hydrogen peroxide diffuses to the MnO_2-modified electrode surface, the chemical reaction takes place, followed by a relatively fast electrochemical re-oxidation of the Mn(II) to Mn(IV) at the electrode surface. On the other hand, when investigating the PAA sensor, we observed the trend (current vs. scan rate) that resembles the adsorption-controlled process with the r^2 of 0.993, whereas the r^2 of 0.969 was calculated if considering the diffusion-controlled process. Taking into account a well-known kinetically sluggish and irreversible electrochemical oxidation process of hydrogen peroxide [42,43], we can assume the observed phenomenon as a combination of the diffusion and adsorption-controlled process.

We investigated the performances of both gas sensors regarding their responses for increasing concentrations of gaseous H_2O_2. In combination with an only 12-minute accumulation, both sensors exhibited acceptable linear response in the same examined concentration range of 15–121 mg m^{-3}, with $r^2 = 0.945$ for the MnO_2/PAA sensor and $r^2 = 0.983$ for the PAA sensor (Fig. 3). The deviation from higher linearity might be due to the accumulation/dissolution/diffusion pattern of H_2O_2 in the viscous sensing membrane and partial decomposition of relatively unstable H_2O_2. The potentials at which we sampled the current signals were 0.66 V for the MnO_2/PAA sensor and 0.82 V for the PAA sensor.

Notably, good sensor-to-sensor repeatability was achieved, i.e., for the series of 10 PAA sensors, a relative standard deviation (RSD) was 4.7% when measuring 15 mg m^{-3} gaseous H_2O_2 and using 12-minute accumulation. The repeatability was slightly lower for the MnO_2/PAA sensor, with an RSD of 10.4% under the same experimental conditions. Although the oxidation signal of gaseous H_2O_2 commences at a slightly less positive potential with the MnO_2/PAA sensor (according to Eqs. (1) and (2) above), the PAA sensor offers improved sensitivity, repeatability, and somewhat enhanced linear operation considering both the concentration and time dependence, along with simpler and faster preparation protocol. Moreover, the sensor's response was checked with a confirmatory method (Fig. S4), i.e., with a standardized spectrophotometric protocol, which is described in Supplementary Information.

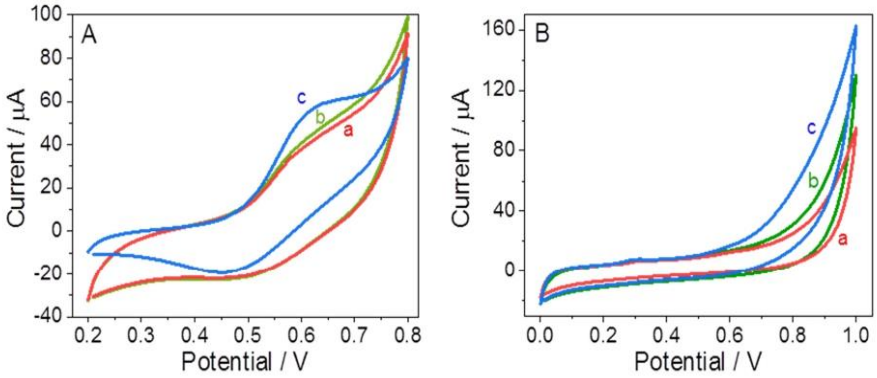

Fig. 5. Cyclic voltammograms obtained at the MnO_2/PAA (A) and PAA sensor (B) for a background (a), in the presence of all five interferences (each 150 mg m^{-3}) (b), and in the presence of all five interferences and 15 mg m^{-3} H_2O_2 (c). Other conditions are as in Fig. 1.

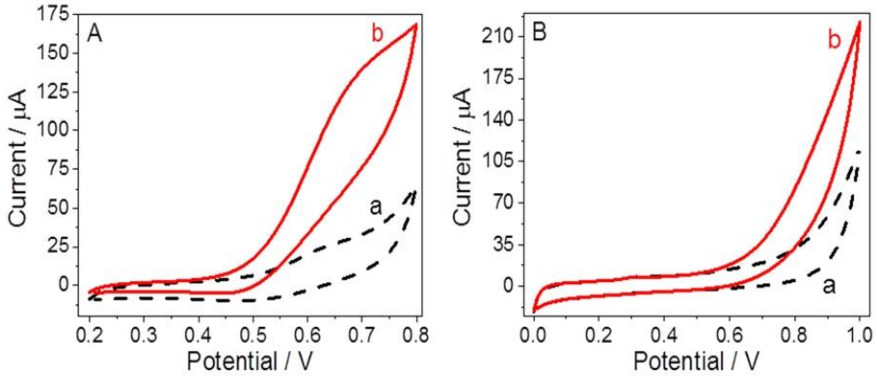

Fig. 6. Cyclic voltammograms obtained at the MnO_2/PAA (A) and PAA (B) sensors for a background (a) and when left for 12 min in a room that was cleaned and disinfected with a 10% H_2O_2 solution. Other conditions are as in Fig. 1.

Both gas sensors were also successfully tested for the detection of even lower H_2O_2 concentration levels. As depicted in Fig. 4, well-defined and readable voltammetric signals could be observed for 20 μg m^{-3} and 10 μg m^{-3} H_2O_2 at the MnO_2/PAA and PAA sensors, respectively, in combination with 40-minute accumulation time. In addition, the calculated limits of detection using the 3σ criterion were 3 μg m^{-3} for the MnO_2/PAA and 2 μg m^{-3} for the PAA sensor; lower limits of detection can be anticipated when using prolonged accumulation times. Since our research focused on the development of gas sensors for rapid H_2O_2 detection, studying the accumulation times over 60 min seemed needless. Moreover, prolonged accumulation times might be accompanied by the negative effect of the H_2O_2 decomposition/oxidation in the sensing membrane. On the other hand, if one needs to measure higher concentrations of H_2O_2, correspondingly shorter accumulation times should be used.

3.3. Interference study

We examined the (in)sensitivity of both gas sensors towards selected interfering gaseous compounds that can be expected in the real environment. The study was carried out by measuring several interferants individually at 150 mg m^{-3} each, followed by the addition of 15 mg m^{-3} H_2O_2. In the absence of H_2O_2, no responses for gaseous methanol, ethanol, formaldehyde, ammonia, and phenol were detected by cyclic voltammetric measurements in the examined potential windows of 0.2–0.8 V for the MnO_2/PAA sensor and 0.0–1.0 V for the PAA sensor (data not shown). Notably, no signal of gaseous phenol was observed under these conditions; the oxidation of phenol is facilitated in an alkaline medium due to the formation of phenolate, whereas in this case, the PAA sensing membrane exhibits acidic pH hindering its oxidation. In the following study, both gas sensors were exposed to a mixture of all these compounds, each of them at a concentration of 150 mg m^{-3} (Fig. 5). In both sets of voltammograms, there was just a slight increase (curve b) of the net signal for all tested compounds representing a total concentration of 750 mg m^{-3}. Moreover, after the addition of only 15 mg m^{-3} H_2O_2, it is evident that the oxidation reaction of H_2O_2 revealed well-defined and readable signals at both gas sensors, as shown in Fig. 5A (curve c) and 5B (curve c). Considering that the concentration of H_2O_2 in the gas phase is 10 times lower than the concentration of each examined interfering compound, we can conclude that both sensors exhibit satisfactory selectivity.

In addition, we also examined the effect of 150 mg m^{-3} $NaNO_2$ (emitting NO and NO_2), 150 mg m^{-3} benzene, 75 mg m^{-3} HNO_3, and pure O_2 upon the sensor's operation (Fig. S5). We observed no readable signals for each of the tested analytes, except in the case of $NaNO_2$, which caused a slight increase in the current signal corresponding to ca. 7 mg m^{-3} gaseous H_2O_2.

3.4. Comparison to other electrochemical H_2O_2 gas sensors

Although there are numerous reports on electrochemical sensors for detecting H_2O_2 in aqueous and non-aqueous media, there are only a few reports on sensors for the detection of gaseous H_2O_2. Thus, the comparison can be made with only a few amperometric/voltammetric sensors and sensors based on chemoresistance. For example, Bontempelli et al. [44] described an amperometric sensor with a deposited porous Pt-electrode on one side of the Nafion membrane, whereas the other, unmodified side of the membrane, faced an internal electrolyte solution in the electrochemical cell. The sensor exhibited the limit of detection of 40 ppbv using an operating potential of 1.0 V; it was reported that a drawback of this sensor might be the selectivity. Wiedemair et al. [45] demonstrated amperometric detection of gaseous H_2O_2 with agarose-coated electrode chips employing a platinum working electrode; the reported limit of detection was 42 ppb. Wang et al. [46] prepared an amperometric sensor based on an agarose-coated Prussian-Blue-modified thick-film carbon electrode exhibiting the limit of detection of 6 ppbv, whereas Dincer et al. [10] demonstrated a paper-based sensor modified with Prussian Blue and pretreated with KCl. The latter sensor was able to measure H_2O_2 in a simulated exhaled breath by providing sufficient humidity; the limit of detection was not reported. There are also reports on chemiresistive H_2O_2 sensors, such as a sensor based on a nanocomposite of a porphyrin derivative (oxo-[5,10,15,20-tetra(4-pyridyl)porphyrinato]titanium(IV)) nanofibers and single-walled carbon nanotubes, operating at room temperature, and revealing the limit of detection of 2 ppb [47], a sensor based on ZnO thin film, which was prepared by spray pyrolysis technique, exhibiting the limit of detection of 10 ppm [48], and a sensor based on platinum nanoparticle-decorated single-walled carbon nanotube networks showing the limit of detection of 27 ppb [49]. This comparison reveals that both gas sensors, which we developed and characterized herein, are undoubtedly competitive and even superior, considering both the overall electroanalytical performances and the ease of preparation.

3.5. Detection of gaseous H_2O_2 in the real environment

Finally, we tested both gas sensors in the real environment, i.e., in a room that was disinfected with a 10% H_2O_2 solution. After measuring the background (before cleaning/disinfecting), the sensors were placed in the disinfected room for 12 min, and then cyclic voltammograms were recorded, as demonstrated in Fig. 6. Both gas sensors showed well-

defined signals for gaseous H_2O_2; after three successive measurements carried out at each sensor, an average concentration of gaseous H_2O_2 was ca. 37 mg m^{-3}.

4. Conclusions

We developed, characterized, and compared two types of sensors for measuring gaseous H_2O_2, which were designed using a viscous polyacrylic-acid-based (PAA) sensing membrane deposited onto the commercial supporting screen-printed electrodes. One type of sensor involves only a PAA sensing membrane (PAA sensor), whereas the other one's working electrode is electrochemically pre-modified with MnO_2 (MnO_2/PAA sensor). Both sensors revealed excellent sensitivity in the low mg m^{-3} concentration range with the limits of detection of 3 μg m^{-3} (MnO_2/PAA) and 2 μg m^{-3} (PAA), favorable operation in the presence of selected interfering gaseous compounds, and were successfully tested in the real environment. In addition, the comprehensive study showed a superior electroanalytical behavior of the PAA sensor, which is also simpler and faster to prepare. This approach provides a solid foundation for further development of sensitive, selective, and robust gas sensing systems that could find their application in several fields, such as environmental monitoring, preservation of cultural heritage, clinical diagnostics (breath analysis), reduction of occupational health hazards, and security screening applications.

CRediT authorship contribution statement

Jelena Isailović: Conceptualization, Methodology, Investigation, Data evaluation, Formal analysis, Visualization, Writing – original draft. **Kristijan Vidović:** Conceptualization, Methodology, Writing – original draft. **Samo B. Hočevar:** Funding acquisition, Conceptualization, Methodology, Supervision, Writing – review & editing.

Declaration of Competing Interest

The authors declare that they have no known competing financial interests or personal relationships that could have appeared to influence the work reported in this paper.

Acknowledgments

This research received funding from the Slovenian Research Agency (Research Program P1-0034) and the Slovenian Research Agency's Young Researchers Programme (grant agreement No. 52020).

Appendix A. Supporting information

Supplementary data associated with this article can be found in the online version at doi:10.1016/j.snb.2021.131053.

References

[1] R. Zhang, W. Chen, Recent advances in graphene-based nanomaterials for fabricating electrochemical hydrogen peroxide sensors, Biosens. Bioelectron. 89 (2017) 249–268.
[2] W. Chen, S. Cai, Q.Q. Ren, W. Wena, Y.D. Zhao, Recent advances in electrochemical sensing for hydrogen peroxide: a review, Analyst 137 (2012) 49–58.
[3] M. Giorgio, M. Trinei, E. Migliaccio, P.G. Pelicci, Hydrogen peroxide: a metabolic by-product or a common mediator of ageing signals? Nat. Rev. Mol. Cell Biol. 8 (2007) 722–728.
[4] E.A. Veal, A.M. Day, B.A. Morgan, Hydrogen peroxide sensing and signaling, Mol. Cell 26 (2007) 1–14.
[5] H. Sies, Hydrogen peroxide as a central redox signaling molecule in physiological oxidative stress: oxidative eustress, Redox Biol. 11 (2017) 613–619.
[6] N. Di Marzo, E. Chisci, R. Giovannoni, The role of hydrogen peroxide in redox-dependent signaling: homeostatic and pathological responses in mammalian cells, Cells 7 (2018) 156.
[7] M. Zhou, Y. Liu, Y. Duan, Breath biomarkers in diagnosis of pulmonary diseases, Clin. Chim. Acta 413 (2012) 1770–1780.
[8] S. Svensson, A.C. Olin, M. Lärstad, G. Ljungkvist, K. Torén, Determination of hydrogen peroxide in exhaled breath condensate by flow injection analysis with fluorescence detection, J. Chromatogr. B 809 (2004) 199–203.
[9] B. Zappacosta, S. Persichilli, F. Mormile, A. Minucci, A. Russo, B. Giardina, P. D. Sole, A fast chemiluminescent method for H_2O_2 measurement in exhaled breath condensate, Clin. Chim. Acta 310 (2001) 187–191.
[10] D. Maier, E. Laubender, A. Basavanna, S. Schumann, F. Güder, G.A. Urban, C. Dincer, Toward continuous monitoring of breath biochemistry: a paper-based wearable sensor for real-time hydrogen peroxide measurement in simulated breath, ACS Sens. 4 (2019) 2945–2951.
[11] R. Stolarek, P. Bialasiewicz, M. Krol, D. Nowak, Breath analysis of hydrogen peroxide as a diagnostic tool, Clin. Chim. Acta 411 (2010) 1849–1861.
[12] D. Vione, V. Maurino, C. Minero, E. Pelizzetti, The atmospheric chemistry of hydrogen peroxide: a review, Ann. Chim. 93 (2003) 477–488.
[13] J.S. Caygill, F. Davis, S.P.J. Higson, Current trends in explosive detection techniques, Talanta 88 (2012) 14–29.
[14] R.M. Burks, D.S. Hage, Current trends in the detection of peroxide-based explosives, Anal. Bioanal. Chem. 395 (2009) 301–313.
[15] J. Wang, Electrochemical sensing of explosives, Electroanal 19 (2007) 415–423.
[16] K. Wang, D.K. Liua, P.P. Wua, X.B. Yu, L.J. Cheng, J.G. Zhang, How hydrogen-storage material affects the decomposition of nitramine explosive: CPMD investigations of LAB-doped CL20, Int. J. Hydrogen Energy 43 (2018) 19825–19840.
[17] A. Üzer, E. Erçağ, R. Apak, Spectrophotometric determination of cyclotrimethylenetrinitramine (RDX) in explosive mixtures and residues with the Berthelot reaction, Anal. Chim. Acta 612 (2008) 53–64.
[18] N.R. Schneider, S.L. Bradley, M.E. Andersen, Toxicology of cyclotrimethylenetrinitramine: distribution and metabolism in the rat and the miniature swine, Toxicol. Appl. Pharmacol. 39 (1977) 531–541.
[19] J.G. Hong, J. Maguhn, D. Freitag, A. Kettrup, Determination of H_2O_2 and organic peroxides by high-performance liquid chromatography with post-column UV irradiation, derivatization and fluorescence detection, Fresen. J. Anal. Chem. 361 (1998) 124–128.
[20] K.B.R. Teodoro, F.L. Migliorini, W.A. Christinelli, D.S. Correa, Detection of hydrogen peroxide (H_2O_2) using a colorimetric sensor based on cellulose nanowhiskers and silver nanoparticles, Carbohydr. Polym. 212 (2019) 235–241.
[21] J. Yuan, A.M. Shiller, Determination of subnanomolar levels of hydrogen peroxide in seawater by reagent-injection chemiluminescence detection, Anal. Chem. 71 (1999) 1975–1980.
[22] Y. Ling, N. Zhang, F. Qu, T. Wen, Z.F. Gao, N.B. Li, H.Q. Luo, Fluorescent detection of hydrogen peroxide and glucose with polyethyleneimine-templated Cu nanoclusters, Spectrochim. Acta A 118 (2014) 315–320.
[23] A.L. Sanford, S.W. Morton, K.L. Whitehouse, H.M. Oara, L.Z. Lugo-Morales, J. G. Roberts, L.A. Sombers, Voltammetric detection of hydrogen peroxide at carbon fiber microelectrodes, Anal. Chem. 82 (2010) 5205–5210.
[24] C.M. Welch, C.E. Banks, A.O. Simm, R.G. Compton, Silver nanoparticle assemblies supported on glassy-carbon electrodes for the electro-analytical detection of hydrogen peroxide, Anal. Bioanal. Chem. 382 (2005) 12–21.
[25] J. Ju, W. Chen, In situ growth of surfactant-free gold nanoparticles on nitrogen-doped graphene quantum dots for electrochemical detection of hydrogen peroxide in biological environments, Anal. Chem. 87 (2015) 1903–1910.
[26] S. Chen, R. Yuan, Y. Chai, F. Hu, Electrochemical sensing of hydrogen peroxide using metal nanoparticles: a review, Microchim. Acta 180 (2013) 15–32.
[27] J. Sophia, G. Muralidharan, Preparation of vinyl polymer stabilized silver nanospheres for electro-analytical determination of H_2O_2, Sens. Actuators B-Chem. 193 (2014) 149–156.
[28] I. Katsounaros, J.C. Meier, K.J.J. Mayrhofer, The impact of chloride ions and the catalyst loading on the reduction of H_2O_2 on high-surface-area platinum catalysts, Electrochim. Acta 110 (2013) 790–795.
[29] T.A. Ivandini, R. Sato, Y. Makide, A. Fujishima, Y. Einaga, Pt-implanted boron-doped diamond electrodes and the application for electrochemical detection of hydrogen peroxide, Diam. Relat. Mater. 14 (2005) 2133–2138.
[30] C. Camacho, J.C. Matías, B. Chico, R. Cao, L. Gómez, B.K. Simpson, R. Villalonga, Amperometric biosensor for hydrogen peroxide, using supramolecularly immobilized horseradish peroxidase on the β-cyclodextrin-coated gold electrode, Electroanal 19 (2007) 2538–2542.
[31] C. Chen, X. Hong, T. Xu, A. Chen, L. Lu, Y. Gao, Hydrogen peroxide biosensor based on the immobilization of horseradish peroxidase onto a poly(aniline-co-N-methylthionine) film, Synth. Met. 212 (2016) 123–130.
[32] A. Salimi, R. Hallaj, S. Soltanian, H. Mamkhezri, Nanomolar detection of hydrogen peroxide on glassy carbon electrode modified with electrodeposited cobalt oxide nanoparticles, Anal. Chim. Acta 594 (2007) 24–31.
[33] B. Šljukić, C.E. Banks, R.G. Compton, An overview of the electrochemical reduction of oxygen at carbon-based modified electrodes, J. Iran. Chem. Soc. 2 (2005) 1–25.
[34] N. Yang, G.M. Swain, X. Jiang, Nanocarbon electrochemistry and electroanalysis: current status and future perspectives, Electroanal 28 (2016) 27–34.
[35] L. Song-Qin, J. Huang-Xian, Renewable reagentless hydrogen peroxide sensor based on direct electron transfer of horseradish peroxidase immobilized on colloidal gold-modified electrode, Anal. Biochem. 307 (2002) 110–116.
[36] H. Shih-Hung, L. Hsiu-Hsien, C. Dong-Hwang, Simultaneous determination of norepinephrine, uric acid, and ascorbic acid at a screen printed carbon electrode modified with polyacrylic acid-coated multi-wall carbon nanotubes, Biosens. Bioelectron. 25 (2010) 2351–2355.
[37] S. Kuwata, Y. Sadaoka, Detection of gaseous hydrogen peroxide using planar-type amperometric cell at room temperature, Sens. Actuators B-Chem. 65 (2000) 325–326.

[38] H. Huang, P.K. Dasgupta, Z. Genfa, J. Wang, A pulse amperometric sensor for the measurement of atmospheric hydrogen peroxide, Anal. Chem. 68 (1996) 2062–2066.
[39] R. Sander, Compilation of Henry's law constants (version 4.0) for water as solvent, Atmos. Chem. Phys. 15 (2015) 4399–4981.
[40] L. Wen-Zhi, L. You-Qin, H. Guang-Qi, Preparation of manganese dioxide modified glassy carbon electrode by a novel film plating/cycling voltammetry method for H_2O_2 detection, J. Chil. Chem. Soc. 54 (2009) 366–371.
[41] L. Limiao, D. Zhifeng, L. Shuang, H. Quanyi, W. Yanguo, L. Qiuhong, W. Taihong, A novel nonenzymatic hydrogen peroxide sensor based on MnO_2/graphene oxide nanocomposite, Talanta 82 (2010) 1637–1641.
[42] R. Gulaboski, V. Mirčeski, R. Kappl, M. Hoth, M. Bozem, Review—quantification of hydrogen peroxide by electrochemical methods and electron spin resonance spectroscopy, J. Electrochem. Soc. 166 (2019) 82–101.
[43] A.L. Sanford, S.W. Morton, K.L. Whitehouse, H.M. Oara, L.Z. Lugo-Morales, J. G. Roberts, L.A. Sombers, Voltammetric detection of hydrogen peroxide at carbon fiber microelectrodes, Anal. Chem. 82 (2010) 5205–5210.
[44] R. Toniolo, P. Geatti, G. Bontempelli, G. Schiavon, Amperometric monitoring of hydrogen peroxide in workplace atmospheres by electrodes supported on ion-exchange membranes, J. Electroanal. Chem. 514 (2001) 123–128.
[45] J. Wiedemair, H.D.S. van Dorp, W. Olthuis, A. van den Berg, Developing an amperometric hydrogenperoxide sensor for an exhaled breathanalysis system, Electrophoresis 33 (2012) 3181–3186.
[46] J. Benedet, D. Lu, K. Cizek, J.L. Belle, J. Wang, Amperometric sensing of hydrogen peroxide vapor for security screening, Anal. Bioanal. Chem. 395 (2009) 371–376.
[47] J.S. Leea, D.W. Jeongb, Y.T. Byun, Porphyrin nanofiber/single-walled carbon nanotube nanocomposite-based sensors for monitoring hydrogen peroxide vapor, Sens. Actuators B-Chem. 306 (2020), 127518.
[48] S. Parthasarathy, V. Nandhini, B.G. Jeyaprakash, Improved sensing response of photo activated ZnO thin film for hydrogen peroxide detection, J. Colloid Interfaces Sci. 482 (2016) 81–88.
[49] D.J. Lee, S.W. Choi, Y.T. Byun, Room temperature monitoring of hydrogen peroxide vapor using platinum nanoparticles-decorated single-walled carbon nanotube networks, Sens. Actuators B-Chem. 256 (2018) 744–750.

Jelena Isailović is a Ph.D. student of Sensor Technologies at the Jožef Stefan International Postgraduate School in Ljubljana. She carries out the research work at the Department of Analytical Chemistry, National Institute of Chemistry.

Dr. Kristijan Vidović received a Ph.D. in Chemistry in 2020 from the Faculty of Chemistry and Chemical Technology, University of Ljubljana, Slovenia. Presently, he works as a researcher at the Department of Analytical Chemistry at the National Institute of Chemistry in Ljubljana. His research interests include the studies of atmospheric reactions/processes and electrochemical detection of gaseous pollutants.

Dr. Samo B. Hočevar received a Ph.D. in Analytical Chemistry in 2002 from the Faculty of Chemistry and Chemical Technology, University of Ljubljana, Slovenia. Presently, he is the Head of the Department of Analytical Chemistry at the National Institute of Chemistry in Ljubljana. His research interests include the development, study, miniaturization, and application of advanced electrochemical sensors, gas sensors, and biosensors.

SUPPLEMENTARY INFORMATION FOR THE MANUSCRIPT:

Simple electrochemical sensors for highly sensitive detection of gaseous hydrogen peroxide using polyacrylic-acid-based sensing membrane

Jelena Isailović[a,b], Kristijan Vidović[a], Samo B. Hočevar[a,*]

[a]*Department of Analytical Chemistry, National Institute of Chemistry, Hajdrihova 19, Ljubljana, Slovenia*

[b]*Jožef Stefan International Postgraduate School, Jamova cesta 39, Ljubljana, Slovenia*

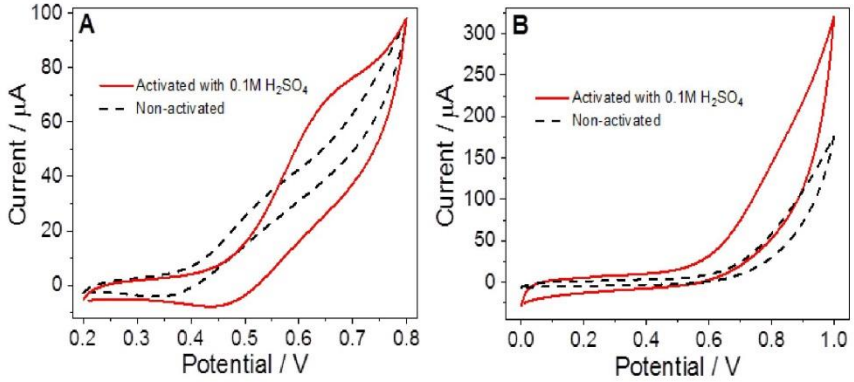

Figure S1. Cyclic voltammograms obtained at the MnO_2/PAA (A) and PAA (B) gas sensors for 50 mg m^{-3} H_2O_2 using non-activated (dashed line) and activated (solid line) supporting screen-printed electrodes. Accumulation time: 15 min; scan rate: 100 mV s^{-1}.

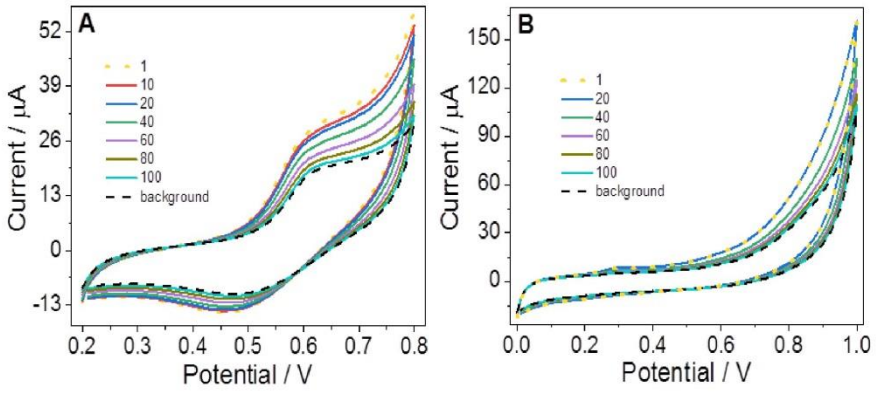

Figure S2. Cyclic voltammograms obtained at the MnO_2/PAA (A) and PAA (B) gas sensors for repetitive measurements of 15 mg m^{-3} H_2O_2. Accumulation time: 12 min; scan rate: 100 mV s^{-1}.

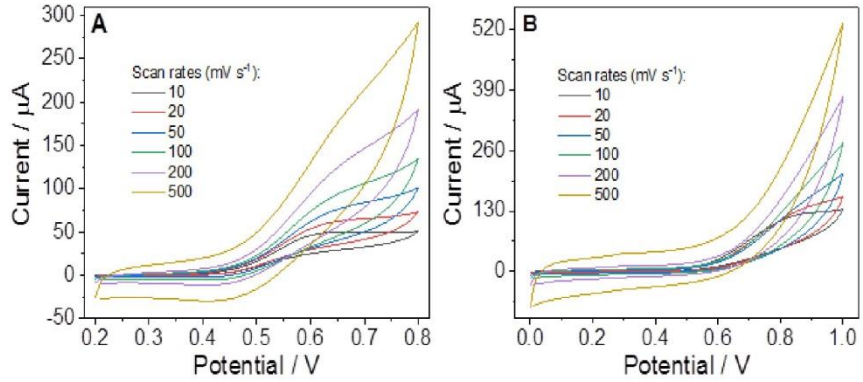

Figure S3. Cyclic voltammograms obtained at the MnO_2/PAA (A) and PAA sensor (B) for increasing scan rates. Accumulation time: 15 min; c(H_2O_2) = 50 mg m^{-3}.

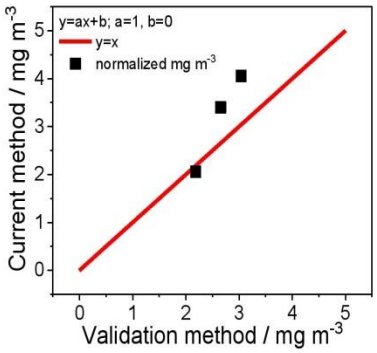

Figure S4. Validation of the electrochemical sensor with a standardized spectrophotometric method. Spectrophotometric method: reduced phenolphthalein in the presence of $CuSO_4x5H_2O$; impinger sampling flow rate of 0.5 L min^{-1} for 5 minutes; extinction measurement at 550 nm. Our electrochemical sensor: accumulation time: 12 min; scan rate: 100 mV s^{-1}.

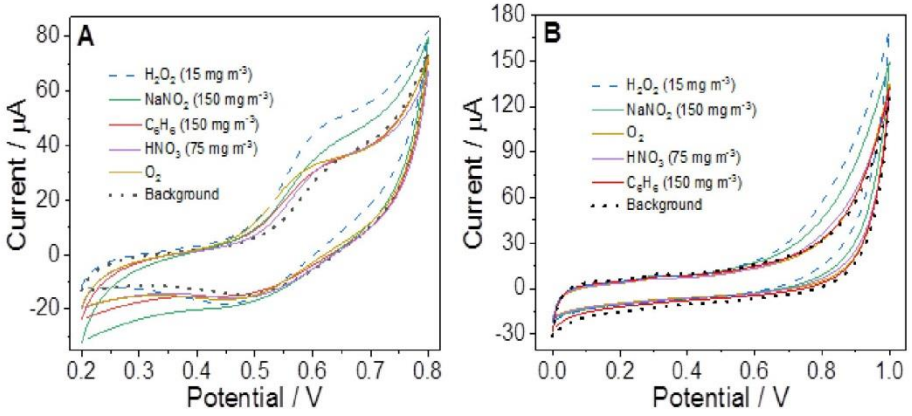

Figure S5. Cyclic voltammograms obtained at the MnO_2/PAA (A) and PAA sensor (B) for a background (dotted line), in the presence of four interferences, and in the presence of 15 mg m^{-3} H_2O_2 (dashed line). Accumulation time: 12 min; scan rate: 100 mV s^{-1}.

3.2 Manuscript 2: "Study of Chitosan-Stabilized $Ti_3C_2T_x$ MXene for Ultrasensitive and Interference-Free Detection of Gaseous H_2O_2"

Published – ACS Applied Materials & Interfaces

In this segment of the dissertation, our aim was to further explore the possibilities for the development of sensitive and selective H_2O_2 gas sensor through a different approach. This includes, among others, the incorporation of a particular material, such as MXenes, without the need for prior activation. After a thorough investigation, we determined that $Ti_3C_2T_x$ MXene was the optimal choice as the electrocatalytic modification layer deposited directly on the ferrocyanide-modified screen-printed carbon electrode surface.

During experimental work, we encountered a challenge regarding the physical/chemical/electrochemical stability of the MXenes, particularly considering their oxidation. To overcome this issue, we introduced a stabilization layer on top of the MXene, utilizing a modification mixture involving chitosan.

Furthermore, we examined the stability and durability of the sensor itself. The sensor was subjected to different storage conditions, including varying storage temperature and humidity levels, overnight in model environments such as the laboratory, refrigerator, and desiccator. Although the sensor exhibited consistent performance across all storage units, a slightly enhanced performance was observed when stored in the desiccator, characterized by low humidity levels and minimal temperature fluctuations. Such a stable environment can assist in minimizing the potential hydrolytic damage and changes in the physicochemical properties of chitosan, which is a component for immobilizing and stabilizing the MXene layer being crucial for assuring sensor's high electroanalytical performance.

Additionally, the sensor's architecture involved a redox pair ($Fe(CN)_6^{4-}/Fe(CN)_6^{3-}$) embedded in the screen-printed carbon electrode playing a vital role in the reduction/detection of H_2O_2. This feature enabled the sensor to operate in the cathodic potential region, thus additionally improve its interference-free operation in comparison with the previous work. The newly developed sensing platform, incorporating all these elements, resulted in an excellent electroanalytical operation considering very low detection limits, good reproducibility, selectivity, and the ability to detect H_2O_2 in a real environment, as demonstrated during the real hair bleaching process.

ACS APPLIED MATERIALS & INTERFACES

www.acsami.org Research Article

Study of Chitosan-Stabilized $Ti_3C_2T_x$ MXene for Ultrasensitive and Interference-Free Detection of Gaseous H_2O_2

Jelena Isailović, Ana Oberlintner, Uroš Novak, Matjaž Finšgar, Filipa M. Oliveira, Jan Paštika, Zdeněk Sofer, Nikola Tasić, Rui Gusmão,* and Samo B. Hočevar*

Cite This: https://doi.org/10.1021/acsami.3c05314 Read Online

ACCESS | Metrics & More | Article Recommendations | Supporting Information

ABSTRACT: The development of sensitive, selective, and reliable gaseous hydrogen peroxide (H_2O_2) sensors operating at room temperature still represents a remaining challenge. In this work, we have investigated and combined the advantageous properties of a two-dimensional $Ti_3C_2T_x$ MXene material that exhibits a large specific surface area and high surface activity, with favorable conducting and stabilizing properties of chitosan. The MXene–chitosan membrane was deposited on the ferrocyanide-modified screen-printed working carbon electrode, followed by applying poly(acrylic acid) as an electrolyte and accumulation medium for gaseous H_2O_2. The sensor showed highly sensitive and selective electroanalytical performance for detecting trace concentrations of gaseous H_2O_2 with a very low detection limit of 4 μg m^{-3} (4 ppbv), linear response in the studied concentration range of 0.5−30.0 mg m^{-3}, and good reproducibility with an RSD of 1.3%. The applicability of the sensor was demonstrated by point-of-interest detection of gaseous H_2O_2 during the real hair bleaching process with a 9 and 12% H_2O_2 solution.

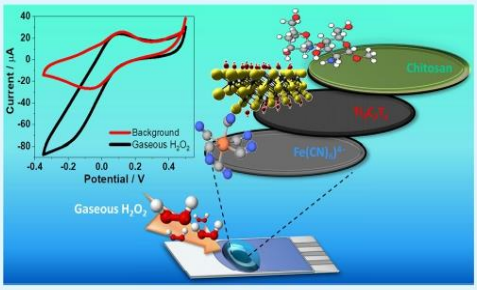

KEYWORDS: *$Ti_3C_2T_x$ MXene, chitosan, hydrogen peroxide, gas sensor, cyclic voltammetry*

INTRODUCTION

In recent years, MXenes have attracted immense attention due to their high metallic conductivity, hydrophilicity, low diffusion barrier, high ion transport properties, biocompatibility, large surface area, and ease of functionalization and thus can serve as a remarkable interface for the development of next-generation sensing strategies.[1−4] This novel class of two-dimensional (2D)-layered materials consists of transition metal carbides or nitrides, with the general formula $M_{n+1}X_nT_x$, where M stands for the transition metal (e.g., Ti, Zr, V, Cr, Nb), X is carbon or nitrogen, and T corresponds to different terminal groups, e.g., O, F, OH, and Cl.[3] Etching of A elements in the MAX phase (A is a p-block element) yields the designated MXenes, as introduced by Gogotsi et al.[5] To date, more than twenty different MXene compounds have been successfully synthesized from the precursor MAX phases by etching and exfoliation methods,[3,6,7] resulting in surface-functionalized MXenes with abundant terminal groups that account for their hydrophilic nature. As such, MXenes can selectively absorb biomolecules and gas molecules through morphology control and surface modification.[8−10] The drawback is that MXenes are highly susceptible to oxidative degradation, leading to impaired functionality and inefficacy. Research efforts related to the specifics of synthesis protocols, storage conditions, or storage media appear to offer some comfort regarding their stability during preparative steps.[11,12] However, for electroanalytical applications, when MXenes are incorporated on the supporting electrodes and subjected to measurements in wide potential windows, an additional application obstacle arises from their innate and irreversible electrooxidation.[13] The existing literature does not yet offer a convincing solution to this problem, which was also addressed in this study.

H_2O_2 is an important molecule that plays a vital role in various fields, such as medicine, clinical diagnostics, biotechnology, chemical synthesis, textile, wood, food, and pharmaceutical industries in the production of cosmetics, dyes, detergents, etc.[14−17] Besides its main property as an oxidant, H_2O_2 is a key molecule in numerous biological systems involving the enzymatic activity of, e.g., oxidases and peroxidases.[18] It is essential as a signaling molecule in the biological processes of the immune system, apoptosis, and root growth.[19,20] As a biomarker, H_2O_2 is associated with oxidative

Received: April 13, 2023
Accepted: June 13, 2023

https://doi.org/10.1021/acsami.3c05314
ACS Appl. Mater. Interfaces XXXX, XXX, XXX−XXX

stress[21,22] and, as a gaseous molecule, with several diseases such as lung cancer and other pulmonary disorders.[23−27] In atmospheric processes, gaseous H_2O_2 accompanies reactions involving UV radiation, free radicals, and the transformation of gaseous pollutants. Its occurrence may also indicate the presence of relatively labile peroxo-explosives.[28] Conventional analytical methods typically used for the determination of H_2O_2 include spectroscopy,[29−31] chemiluminescence,[24,32−34] colorimetry,[35] fluorimetry,[36] gas chromatography−mass spectrometry (GC−MS),[37] and others.[38,39] Most of these techniques can achieve satisfactory detection limits, sensitivity, and selectivity; however, expensive and robust equipment, limited portability, and relatively complex sample preparation are persistent challenges that must be overcome. On the other hand, electrochemical sensing offers an attractive alternative to conventional methods, especially in terms of low-cost and compact instrumentation, portability, capability for point-of-interest detection, sensitivity, and relative ease of operation.[40] Many powerful electrochemical sensors have been developed for the detection of H_2O_2 in liquid samples, incorporating numerous redox modifiers, metal, metal oxide, and nonmetallic nanoparticles, enzymes, polymeric membranes, and combinations thereof.[41,42] However, to the best of our knowledge, there are very few reports of electrochemical sensors for detecting considerably more challenging gaseous H_2O_2.[43−48]

In this work, we have investigated the integration of $Ti_3C_2T_x$ MXene into the sensing membrane to construct a disposable, ultrasensitive, and interference-free electrochemical sensor for onsite detection of gaseous H_2O_2. Moreover, through a synergistic effect between $Ti_3C_2T_x$ MXene and chitosan membrane, we successfully stabilized the 2D-layered MXene. We exploited the electrocatalytic characteristics of MXene by combining it with a ferrocyanide-modified working carbon electrode and poly(acrylic acid), the latter simultaneously serving as a suitable accumulation and electrolyte medium for gaseous H_2O_2. We characterized the sensing interface, including the interaction between chitosan and MXene and the stabilization of MXene.

■ EXPERIMENTAL SECTION

Apparatus. Electrochemical studies were carried out using a portable potentiostat/galvanostat PalmSens4 (PalmSens BV, Houten, Netherlands) in combination with a cable connector for screen-printed electrodes (DRP-CAC 71606, Metrohm DropSens, Herisau, Switzerland) and PSTrace 5.9 software (PalmSens BV). The supporting screen-printed electrode system consisted of a ferrocyanide-bulk-modified carbon working electrode (FCN-SPCE, the diameter of the working electrode was 4 mm), a silver quasi-reference electrode, and a carbon counter electrode (DRP-F10, Metrohm DropSens) designed to work with microvolume solution droplets.

Reagents and Solutions. Methanol (VWR International, Radnor, Pennsylvania), ethanol, benzene (Carlo Erba Reagents, Milano, Italy), H_2O_2 (30%), ammonia, formaldehyde, nitric acid (65%), glycerol, sulfuric acid (95−98%) (all from Merck, Rahway, New Jersey), phenol, high-molecular-weight chitosan (310−375 kDa; ≥75% deacetylated), lactic acid (85%), and sodium nitrite (97%) (all from Sigma-Aldrich, St. Louis, Missouri) were of the analytical grade purity. Pure O_2 (N5.0) was purchased from Messer (Frankfurt, Germany). The chitosan blend (CHI) was prepared as follows: 1.5% (w/v) chitosan and 30.0% (w/w) glycerol were dissolved in 100.0 mL of 1.0% (v/v) aqueous solution of lactic acid, and the mixture was continuously stirred (Ika, Staufen, Germany) overnight at room temperature (24 °C), as reported previously.[49] Test solutions yielding the desired gaseous-phase H_2O_2 concentrations above the solution were prepared in 100.0 mL glass flasks according to Henry's law[50] in the presence of the ambient atmosphere, i.e., no purging was applied. The corresponding Henry constants were given in ref 50. All solutions used in this work were prepared using water purified with the Elix 10/Milli-Q Gradient unit (Millipore, Bedford).

Synthesis and Characterization of the $Ti_3C_2T_x$ MXene. For MXene synthesis, 5.0 g of Ti_3AlC_2 MAX phase material (Jinzhou Haixin Metal Materials, China) was immersed in 250.0 mL of hydrofluoric acid solution (Sigma-Aldrich) with 40.0 vol % and stirred continuously for four days. Then, the sample was stirred for two days in lithium fluoride/hydrochloric acid. Finally, the sample was subjected to iterative cycles of centrifugation and redispersement in water until obtaining a neutral pH value in the residual water. The obtained sample was dried for 24 h in a vacuum oven set at 50 °C.

The morphology of $Ti_3C_2T_x$ MXene was examined by scanning electron microscopy (SEM) with a field emission gun (FEG) electron source (Tescan Lyra dual-beam microscope) at 5 kV acceleration voltage. Elemental composition was investigated by energy-dispersive X-ray spectroscopy (EDXS) using an X-Max^N detector from Oxford Instruments at 20 kV acceleration voltage. For both SEM and EDXS analyses, the colloidal suspension of $Ti_3C_2T_x$ MXene was drop-cast on carbon tape. STEM was performed with the same instrument as SEM but with a STEM sample holder. Diluted suspension of Mxene was drop-cast on a 200 mesh Cu TEM grid and then dried. STEM measurements were carried out using a 30 kV electron beam.

X-ray diffraction (XRD) measurements were carried out using a Bruker D8 Discoverer (Bruker, Germany) diffractometer in Bragg−Brentano parfocal geometry equipped with a Cu Kα radiation source (λ = 0.15418 nm, U = 40 kV, and I = 40 mA). The diffraction pattern was acquired in the scan range of 2θ from 5 to 70° at room temperature. The data were evaluated by HighScore Plus 4.9 software. For the sample preparation, 3.0 μL of a colloidal suspension of $Ti_3C_2T_x$ MXene was drop-cast on a Si/SiO_2 substrate, followed by evaporation of the solvent at room temperature.

An InVia Raman microscope (Renishaw, England) was used for Raman spectroscopy measurements in backscattering geometry with a CCD detector. An Nd:YAG laser (532 nm, 50 mW) with a 2400 line mm^{-1} diffraction grating, an applied power of 1.25%, and a 20x objective were used for the measurements. The Raman spectrum was collected with 200 accumulations in the Raman range of 100−800 cm^{-1} at room temperature. For the sample preparation, the same procedure was used as in the case of XRD measurements.

Atomic force microscopy (AFM) measurements were carried out on a Ntegra Spectra from NT-MDT in a tapping mode using a cantilever with a strain constant of 1.5 kN m^{-1} equipped with a standard silicon tip with a curvature radius less than 10 nm. Sample suspensions of exfoliated material were prepared and drop-cast on a freshly cleaved mica substrate. The measurements were carried out under ambient conditions with a scan rate of 1 Hz and 512 scan lines.

Modification of the Working Electrode and Fabrication of the Sensor. The working electrode was first modified with $Ti_3C_2T_x$ MXene. Before the modification, the MXene solution was sonicated and stirred for 3 min, followed by drop-casting 1.0 μL of the 250.0 mg mL^{-1} solution on the surface of the FCN-SPCE. After drying in air for 10 min, an 8.0 μL droplet of chitosan blend (CHI, from the Reagents and Solutions section) was applied to the working electrode, i.e., on the top of the MXene layer. After drying under laboratory conditions overnight, the whole screen-printed electrode system was modified via drop-casting 20.0 μL of a viscous mixture consisting of 1.0 g of polyacrylic acid (450.000 g mol^{-1}; Sigma-Aldrich) and 10.0 mL of 0.1 M phosphate buffer solution (pH = 7.2), resulting in a polyacrylic gel-like accumulation/electrolyte membrane.

XPS Measurements. XPS measurements were performed with a Supra plus device (Kratos, Manchester, UK) equipped with an Al Kα excitation source. During the spectra acquisition, the charge neutralizer was on. The binding energy scale was corrected using the C−C/C−H peak at 284.8 eV in the C 1s spectra. The screen-printed electrodes were attached to the sample holder using carbon tape. Measurements were carried out at a 90° take-off angle at a pass energy of 20.0 eV and a step of 0.1 eV. The analysis area was 300 by

https://doi.org/10.1021/acsami.3c05314
ACS Appl. Mater. Interfaces XXXX, XXX, XXX−XXX

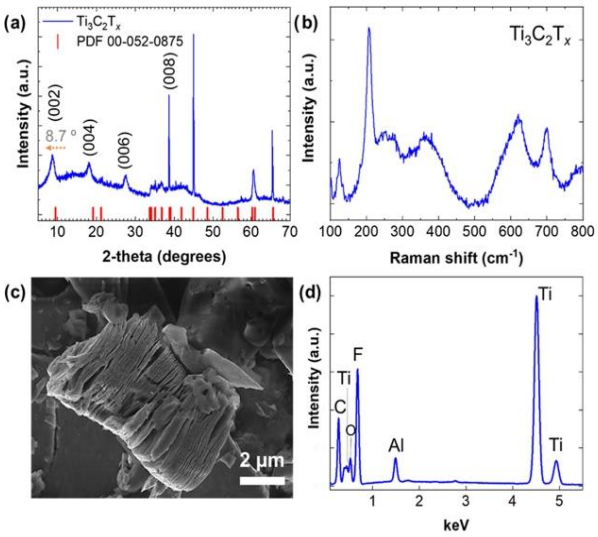

Figure 1. Structural and morphological characterization of $Ti_3C_2T_x$ MXene by XRD (a), Raman spectroscopy (b), SEM (c), and EDXS (d).

700 μm. Spectra were measured and processed using ESCApe 1.5 software (Kratos).

ToF-SIMS Measurements. ToF-SIMS measurements were performed with an M6 device (IONTOF, Münster, Germany). During the spectra acquisition, the flood gun was on. The spectra were calibrated using the peak for CH_3^+ at m/z 15.02, $C_2H_3^+$ at m/z 27.02, and $C_4H_7^+$ at m/z 55.05. The 30.0 keV Bi^+ with a target current of 1.2 pA was employed as the primary ion beam. Sputtering was performed on 500 by 500 μm using the 5.0 keV Ar_{1200}^+ gas cluster ion beam (GCIB), while the analysis was carried out on a 300 by 300 μm in the center of the sputter crater. Spectra were measured and processed, and 3D profiles were constructed using SurfaceLab 7.3 software (IONTOF). The depth (z-scale) of the sputter crater created by the ToF-SIMS sputtering was analyzed using a DektakXT stylus profilometer (Bruker, Karlsruhe, Germany).

Electrochemical Measurements. Cyclic voltammetric measurements were carried out in a potential range of +0.50 to −0.35 V (unless otherwise specified) using a scan rate of 100 mV s^{-1} vs Ag quasi-reference electrode. The gas sensor attached to the electrode holder was inserted tightly into the narrow opening of the chamber, created specifically for the dimensions of a screen-printed electrode, in the area above the solution. All measurements were performed at room temperature (22−23 °C) in a model atmosphere (unless otherwise specified) above the corresponding H_2O_2 solution in the presence of atmospheric gases. For studying the stabilization effect of chitosan on $Ti_3C_2T_x$ MXene, square-wave voltammetry was used in the range of −0.5 to +1.0 V vs Ag quasi-reference electrode.

RESULTS AND DISCUSSION

Characterization of $Ti_3C_2T_x$ MXene. The $Ti_3C_2T_x$ MXene was obtained by selectively etching the Ti_3AlC_2 MAX phase as described in the Experimental Section and illustrated in Scheme S1. The physical and chemical properties of the obtained $Ti_3C_2T_x$ MXene were investigated by X-ray diffraction (XRD), Raman spectroscopy, scanning electron microscopy (SEM) combined with X-ray spectroscopy (EDXS), and atomic force microscopy (AFM).

The XRD pattern of $Ti_3C_2T_x$ MXene is shown in Figure 1a, and its successful synthesis is confirmed by the presence of characteristic diffraction peaks at 8.7, 18.2, 27.6, and 38.6°, which are related to the (002), (004), (006), and (008) planes of this MXene, respectively.[51] For a better understanding of the successful synthesis of $Ti_3C_2T_x$, the powder diffraction file (PDF) of its precursor MAX phase Ti_3AlC_2 (PDF 00-052-0875) was included for comparison. The selective etching of aluminum (Al) is confirmed by a noticeable shift in the (002) diffraction of Ti_3AlC_2 from 9.5 to 8.7° in $Ti_3C_2T_x$. This downshift not only signifies the removal of Al but also indicates the introduction of surface terminations (T_x = −F, −O) in the structural composition of $Ti_3C_2T_x$.

The Raman spectrum in Figure 1b is in agreement with previous studies[52,53] on the vibration modes of $Ti_3C_2T_x$ flakes because typical vibrations related to titanium A_{1g}(Ti, C, O) at 206.5 cm^{-1} and broad peaks in the region of 230−470 cm^{-1} assigned to in-plane (E_g) modes of surface groups attached to Ti atoms are identified. In the 580−730 cm^{-1} region, also designated as the carbon region, the peaks occurring at 621.3 and 700.3 cm^{-1} are associated, respectively, with the vibrations of Ti (E_g) and C (A_{1g}). The peak at 126.1 cm^{-1} is a characteristic resonant peak of laser use during the measurements.[53] The numerical data regarding the identified vibrational modes are summarized in Table S1 and are compared with the reported literature.[52,53] The observed deviations between the Raman spectrum obtained in this work and those reported in the literature (see Table S1) can be attributed to differences arising from material purities and the presence and abundance of terminal groups. Additionally, deviations between experimental results from stacked sheets and theoretical calculations performed on residual-stress-free monosheet models should also be taken into consideration.[52] SEM analysis showed that most Al layers of the Ti_3AlC_2 MAX phase were eliminated after the etching procedure, obtaining the typical accordion-like morphology of the multilayer $Ti_3C_2T_x$ MXene (Figure 1c).[51] The EDXS spectra performed within the same view field (Figure 1d) confirmed the expected C/Ti atomic concentration ratio of 2:3 for $Ti_3C_2T_x$ MXene

https://doi.org/10.1021/acsami.3c05314
ACS Appl. Mater. Interfaces XXXX, XXX, XXX−XXX

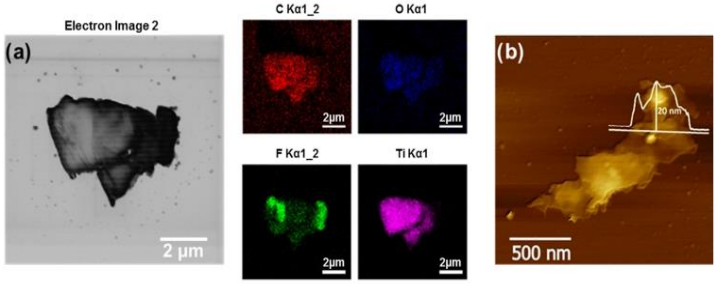

Figure 2. Characterization of $Ti_3C_2T_x$ MXene flakes: STEM image and respective mapping of elements; the scale bar represents 2 μm (a). AFM image with a height profile; the scale bar represents 500 nm (b).

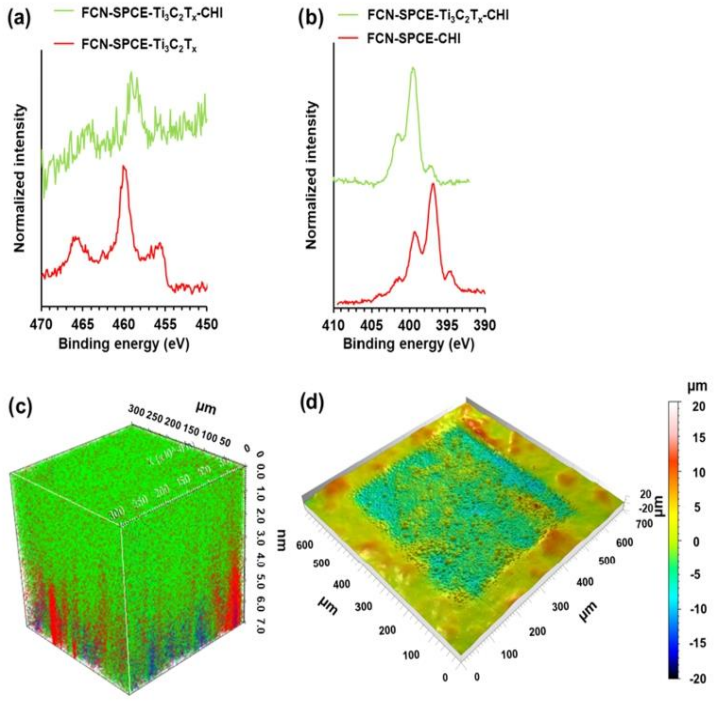

Figure 3. High-resolution Ti 2p (a) and N 1s (b) XPS spectra of FCN-SPCE-$Ti_3C_2T_x$-CHI (green) and FCN-SPCE-$Ti_3C_2T_x$ (red) (a) and FCN-SPCE-$Ti_3C_2T_x$-CHI (green) and FCN-SPCE-CHI (red) (b). 3D ToF-SIMS image of the FCN-SPCE coated with CHI (green), $Ti_3C_2T_x$ MXene (red), and ferrocyanide (blue) (c) and the sputter crater in the sensing membrane measured with a stylus profilometer (d).

besides the residual presence of Al (Table S2). The spectra also show O and F due to their presence as MXene surface terminations (T_x = −OH, −O, −F, etc.). An example of SEM-EDX elemental mapping of $Ti_3C_2T_x$ MXene is shown in Figure S1.

Separated $Ti_3C_2T_x$ MXene flakes were obtained after sonication to form a stable suspension, as observed by STEM and shown in Figures 2a and S2, which typically exhibited micron size in the lateral scale. The elemental maps confirm the composition and distribution of Ti, C, and O, although there was a nonuniform structural feature of F in the $Ti_3C_2T_x$ MXene flake (Figure 2a). The selected elemental line profiles of Ti and C within the same region show a clear higher intensity of both elements within a length of 2.8 μm (Figure S3); positions with a higher Ti concentration match those with a higher C concentration. The AFM image (Figure 2b) shows the corresponding height profile of the $Ti_3C_2T_x$ MXene flake, up to 20 nm, with a lateral size of approximately 1.5 μm. The layer number can be estimated from the theoretical value for a single layer of $Ti_3C_2T_x$ (ca. 0.9 nm) and the measured flake thickness which points to ca. 22 layers. In practical terms, gaps occur between some of the layers, which can be seen in SEM images (Figures 1c and S1); thus, it is possible that the actual number of layers can be lower than the predicted.

Surface Analysis. Figure 3a shows high-resolution Ti 2p spectra for the ferrocyanide-modified screen-printed carbon

https://doi.org/10.1021/acsami.3c05314
ACS Appl. Mater. Interfaces XXXX, XXX, XXX−XXX

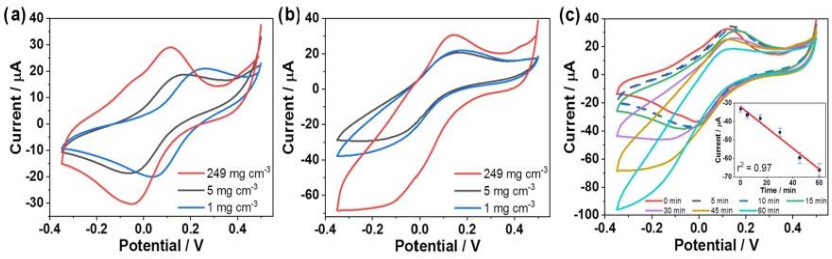

Figure 4. Cyclic voltammograms (CVs) recorded with the sensors prepared using different concentrations of MXene in the absence (a) and presence (b) of 10 mg m^{-3} gaseous H_2O_2 using a 20 min accumulation and a scan rate of 100 mV s^{-1}. CVs recorded for successive increments of accumulation time in the range of 0−60 min together with a background response (red) for 5 mg m^{-3} gaseous H_2O_2 using a scan rate of 100 mV s^{-1} (c) (seven different sensors were used per each time point). All experiments were carried out using completely assembled sensors (FCN-SPCE-MXene-CHI).

electrode (FCN-SPCE) coated with $Ti_3C_2T_x$ (FCN-SPCE-$Ti_3C_2T_x$) and the FCN-SPCE electrode coated with $Ti_3C_2T_x$ and chitosan (CHI), i.e., FCN-SPCE-$Ti_3C_2T_x$-CHI. The main Ti 2p peak for FCN-SPCE-$Ti_3C_2T_x$ is located at 460.0 eV, whereas the Ti 2p spectrum for the electrode that was additionally coated with CHI, i.e., FCN-SPCE-$Ti_3C_2T_x$-CHI, shifts to more negative binding energies, which suggest bonding of Ti-containing species and CHI.

A higher degree of noise is present in the Ti 2p spectrum for FCN-SPCE-$Ti_3C_2T_x$-CHI as $Ti_3C_2T_x$ was underneath the CHI layer, and less signal was obtained for Ti 2p. Figure 3b shows N 1s spectra for the FCN-SPCE electrode coated with CHI (FCN-SPCE-CHI) and the FCN-SPCE electrode coated with $Ti_3C_2T_x$ and CHI (FCN-SPCE-$Ti_3C_2T_x$-CHI). The main peak in the N 1s spectrum for FCN-SPCE-CHI is located at 397.0 eV, while this main peak for FCN-SPCE-$Ti_3C_2T_x$-CHI is shifted to the more positive binding energy. Additional deconvolution of Ti 2p and N 1s spectra with peak assignments is given in the Supporting Information as Figure S5, along with the corresponding discussion. Both peak shifts in the Ti 2p and N 1s spectra indicate that an interaction between CHI and $Ti_3C_2T_x$ occurred, which can explain the electrochemical stabilization of MXene by CHI.

The remarkable stabilization effect was confirmed by the electrochemical characterization of $Ti_3C_2T_x$ MXene in the presence and absence of CHI, as shown in Figure S4. The study compares the square-wave voltammetric responses obtained with bare SPCE (black), CHI-modified SPCE (green), $Ti_3C_2T_x$-modified SPCE (blue), and CHI-$Ti_3C_2T_x$-modified SPCE (red) in 0.1 M KCl as the supporting electrolyte. The signal at ca +0.55 V can be attributed to the typical oxidation of $Ti_3C_2T_x$ MXene deposited on the SPCE.[13] On the other hand, when the $Ti_3C_2T_x$ MXene was codeposited with CHI (red), no oxidation signal was observed at this potential, indicating a favorable stabilization effect of CHI. Clearly, the signal at ca +0.0 V belongs to CHI. In this study, a supporting SPCE was used instead of FCN-SPCE since the latter exhibits a redox activity in the potential window significant for both studied species, i.e., MXene and CHI.

The ToF-SIMS technique was employed to determine the spatial distribution of the species in the gas-sensing membrane. Signals for CH_4N^+ at m/z 30.03, $C_2H_4NO^+$ at m/z 58.03, $C_2H_5NO^+$ at m/z 59.04, $C_3H_6NO^+$ at m/z 72.05, and $C_6H_{10}NO_3^+$ at m/z 144.09[54−57] were used to determine the 3D distribution of chitosan. The spatial distribution of $Ti_3C_2T_x$ was characterized by the signal for Ti^+ at m/z 47.95, and the position of ferrocyanide was characterized by the signal for Fe^+ at m/z 55.94. The obtained depth profile was processed to obtain a 3D image, which is presented in Figure 3c. Chitosan covers the topmost position (green area with a thickness of ca 4 μm), followed by $Ti_3C_2T_x$ (red spots), which is deposited on the ferrocyanide-modified (blue spots) screen-printed carbon electrode. The ToF-SIMS 3D imaging, therefore, confirms the layered design of the sensor, whereas Figure 3d shows the topography of the sensing membrane and the depth of the sputter crater (ca 7 μm) measured by the stylus profilometer.

Electroanalytical Performance. Since the initial experiments showed a positive effect of MXene upon the detection of gaseous H_2O_2, we investigated the cyclic voltammetric behavior of gas sensors that were prepared using different concentrations of MXene in the modification layer.

Figure 4 shows the cyclic voltammetric responses of such gas sensors in the absence (a) and presence (b) of 10 mg m^{-3} gaseous H_2O_2. In the absence of H_2O_2, the sensor revealed two well-developed redox signals corresponding to the oxidation and reduction of $Fe(CN)_6^{4-}/Fe(CN)_6^{3-}$ redox couple between ca +0.00 and −0.20 V vs Ag quasi-reference electrode (Figure 4a). The most pronounced effect of MXene was observed at the highest concentration tested (249 mg cm^{-3}) at the electrode surface, whereas the modification with 5 mg cm^{-3} MXene resulted only in shifted peaks of the $Fe(CN)_6^{4-}/Fe(CN)_6^{3-}$ redox couple toward more negative potentials for ca 100 mV. After only 20 min of exposure to gaseous H_2O_2, a substantial increase in the reduction signal was observed, as shown in Figure 4b.

In the presence of H_2O_2, $(Fe(CN)_6)^{4-}$ is chemically re-oxidized to $(Fe(CN)_6)^{3-}$, followed by immediate electrochemical re-reduction at the electrode surface. Consequently, the voltammogram displayed an increased reduction signal during the cathodic potential scan. It can be perceived that the highest examined concentration of MXene resulted in the highest cathodic response toward gaseous H_2O_2. On the other hand, it is also evident that the sensor containing the highest concentration of MXene exhibited a somewhat higher anodic signal, implying favorable electrocatalytic characteristics of MXene.

To gain further insight into the electroanalytical properties of the gas sensor, we investigated the effect of accumulation time on its voltammetric response; each measurement was performed with a newly fabricated sensor (Figure 4c). It was found that the current signal increased almost linearly with increasing accumulation time in the examined time range of

https://doi.org/10.1021/acsami.3c05314
ACS Appl. Mater. Interfaces XXXX, XXX, XXX−XXX

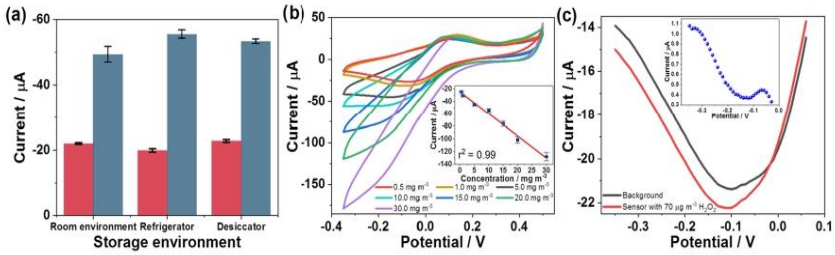

Figure 5. CV signal dependence on different storage conditions in the absence (red) and presence (blue) of 10 mg m^{-3} H_2O_2: refrigerator (ca 4 °C, 65% RH), laboratory (ca 26 °C, 59% RH), and desiccator (ca 26 °C, 10% RH) (a). CVs recorded for successive increments of gaseous H_2O_2 concentrations in the range of 0.5−30.0 mg m^{-3} using a 50 min accumulation and the corresponding calibration plot (b). CVs recorded for 70 μg m^{-3} gaseous H_2O_2 (red) together with background response (black) using a 60 min accumulation; a background subtracted voltammogram is shown in the inset (dotted blue) (c). Other conditions are as in Figure 4c.

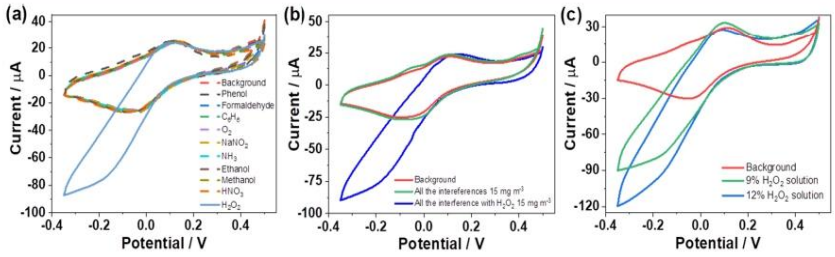

Figure 6. CVs recorded individually for nine potential gaseous interferants of 15 mg m^{-3} each (a) and in the presence of all nine interferants together (of 15 mg m^{-3} each) (b), along with the addition of 15 mg m^{-3} H_2O_2 and a background response using a 20 min accumulation. CVs recorded for a background (red) and when the gas sensor was left for 20 min in a room, where hair bleaching was carried out using 9% (green) and 12% (blue) H_2O_2 solution (c). Other conditions are as in Figure 4c.

0−60 min. In this range, we did not observe any concentration saturation. On the contrary, apart from a linear increase of the signal (r^2 = 0.97) at longer exposure times, excellent reproducibility was observed for each data point, as shown by the small error bars in Figure 4c. An even higher response could be achieved by further increasing the accumulation time; however, considerably longer accumulation times are associated with the inherent instability of gaseous H_2O_2.

With longer accumulation times and consequently with higher concentrations of gaseous H_2O_2 in the sensing membrane, the signal waveform gradually changes from a peak-shaped to a steady state-shaped voltammogram and then, with even longer accumulation times, to a situation with a well-visible deflection point. This process is also accompanied by a gradual shift of the reduction potential toward more negative values. This is due to the change in the diffusion profile with more accumulated H_2O_2 and electrogenerated product as a result of H_2O_2 reduction in the vicinity of the electrode surface, along with the inherently irreversible reduction reaction of H_2O_2.

In addition, the stability study of the sensor was conducted at various temperatures and humidity, as shown in Figure 5a. The sensors were stored overnight in different environments, i.e., in the laboratory, refrigerator, and desiccator; they were tested in triplicate. It can be observed that the background responses of the sensors stored in different ways are practically the same, i.e., within the range of standard deviation. Interestingly, storage in the desiccator did not affect the sensor response, i.e., the dry atmosphere did not compromise the electroanalytical performance of the gas sensor. A slightly lower response toward the gaseous analyte was observed when the sensor was stored under ambient conditions. This could be due to the combination of higher ambient humidity and temperature (at more than 5 °C), which could accelerate the hydrolytic damage degree of the chitosan and change its physicochemical properties.[58,59]

We followed the performance of the sensor in terms of its response to increasing concentrations of gaseous H_2O_2. In combination with a 50 min accumulation, the sensor exhibited a well-developed and satisfactory linear response in the examined concentration range of 0.5−30 mg m^{-3} with r^2 of 0.99 (Figure 5b). The deviation from the higher linearity is due to the accumulation/dissolution/diffusion pattern of H_2O_2 in the viscous sensing membrane and the partial decomposition of relatively unstable H_2O_2.

The gas sensor was also successfully tested for the detection of lower H_2O_2 concentration; as depicted in Figure 5c, a well-readable voltammetric signal was obtained for 70 μg m^{-3} in conjunction with an accumulation time of only 60 min. The sensor unveiled a very low limit of detection (3σ criterion) of 4 μg m^{-3}. Moreover, surprisingly, good sensor-to-sensor repeatability was achieved, with a relative standard deviation (RSD) of only 1.30% when measuring 70 μg m^{-3} gaseous H_2O_2.

Selectivity Study. The operation of the gas sensor was investigated in the presence of selected potential gaseous compounds expected in the real environment. The study was performed by measuring the potential interferants individually at a concentration of 15 mg m^{-3} each, followed by the addition of 15 mg m^{-3} H_2O_2, as shown in Figure 6a.

https://doi.org/10.1021/acsami.3c05314
ACS Appl. Mater. Interfaces XXXX, XXX, XXX−XXX

In the absence of gaseous H_2O_2, no analytical signal was detected for gaseous methanol, ethanol, formaldehyde, phenol, ammonia, benzene, oxygen, nitric acid, and sodium nitrite in the applied potential range of +0.50 to −0.35 V. In addition, the sensor was exposed to a mixture of all of these gaseous compounds at a concentration of 15 mg m^{-3} each. After the addition of 15 mg m^{-3} H_2O_2, a well-defined reduction signal of H_2O_2 was formed with no visible effects of the nine gaseous compounds present, confirming the excellent selectivity of the gas sensor (Figure 6b).

Real Sample Detection. Finally, the performance of the gas sensor was tested in a real environment during the bleaching treatment of human hair. The experiment was carried out in a fume hood by applying 10.0 mL of a 9% H_2O_2 solution to the wig; each of the three sensors was exposed for 20 min. After washing and drying the wig, the same procedure was repeated with 10.0 mL of a 12% H_2O_2 solution (Figure 6c). In both cases, the background was measured in the absence of gaseous H_2O_2. The sensor exhibited distinct signals for both concentrations of gaseous H_2O_2; after three successive measurements, an average determined concentration of ca 18 mg m^{-3} for 9% H_2O_2 solution and ca 24 mg m^{-3} for 12% H_2O_2 solution was obtained.

CONCLUSIONS

In this work, we have demonstrated a synergistic effect of the advantageous physicochemical properties of exfoliated $Ti_3C_2T_x$ MXene and the stabilizing characteristics of chitosan, together with the redox activity of the ferrocyanide-modified screen-printed carbon electrode for ultrasensitive point-of-interest detection of gaseous H_2O_2. The poly(acrylic acid)-based membrane served simultaneously as an electrolyte and a suitable accumulation medium for the gaseous analyte. The sensor showed excellent interference-free operation in the cathodic potential range along with good sensor-to-sensor reproducibility, favorable stability, and a very low detection limit of only 4 μg m^{-3} (ppbv). The applicability of the $Ti_3C_2T_x$ MXene-based gas sensor was successfully demonstrated by measuring H_2O_2 during the treatment of real human hair with a bleaching agent.

ASSOCIATED CONTENT

Supporting Information

The Supporting Information is available free of charge at https://pubs.acs.org/doi/10.1021/acsami.3c05314.

Synthesis route to prepare $Ti_3C_2T_x$ MXene from the precursor Ti_3AlC_2 MAX phase (Scheme S1); SEM micrograph of $Ti_3C_2T_x$ MXene and mapping of elements (Figure S1); bright-mode STEM image of $Ti_3C_2T_x$ MXene flakes (Figure S2); mapping of elements of $Ti_3C_2T_x$ MXene flakes and relative intensity profiles (Figure S3); Raman shift positions for Raman-active modes of $Ti_3C_2T_x$ (Table S1); EDXS element quantification of $Ti_3C_2T_x$ MXene (Table S2); square-wave voltammograms of MXene stabilization study (Figure S4); and deconvolution of the high-resolution Ti 2p XPS spectra and N 1s XPS spectra for sensing layers (Figure S5) (PDF)

AUTHOR INFORMATION

Corresponding Authors

Rui Gusmão − *Department of Inorganic Chemistry, University of Chemistry and Technology Prague, 16628 Prague, Czech Republic*; orcid.org/0000-0001-6358-7601; Email: rui.gusmao@vscht.cz

Samo B. Hočevar − *Department of Analytical Chemistry, National Institute of Chemistry, 1000 Ljubljana, Slovenia*; orcid.org/0000-0003-2980-4822; Email: samo.hocevar@ki.si

Authors

Jelena Isailović − *Department of Analytical Chemistry, National Institute of Chemistry, 1000 Ljubljana, Slovenia; International Postgraduate School Jožef Štefan, 1000 Ljubljana, Slovenia*

Ana Oberlintner − *International Postgraduate School Jožef Štefan, 1000 Ljubljana, Slovenia; Department of Catalysis and Chemical Reaction Engineering, National Institute of Chemistry, 1000 Ljubljana, Slovenia*

Uroš Novak − *Department of Catalysis and Chemical Reaction Engineering, National Institute of Chemistry, 1000 Ljubljana, Slovenia*; orcid.org/0000-0003-0561-8427

Matjaž Finšgar − *Faculty of Chemistry and Chemical Engineering, University of Maribor, 2000 Maribor, Slovenia*; orcid.org/0000-0002-8302-9284

Filipa M. Oliveira − *Department of Inorganic Chemistry, University of Chemistry and Technology Prague, 16628 Prague, Czech Republic*; orcid.org/0000-0001-7268-3144

Jan Paštika − *Department of Inorganic Chemistry, University of Chemistry and Technology Prague, 16628 Prague, Czech Republic*

Zdeněk Sofer − *Department of Inorganic Chemistry, University of Chemistry and Technology Prague, 16628 Prague, Czech Republic*; orcid.org/0000-0002-1391-4448

Nikola Tasić − *Department of Analytical Chemistry, National Institute of Chemistry, 1000 Ljubljana, Slovenia*; orcid.org/0000-0002-0582-2252

Complete contact information is available at: https://pubs.acs.org/10.1021/acsami.3c05314

Notes

The authors declare no competing financial interest.

ACKNOWLEDGMENTS

The work was supported by the Slovenian Research Agency (P1-0034, P2-0118) and the Slovenian Research Agency's Young Researchers Programme (grant agreement no. 52020). The project is co-financed by the Republic of Slovenia, the Ministry of Education, Science and Sport, and the European Union under the European Regional Development Fund. Z.S. was supported by Czech Science Foundation (GAČR No. 20-16124J). J.P. acknowledges support from the grant of specific university research—A2_FCHT_2023_102.

REFERENCES

(1) Ho, D. H.; Choi, Y. Y.; Jo, S. B.; Myoung, J.-M.; Cho, J. H. Sensing with MXenes: Progress and Prospects. *Adv. Mater.* **2021**, *33*, No. 2005846.

(2) Sinha, A.; Dhanjai; Zhao, H.; Huang, Y.; Lu, X.; Chen, J.; Jain, R. MXene: An Emerging Material for Sensing and Biosensing. *TrAC, Trends Anal. Chem.* **2018**, *105*, 424−435.
(3) Verger, L.; Natu, V.; Carey, M.; Barsoum, M. W. MXenes: An Introduction of Their Synthesis, Select Properties, and Applications. *Trends Chem.* **2019**, *1*, 656−669.
(4) Oliveira, F. M.; Gusmão, R. Recent Advances in the Electromagnetic Interference Shielding of 2D Materials Beyond Graphene. *ACS Appl. Electron. Mater.* **2020**, *2*, 3048−3071.
(5) Naguib, M.; Kurtoglu, M.; Presser, V.; Lu, J.; Niu, J.; Heon, M.; Hultman, L.; Gogotsi, Y.; Barsoum, M. W. Two-Dimensional Nanocrystals Produced by Exfoliation of Ti_3AlC_2. *Adv. Mater.* **2011**, *23*, 4248−4253.
(6) Gogotsi, Y.; Anasori, B. The Rise of MXenes. *ACS Nano* **2019**, *13*, 8491−8494.
(7) Haemers, J.; Gusmão, R.; Sofer, Z. Synthesis Protocols of the Most Common Layered Carbide and Nitride MAX Phases. *Small Methods* **2020**, *4*, No. 1900780.
(8) Ding, L.; Wei, Y.; Li, L.; Zhang, T.; Wang, H.; Xue, J.; Ding, L.-X.; Wang, S.; Caro, J.; Gogotsi, Y. MXene Molecular Sieving Membranes for Highly Efficient Gas Separation. *Nat. Commun.* **2018**, *9*, No. 2002.
(9) Lee, E.; Kim, D.-J. Review—Recent Exploration of Two-Dimensional MXenes for Gas Sensing: From a Theoretical to an Experimental View. *J. Electrochem. Soc.* **2020**, *167*, No. 037515.
(10) Dixit, F.; Zimmermann, K.; Alamoudi, M.; Abkar, L.; Barbeau, B.; Mohseni, M.; Kandasubramanian, B.; Smith, K. Application of MXenes for Air Purification, Gas Separation and Storage: A review. *Renewable Sustainable Energy Rev.* **2022**, *164*, No. 112527.
(11) Iqbal, A.; Hong, J.; Ko, T. Y.; Koo, C. M. Improving Oxidation Stability of 2D MXenes: Synthesis, Storage Media, and Conditions. *Nano Convergence* **2021**, *8*, 9.
(12) Habib, T.; Zhao, X.; Shah, S. A.; Chen, Y.; Sun, W.; An, H.; Lutkenhaus, J. L.; Radovic, M.; Green, M. J. Oxidation Stability of $Ti_3C_2T_x$ MXene Nanosheets in Solvents and Composite Films. *npj 2D Mater. Appl.* **2019**, *3*, 8.
(13) Nayak, P.; Yang, M.; Wang, Z.; Li, X.; Miao, R.; Compton, R. G. Single-Entity $Ti_3C_2T_x$ MXene Electro-Oxidation. *Appl. Mater. Today* **2022**, *26*, No. 101335.
(14) Eul, W.; Moeller, A.; Steiner, N.Hydrogen Peroxide *Wiley, Kirk-Othmer Encyclopedia of Chemical Technology* 2000; Vol. *13*, p 1.
(15) Chen, W.; Fan, H.; Balakrishnan, K.; Wang, Y.; Sun, H.; Fan, Y.; Gandhi, V.; Arnold, L. A.; Peng, X. Discovery and Optimization of Novel Hydrogen Peroxide Activated Aromatic Nitrogen Mustard Derivatives as Highly Potent Anticancer Agents. *J. Med. Chem.* **2018**, *61*, 9132−9145.
(16) Müller, G.; Chylenski, P.; Bissaro, B.; Eijsink, V.G.-H.; Horn, S. J. The Impact of Hydrogen Peroxide Supply on LPMO Activity and Overall Saccharification Efficiency of a Commercial Cellulase Cocktail. *Biotechnol. Biofuels* **2018**, *11*, 209.
(17) Holkar, C. R.; Jadhav, A. J.; Pinjari, D. V.; Mahamuni, N. M.; Pandit, A. B. A Critical Review on Textile Wastewater Treatments: Possible Approaches. *J. Environ. Manage.* **2016**, *182*, 351−366.
(18) Giorgio, M.; Trinei, M.; Migliaccio, E.; Pelicci, P. G. Hydrogen Peroxide: A Metabolic By-Product or a Common Mediator of Ageing Signals? *Nat. Rev. Mol. Cell Bio.* **2007**, *8*, 722−728.
(19) Wu, J.; Shu, S.; Li, C.; Sun, J.; Guo, S. Spermidine-Mediated Hydrogen Peroxide Signaling Enhances the Antioxidant Capacity of Salt-Stressed Cucumber Roots. *Plant Physiol. Biochem.* **2018**, *128*, 152−162.
(20) Whittemore, E. R.; Loo, D. T.; Cotman, C. W. Exposure to Hydrogen Peroxide Induces Cell Death via Apoptosis in Cultured Rat Cortical Neurons. *Neuroreport* **1994**, *5*, 1485−1488.
(21) Veal, E. A.; Day, A. M.; Morgan, B. A. Hydrogen Peroxide Sensing and Signaling. *Mol. Cell* **2007**, *26*, 1−14.
(22) Sies, H. Hydrogen Peroxide as a Central Redox Signaling Molecule in Physiological Oxidative Stress: Oxidative Eustress. *Redox Biol.* **2017**, *11*, 613−619.
(23) Zhou, M.; Liu, Y.; Duan, Y. Breath Biomarkers in Diagnosis of Pulmonary Diseases. *Clin. Chim. Acta* **2012**, *413*, 1770−1780.
(24) Zappacosta, B.; Persichilli, S.; Mormile, F.; Minucci, A.; Russo, A.; Giardina, B.; Sole, P. D. A Fast Chemiluminescent Method for H_2O_2 Measurement in Exhaled Breath Condensate. *Clin. Chim. Acta* **2001**, *310*, 187−191.
(25) Stolarek, R.; Bialasiewicz, P.; Krol, M.; Nowak, D. Breath Analysis of Hydrogen Peroxide as a Diagnostic Tool. *Clin. Chim. Acta* **2010**, *411*, 1849−1861.
(26) Svensson, S.; Olin, A. C.; Lärstad, M.; Ljungkvist, G.; Torén, K. Determination of Hydrogen Peroxide in Exhaled Breath Condensate by Flow Injection Analysis with Fluorescence Detection. *J. Chromatogr. B* **2004**, *809*, 199−203.
(27) Chan, H. P.; Lewis, C.; Thomas, P. S. Exhaled Breath Analysis: Novel Approach for Early Detection of Lung Cancer. *Lung Cancer* **2009**, *63*, 164−168.
(28) Klapötke, T. M.; Włoka, T. Peroxide Explosives. *PATAI's Chem. Funct. Groups* **2009**, 1−28.
(29) Meyer, J.; Karst, U. Workplace Monitoring of Gas Phase Hydrogen Peroxide by Means of Fluorescence Spectroscopy. *Anal. Chim. Acta* **1999**, *401*, 191−196.
(30) Voraberger, H.; Ribitsch, V.; Janotta, M.; Mizaikoff, B. Application of Mid-Infrared Spectroscopy: Measuring Hydrogen Peroxide Concentrations in Bleaching Baths. *Appl. Spectrosc.* **2003**, *57*, 574−579.
(31) Stewart, S. P.; Bell, S.E.J.; McAuley, D.; Baird, I.; Speers, S. J.; Kee, G. Determination of Hydrogen Peroxide Concentration Using a Handheld Raman spectrometer: Detection of an Axplosives Precursor. *Forensic Sci. Int.* **2012**, *216*, e5−e8.
(32) Navas, M. J.; Jiménez, A. M.; Galán, G. Air Analysis: Determination of Hydrogen Peroxide by Chemiluminescence. *Atmos. Environ.* **1999**, *33*, 2279−2283.
(33) Li, J.; Dasgupta, P. K. Measurement of Gaseous Hydrogen Peroxide with a Liquid Core Waveguide Chemiluminescence Detector. *Anal. Chim. Acta* **2001**, *442*, 63−70.
(34) Tahirović, A.; Čopra, A.; Omanović-Mikličanin, E.; Kalcher, K. A Chemiluminescence Sensor for the Determination of Hydrogen Peroxide. *Talanta* **2007**, *72*, 1378−1385.
(35) Xu, M.; Bunes, B. R.; Zang, L. Paper-Based Vapor Detection of Hydrogen Peroxide: Colorimetric Sensing with Tunable Interface. *ACS Appl. Mater. Interfaces* **2011**, *3*, 642−647.
(36) Sanchez, J. C.; Trogler, W. C. Polymerization of a Boronate-Functionalized Fluorophore by Double Transesterification: Applications to Fluorescence Detection of Hydrogen Peroxide Vapor. *J. Mater. Chem.* **2008**, *18*, 5134−5141.
(37) Chen, L. C.; Hiroaki, S.; Kunihiko, M.; Osamu, A.; Kenzo, H. Mass Spectrometric Detection of Gaseous Hydrogen Peroxide in Ambient Air Using Dielectric Barrier Discharge as an Excitation Source. *Chem. Lett.* **2009**, *38*, 520−521.
(38) Kirchner, P.; Oberländer, J.; Suso, H-P.; Rysstad, G.; Keusgen, M.; Schöning, M. J. Monitoring the Microbicidal Effectiveness of Gaseous Hydrogen Peroxide in Sterilisation Processes by Means of a Calorimetric Gas Sensor. *Food Control* **2013**, *31*, 530−538.
(39) Steinberg, S. M. High-Performance Liquid Chromatography Method for Determination of Hydrogen Peroxide in Aqueous Solution and Application to Simulated Martian Soil and Related Materials. *Environ. Monit. Assess.* **2013**, *185*, 3749−3757.
(40) Kimmel, D. W.; LeBlanc, G.; Meschievitz, M. E.; Cliffel, D. E. Electrochemical Sensors and Biosensors. *Anal. Chem.* **2012**, *84*, 685−707.
(41) Gulaboski, R.; Mirčeski, V.; Kappl, R.; Hoth, M.; Bozem, M. Review—Quantification of Hydrogen Peroxide by Electrochemical Methods and Electron Spin Resonance Spectroscopy. *J. Electrochem. Soc.* **2019**, *166*, G82.
(42) Yu, Y.; Pan, M.; Peng, J.; Hu, D.; Hao, Y.; Qian, Z. A Review on Recent Advances in Hydrogen Peroxide Electrochemical Sensors for Applications in Cell Detection. *Chin. Chem. Lett.* **2022**, *33*, 4133−4145.

https://doi.org/10.1021/acsami.3c05314
ACS Appl. Mater. Interfaces XXXX, XXX, XXX−XXX

(43) Kuwata, S.; Yoshihiko, S. Detection of Gaseous Hydrogen Peroxide Using Planar-Type Amperometric Cell at Room Temperature. *Sens. Actuators, B* **2000**, *65*, 325−326.
(44) Toniolo, R.; Geatti, P.; Bontempelli, G.; Schiavon, G. Amperometric Monitoring of Hydrogen Peroxide in Workplace Atmospheres by Electrodes Supported on Ion-Exchange Membranes. *J. Electroanal. Chem.* **2001**, *514*, 123−128.
(45) Aroutiounian, V.; Arakelyan, V.; Aleksanyan, M.; Sayunts, A.; Shahnazaryan, G.; Kacer, P.; Picha, P.; Kovarik, J.; Pekarek, J.; Joost, B. Nanostructured Sensors for Detection of Hydrogen Peroxide Vapours. *Sens. Transducers* **2017**, *213*, 46.
(46) Isailović, J.; Vidović, K.; Hočevar, S. B. Simple Electrochemical Sensors for Highly Sensitive Detection of Gaseous Hydrogen Peroxide Using Polyacrylic-Acid-Based Sensing Membrane. *Sens. Actuators, B* **2022**, *352*, No. 131053.
(47) Maier, D.; Laubender, E.; Basavanna, A.; Schumann, S.; Güder, F.; Urban, G. A.; Dincer, C. Toward Continuous Monitoring of Breath Biochemistry: A Paper-Based Wearable Sensor for Real-Time Hydrogen Peroxide Measurement in Simulated Breath. *ACS Sens.* **2019**, *4*, 2945−2951.
(48) Giaretta, J. E.; Oveissi, F.; Dehghani, F.; Naficy, S. Paper-Based, Chemiresistive Sensor for Hydrogen Peroxide Detection. *Adv. Mater. Technol.* **2021**, *6*, No. 2001148.
(49) Bajić, M.; Ročnik, T.; Oberlintner, A.; Scognamiglio, F.; Novak, U.; Likozar, B. Natural Plant Extracts as Active Components in Chitosan-Based Films: A Comparative Study. *Food Packag. Shelf Life* **2019**, *21*, No. 100365.
(50) Sander, R. Compilation of Henry's Law Constants (Version 4.0) for Water as Solvent. *Atmos. Chem. Phys.* **2015**, *15*, 4399−4981.
(51) Alhabeb, M.; Maleski, K.; Anasori, B.; Lelyukh, P.; Clark, L.; Sin, S.; Gogotsi, Y. Guidelines for Synthesis and Processing of Two-Dimensional Titanium Carbide ($Ti_3C_2T_x$ MXene). *Chem. Mater.* **2017**, *29*, 7633−7644.
(52) Hu, T.; Wang, J.; Zhang, H.; Li, Z.; Hu, M.; Wang, X. Vibrational Properties of Ti_3C_2 and $Ti_3C_2T_2$ (T = O, F, OH) Monosheets by First-Principles Calculations: A Comparative Study. *Phys. Chem. Chem. Phys.* **2015**, *17*, 9997−10003.
(53) Sarycheva, A.; Gogotsi, Y. Raman Spectroscopy Analysis of the Structure and Surface Chemistry of $Ti_3C_2T_x$ MXene. *Chem. Mater.* **2020**, *32*, 3480−3488.
(54) Hashmi, A.; Sodhi, R. N. S.; Kishen, A. Interfacial Characterization of Dentin Conditioned with Chitosan Hydroxyapatite Precursor Nanocomplexes Using Time-of-flight Secondary Ion Mass Spectrometry. *J. Endod.* **2019**, *45*, 1513−1521.
(55) D'Almeida, M.; Attik, N.; Amalric, J.; Brunon, C.; Renaud, F.; Abouelleil, H.; Toury, B.; Grosgogeat, B. Chitosan Coating as an Antibacterial Surface for Biomedical Applications. *PLoS One* **2017**, *12*, No. e0189537.
(56) Wu, T.; Du, Y.; Yan, N.; Farnood, R. Cellulose Fiber Networks Reinforced with Glutaraldehyde−Chitosan Complexes. *J. Appl. Polym. Sci.* **2015**, *132*, 42375.
(57) Finšgar, M.; Ristić, T.; Fardim, P.; Zemljič, L. F. Time-of-Flight Secondary Ion Mass Spectrometry Analysis of Chitosan-Treated Viscose Fibres. *Anal. Biochem.* **2018**, *557*, 131−141.
(58) Qin, C. Q.; Du, Y. M.; Xiao, L. Effect of Hydrogen Peroxide Treatment on the Molecular Weight and Structure of Chitosan. *Polym. Degrad. Stab.* **2002**, *76*, 211−218.
(59) Szymańska, E.; Winnicka, K. Stability of Chitosan—A Challenge for Pharmaceutical and Biomedical Applications. *Mar. Drugs* **2015**, *13*, 1819−1846.

https://doi.org/10.1021/acsami.3c05314
ACS Appl. Mater. Interfaces XXXX, XXX, XXX−XXX

Supporting Information

Study of Chitosan-Stabilized $Ti_3C_2T_x$ MXene for Ultrasensitive and Interference-Free Detection of Gaseous H_2O_2

Jelena Isailović,[a,c] Ana Oberlintner,[c,d] Uroš Novak,[d] Matjaž Finšgar,[e] Filipa M. Oliveira,[b] Jan Paštika,[b] Zdeněk Sofer,[b] Nikola Tasić,[a] Rui Gusmão,[b,] Samo B. Hočevar[a,*]*

[a] Department of Analytical Chemistry, National Institute of Chemistry, Hajdrihova 19, 1000 Ljubljana, Slovenia

[b] Department of Inorganic Chemistry, University of Chemistry and Technology Prague, Technická 5, 166 28 Prague, Czech Republic

[c] International Postgraduate School Jožef Štefan, Jamova cesta 39, 1000 Ljubljana, Slovenia

[d] Department of Catalysis and Chemical Reaction Engineering, National Institute of Chemistry, Hajdrihova 19, 1000 Ljubljana, Slovenia

[e] Faculty of Chemistry and Chemical Engineering, University of Maribor, Smetanova ulica 17, 2000 Maribor, Slovenia

*Samo. B. Hočevar (e-mail: samo.hocevar@ki.si)

*Rui Gusmão (e-mail: rui.gusmao@vscht.cz)

KEYWORDS: $Ti_3C_2T_x$ MXene, Chitosan, Hydrogen peroxide, Gas sensor, Cyclic Voltammetry.

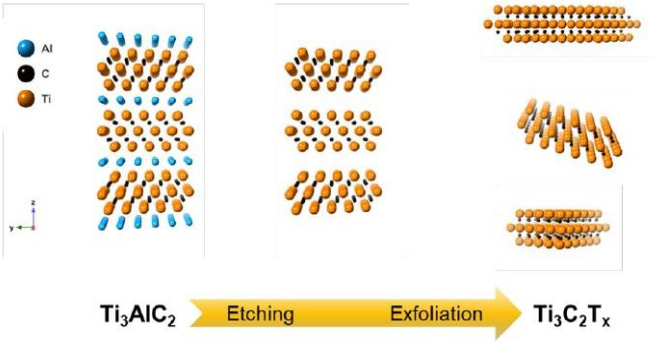

Scheme S1. Representation of the synthesis route to prepare $Ti_3C_2T_x$ MXene from the precursor Ti_3AlC_2 MAX phase.

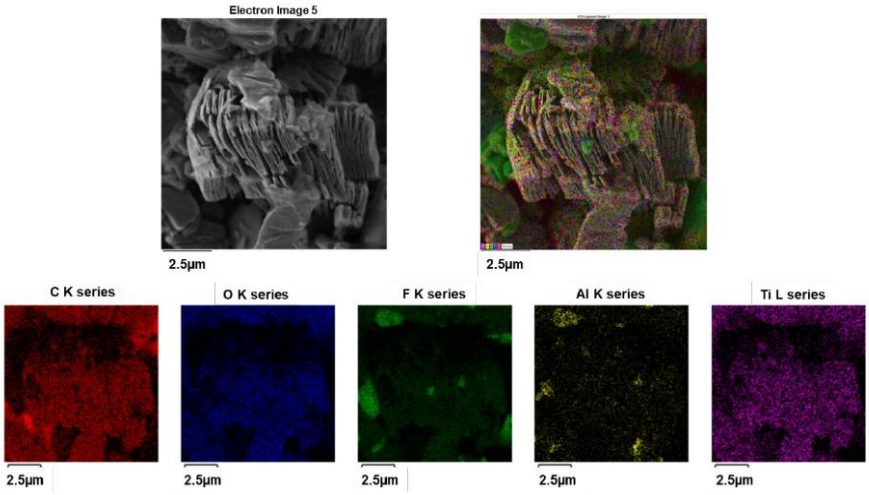

Figure S1. SEM micrograph of $Ti_3C_2T_x$ MXene (top left) with the overlay colored mapping of elements (top right). Individual mapping of elements for C, O, F, Al, and Ti (bellow). The scale bar represents 2.5 µm.

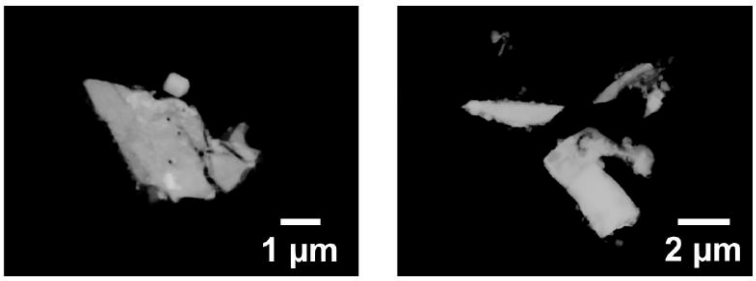

Figure S2. Bright mode STEM image of $Ti_3C_2T_x$ MXene flakes.

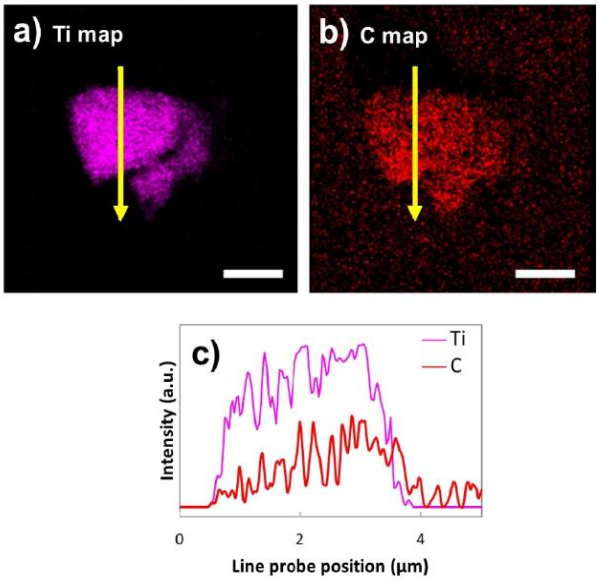

Figure S3. Mapping of elements of $Ti_3C_2T_x$ MXene flakes: Ti (a), C (b). The yellow arrow denotes the EDXS elemental line probe for Ti and C elements for which the relative intensity profiles were obtained (c). Scale bars represent 2 µm.

Table S1. Raman shift positions for Raman-active modes of $Ti_3C_2T_x$. All the values are given in cm^{-1}.

Material	**Resonant peak**	A_{1g} (Ti, C, O)	E_g (C)	A_{1g} (C)	**Ref.**
$Ti_3C_2T_x$	126.1	206.5	621.3	700.3	**This work**
$Ti_3C_2T_x$ (HF-HCl Multilayer)	122.2	202.8	~ 620	721.8	[1]
$Ti_3C_2T_x$ (DFT calculations)	-	228	621	-	[2]

[52] Sarycheva, A.; Gogotsi, Y. Raman Spectroscopy Analysis of the Structure and Surface Chemistry of $Ti_3C_2T_x$ MXene. *Chem. Mater.* 2020, *32* (8), 3480–3488.

[53] Hu, T.; Wang, J.; Zhang, H.; Li, Z.; Hu, M.; Wang, X. Vibrational Properties of Ti_3C_2 and $Ti_3C_2T_2$ (T = O, F, OH) Monosheets by First-Principles Calculations: A Comparative Study. *Phys. Chem. Chem. Phys.* 2015, *17* (15), 9997–10003.

Table S2. EDXS element quantification of $Ti_3C_2T_x$ MXene.

at.%	C	O	F	Al	Ti
Average	19.6	19.2	31.2	1.7	28.2
Standard deviation	2.3	1.9	2.4	0.2	3.1

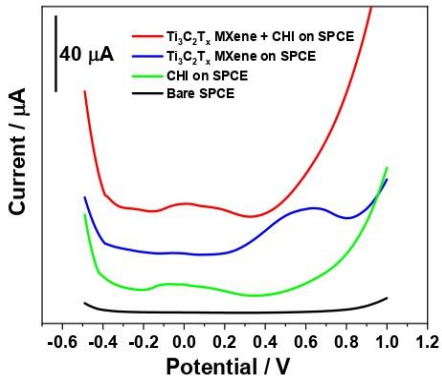

Figure S4. Square-wave voltammograms recorded in 0.1 M KCl using bare SPCE (black), CHI-modified SPCE (green), $Ti_3C_2T_x$ MXene-modified SPCE (blue), and $Ti_3C_2T_x$ MXene + CHI-modified SPCE (red), using an amplitude of 100 mV, a frequency of 20 Hz and a step potential of 10 mV.

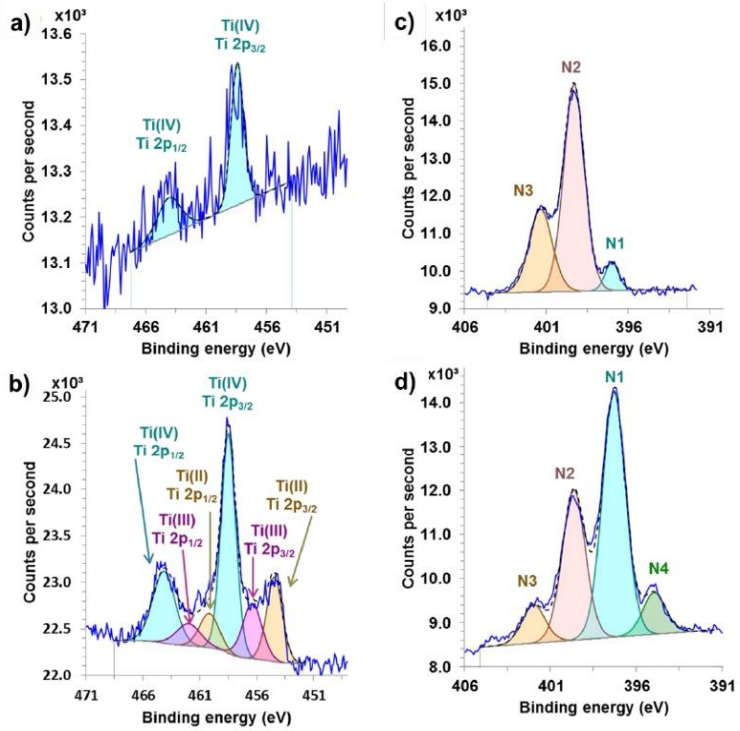

Figure S5. Deconvolution of the high-resolution Ti 2p XPS spectra for FCN-SPCE-$Ti_3C_2T_x$-CHI (a) and FCN-SPCE-$Ti_3C_2T_x$ (b), and deconvolution of the high-resolution N 1s XPS spectra for FCN-SPCE-$Ti_3C_2T_x$-CHI (c) and FCN-SPCE-CHI (d).

Figure S5 shows deconvoluted Ti 2p spectra for FCN-SPCE-$Ti_3C_2T_x$-CHI (Figure S5a) and FCN-SPCE-$Ti_3C_2T_x$ (Figure S5b). A higher degree of noise is present in Figure S5a due to the coverage of the surface (also Ti-containing species) with CHI. The positions of the Ti $2p_{3/2}$ and Ti $2p_{1/2}$ peaks correspond to Ti(IV) oxidation state. In the case of FCN-SPCE-$Ti_3C_2T_x$, i.e., the sample that was not covered with CHI, the Ti 2p spectrum is different and can be fitted with three oxidation states, i.e., Ti(IV), Ti(III), and Ti(II) (Figure S5b). As this sample was not covered with CHI, the XPS excitation signal also reached regions with Ti(II) and Ti(III) oxidation states of the MXene. The peaks for the Ti(II) and Ti(III) oxidation states were less intense compared to the peak for Ti(IV), implying lower surface atomic concentrations of these species compared to Ti(IV)-containing species. In the case of FCN-SPCE-$Ti_3C_2T_x$-CHI, Ti(II)- and Ti(III)-containing species were deeper in the subsurface

region compared to Ti(IV)-containing species, and the XPS excitation signal did not reach them (hence the peaks for these species are missing in Figure S5a).

Figures S5c and S5d show deconvoluted N 1s spectra for FCN-SPCE-$Ti_3C_2T_x$-CHI and FCN-SPCE-CHI, respectively. Deconvoluted peaks designated as N3 and N2 correspond to NH_3^+ and NH_2 in the CHI molecule. The deconvoluted peak N1 might originate from nonbounded hexacyanoferrate, and the deconvoluted peak N4 to hexacyanoferrate bonded to SPCE. The N4 peak in the case of FCN-SPCE-$Ti_3C_2T_x$-CHI (Figure S5c) was not developed, which is most likely due to the too-thick surface layer (as an additional layer of $Ti_3C_2T_x$ was present), and the XPS excitation signal did not reach the SPCE, where the connection of hexacyanoferrate with SPCE occurred. The same is most likely the reason for a less intense N1 peak in the case of FCN-SPCE-$Ti_3C_2T_x$-CHI (Figure S5c) compared to FCN-SPCE-CHI (Figure S5d), where more signal for nonbounded hexacyanoferrate was obtained for the latter as the surface layer was thinner (as MXene was not present).

Chapter 4

Conclusion

The main objective of this dissertation was to study and develop sensitive and selective electrochemical gas sensors for detecting low-concentration levels of gaseous H_2O_2. The initial objective was to comprehensively investigate and improve the electrochemical properties of disposable screen-printed supporting electrodes. We aimed to improve key aspects such as conductivity, electrocatalytic activity, reproducibility, and signal-to-noise ratio through chemical and electrochemical methodologies and treatments. The next objective was to investigate and select suitable redox/catalytic modification materials, including state-of-the-art 2D nanomaterials and metal oxides, to enhance the electroanalytical performances of gas sensors, such as sensitivity, selectivity, and robustness.

Another important aspect of our research was the development of suitable multi-functional gas sensing membranes, serving simultaneously as an electrolyte, accumulation medium, and protective/stabilization membrane to facilitate improved detection of gaseous H_2O_2. We strived to develop membranes that would enhance the sensitivity and selectivity of the sensors, allowing for more precise and accurate quantification of gaseous H_2O_2.

The ambition was also to provide and demonstrate real environmental detection of gaseous H_2O_2, making it possible to identify and quantify this analyte in minute concentrations.

We have successfully accomplished all the foreseen goals by conducting extensive research, optimization, and studies and implementing the methodologies and techniques outlined in this dissertation. Our findings and experimental results demonstrate that gaseous H_2O_2 can indeed be detected in simulated and real environments, even at its extremely low concentrations.

The candidate's Ph.D. research work is summarized in two manuscripts published in peer-reviewed renowned international journals:

1. **Manuscript:** In the context of several hypotheses, we dedicated our efforts to develop, characterize, and compare two distinct types of sensors for measuring gaseous H_2O_2. These sensors were carefully designed by incorporating a viscous poly(acrylic acid)-based (PAA) sensing membrane onto commercially available screen-printed carbon electrodes. The membrane was composed of optimized amounts of PAA and phosphate buffer solution, providing convenient ionic conductivity, accumulation of gaseous analyte, and physically stable gel-like material. The first type of sensor focused solely on the PAA sensing

membrane (referred to as the PAA sensor), while the second type involved electrochemical pre-modification of the working electrode surface with electrodeposited film of MnO_2 (known as the MnO_2/PAA sensor). Both sensor types exhibited outstanding sensitivity within the low $mg\,m^{-3}$ concentration range, with detection limits of $3\,\mu g\,m^{-3}$ for the MnO_2/PAA sensor and $2\,\mu g\,m^{-3}$ for the PAA sensor. The sensors demonstrated favorable operation even in the presence of selected interfering gaseous compounds and were successfully tested in real environments. Moreover, our comprehensive study unveiled the superior electroanalytical performance of the PAA sensor, which also offered the advantage of simpler and faster preparation. This particular approach has established a solid foundation for further advancements in the development of sensitive, selective, and robust gas sensing systems. Such systems hold significant potential for diverse applications, including environmental monitoring, food safety (disinfection), preservation of cultural heritage, clinical diagnostics through breath analysis, mitigation of occupational health hazards, and security screening.

2. **Manuscript:** This study demonstrates the remarkable combination of the advantageous physicochemical properties of 2D MXene material ($Ti_3C_2T_x$), the stabilizing effect of chitosan, and the redox activity of a ferrocyanide-modified screen-printed carbon electrode. The electrochemical signal, as a consequence of the chemical and electrochemical (reduction) reaction of H_2O_2 at the ferrocyanide-modified screen-printed carbon electrode surface, was enhanced by the electrocatalytic properties of the MXene material. Moreover, we demonstrated favorable immobilization/stabilization properties of chitosan towards MXene, enabling the entrapment of MXene at the electrode surface and improving its chemical stability. This phenomenon was also demonstrated through a short electrochemical study. Together, these elements contribute to an ultrasensitive and accurate point-of-interest detection of low-concentration levels of gaseous H_2O_2. By incorporating a poly(acrylic acid)-based membrane into our sensor architecture, we took advantage of its multifunctional properties to accomplish two essential tasks simultaneously, i.e., first, the membrane acted as an electrolyte, facilitating the necessary ion transport and enabling efficient electrochemical reactions/detection at the sensor interface, and second, it served as an ideal medium for the accumulation of the gaseous analyte, providing improved sensitivity and reliable detection of gaseous H_2O_2. The developed sensor showed exceptional performance in the cathodic potential range, ensuring enhanced interference-free operation. It exhibited excellent reproducibility between sensors, favorable stability, and a very low detection limit of 4 $\mu g\ m^{-3}$ (ppbv). To demonstrate the practical applicability of the $Ti_3C_2T_x$ MXene-based gas sensor, real human hair was treated with a bleaching agent, and the sensor successfully measured the H_2O_2 generated during the process.

Given the fulfillment of all hypotheses, the remarkable performance of the electrochemical gas sensors highlighted in this dissertation can be further interpreted by comparing them with other electrochemical gas sensors in a comparative manner. Despite the increasing research interest in gaseous electrochemical H_2O_2 sensors due to their versatile importance and applications in industrial and biological processes, the construction of electrochemical sensors for the detection of gaseous H_2O_2 remains a

challenge, along with relatively limited reports. This scarceness can be attributed to several factors, primarily the inherent properties of gaseous H_2O_2 molecules, including their rapid degradation under the influence of UV radiation, susceptibility to environmental variables like temperature and humidity, etc. These properties have considerably influenced the progression of electrochemical gas sensor development in this specific context. Given the limited availability of electrochemical sensors designed specifically for detecting gaseous H_2O_2, the impact and importance of the presented sensors in the dissertation become even more pronounced.

A relatively strong redox activity of H_2O_2 is pivotal for its detection through various electrochemical methods. Among these methods, electrochemical sensors hold a prominent position predominantly due to their higher sensitivity, selectivity, cost-effectiveness, shorter response times, and potential for miniaturization. At this point, it is important to note that there exist numerous studies addressing the development of H_2O_2 sensors for liquid samples; probably as the most recognized are the sensors for measuring blood glucose. Within the domain of electrochemical sensors, amperometric sensors stand out for their simplicity and ease of operation. They exhibit high selectivity, as target analytes possess specific redox signals depending upon their chemical structures. By tuning the applied potential to match the oxidation/reduction potential of a particular analyte, amperometric sensors can selectively target and quantify that specific compound. For example, J. Kulys is credited with pioneering one of the early amperometric sensors designed for the detection of gaseous H_2O_2 [193]. This sensor adopted a flow-through configuration featuring a three-electrode system composed of a platinum electrode, a silver/silver chloride reference electrode, and a titanium auxiliary electrode. It operated within a buffer solution containing 0.05-1.0 M sodium acetate at a pH of 5.5, complemented by 0.01–1.0 M potassium chloride. Air was introduced into the sensor via a membrane air pump to facilitate the analysis, with flow rates of either 0.5 or 1.0 l/min. The sensor exhibited a commendably low limit of detection, calculated at 0.01 ppmv, although the response time was found to vary with the concentration of H_2O_2 vapor. A noteworthy limitation of this sensor was its stability, which affected particularly its sensitivity. Additionally, altering the airflow, transitioning from 1.0 to 0.5 l/min, led to an increased response time of approximately 20-30%. Furthermore, the sensor's selectivity remained unexplored; it was presumed that the utilization of an acetate buffer solution and the relatively low platinum electrode potential would mitigate interference, though it was acknowledged that certain gases, such as H_2S, could potentially affect the determination of H_2O_2. S. D. Holmstrom and J. A. Cox introduced an innovative approach based on a base-catalyzed sol-gel process for H_2O_2 detection [194]. Their method incorporated Triton X-114 surfactant to enhance sensitivity and a 1.3 M $MgCl_2$ solution within the sol. The outcome was the creation of material capable of extracting H_2O_2 from the gas phase while simultaneously acting as electrolytes for the voltammetric oxidation of HO_2^{-1} species. Remarkably, this was achieved without the need for a contacting liquid phase. Their sensor employed a combination of techniques, including a 60-minute preconcentration step via solid-phase extraction into the xerogel's pore water, followed by differential pulse voltammetry. Such an approach delivered an impressive detection limit of 10.2 ppbv H_2O_2. However, it is important to note certain limitations of this sensor; it exhibited poorer reproducibility, extended recovery times between measurements, which diminished its overall sensitivity, and challenges regarding selectivity. Specifically, the system could not differentiate among gases that displayed electroactivity at approximately 0.7 V, potentially introducing interference issues for specific applications. V. Mirceski et al. conducted a comprehensive investigation focusing on the kinetics and mechanisms underlying an H_2O_2 sensor [154]. This sensor featured a screen-printed carbon electrode or glassy carbon electrode with a film consisting of 1%

aqueous polyacrylic acid and Cu^{2+} ions. The researchers employed cyclic staircase voltammetry (CV), square-wave voltammetry (SWV), and chronoamperometry (CA) to scrutinize the redox reactions involving the Cu^{2+}/Cu^{+} couple, which also functioned as a redox mediator facilitating the reduction of H_2O_2. In terms of sensitivity, the limits of detection were determined for each technique; CV exhibited a detection limit of $3.49 \cdot 10^{-2}$ µg dm^{-3}, SWV demonstrated a detection limit of $1.44 \cdot 10^{-1}$ µg dm^{-3}, and CA showcased a detection limit of $4.58 \cdot 10^{-2}$ µg dm^{-3}. Importantly, these measurements were obtained following a one-minute gas equilibration period. Similarly, V. Jovanovski et al. presented an H_2O_2 gas sensor design, which incorporated a gel electrolyte containing a mixture of polyacrylic acid and NaOH and integrated Cu(II) ions to serve as a redox mediator [195]. This sensor was prepared on readily available screen-printed carbon electrodes and showed a detection limit of 0.53 mg m^{-3}, with a 5-minute accumulation time employed during the measurements.

On the other hand, chemiresistive gas sensors, commonly referred to as chemiresistors, are sensor devices relying on various (semiconducting) materials to alter their electrical resistance in response to alterations in the surrounding chemical environment or the presence of an analyte. A fundamental chemiresistor setup comprises a sensing material that either bridges the gap between two electrodes or coats a pair of interdigitated electrodes – a design characterized by two comb-shaped arrays of metallic electrodes interlocking with each other. The sensing material's intrinsic resistance can be adjusted based on the presence or absence of the analyte of interest. When exposed to the target analyte, interactions transpire between the analyte molecules and the sensing material, leading to discernible fluctuations in the resistance readings. Chemiresistors designed for gaseous analyte detection exhibit favorable analytical features, including high sensitivity and rapid detection times. However, it is essential to recognize that the effectiveness of these sensors strongly relies on the choice of sensing materials incorporated within their architecture. The selection of sensing materials can significantly enhance the sensor's overall performance, elevating its sensitivity and responsiveness. Despite these advantages, chemiresistors do present certain limitations. Typically, they exhibit poorer selectivity, making them more susceptible to interference from other compounds when compared to electrochemical, i.e., voltammetric sensors for gaseous H_2O_2. Additionally, many chemiresistors require elevated operating temperatures, which can be a drawback in terms of energy efficiency and operational convenience. F. I. Bohrer et al. studied crafting chemiresistor arrays constructed from ultra-thin films (50 nm) of metallophthalocyanines (MPcs) [196]. These MPcs, characterized by their redox-selective nature, exhibited the ability to detect vaporized H_2O_2 with good sensitivity. In cobalt phthalocyanine sensors, the current decreased, while in nickel, copper, and metal-free phthalocyanine sensors, the current increased in response to the presence of H_2O_2; the phenomenon was attributed to the catalytic oxidation (and reduction) of H_2O_2 at the phthalocyanine surface. This marked the first example of such a sensor system. The intrinsic variability linked to the metal center of the phthalocyanines holds great promise for selectivity, although it should be noted that the sensor's performance in the presence of other potentially interfering gaseous molecules remains practically untested. The reported detection limit of 50 ppb, achieved through a combination of preconcentration and a 10-minute detection time, demonstrates good sensitivity at the operating temperature of 50 ± 0.1 °C. However, it is important to acknowledge that a 90-minute recovery period between measurements can be somewhat limiting for the practical application of this sensor. J.-S. Lee et al. engineered an H_2O_2 vapor sensor utilizing advanced nanocomposites [197]. Their design incorporated nanofibers comprising a porphyrin derivative known as oxo-[5,10,15,20-tetra(4 pyridyl)porphyrinato] titanium(IV) (TiOTPyP) and single-walled carbon nanotubes (SWCNTs). What made this sensor

advantageous was its ability to operate efficiently at room temperature. This sensor demonstrated rapid response and recovery times, particularly within the H_2O_2 vapor concentration range of 0.1 to 10 ppm. Notably, the sensor's selectivity was tested, revealing negligible responses to various potential interferents such as carbon monoxide, toluene, acetone, hexane, and NO and NO_2. While there was a weak response to ammonia, it remained within acceptable limits for practical application. Furthermore, the sensor's stability was assessed over a span of 100 days, and the results were satisfactory. However, it is worth noting that humidity did exhibit a slight influence, i.e., causing a marginal decrease in performance of about 5%. J. E. Giaretta et al. created a paper-based sensor composed of poly(3,4 ethylenedioxythiophene) and poly(styrenesulfonate) (PEDOT: PSS), embellished with horseradish peroxidase, designed for the detection of H_2O_2 molecules in both liquid and gas phases [142]. Their sensor demonstrated a clear relationship between its electrical resistance signal and the concentration of H_2O_2. This correlation was found to be strongly dependent on the level of the integrated enzyme. The sensor exhibited a few limitations, like relatively prolonged detection times, whereas the maximum performance could be achieved only under conditions of 100% humidity, which could restrict its utility in environments with lower moisture content. Additionally, while the detection limit was determined for the detection in liquid samples, it was not assessed for gas-phase detection. X. Xie et al. have introduced a composite material consisting also of poly(3,4-ethylenedioxythiophene) and polystyrene sulfonate (PEDOT: PSS) doped with ammonium titanyl oxalate (ATO) [198]. The composite material serves as the basis for a chemiresistive sensor designed specifically for detecting H_2O_2 vapor, primarily for breath analysis. The sensor exhibited a relatively rapid detection time of 14 minutes. However, its optimal performance in terms of detection speed was achieved under high-humidity conditions.

Finally, we can conclude that this research project has achieved important milestones in the challenging field of electrochemical gas sensing, explicitly in the sensing of gaseous H_2O_2 as an important and omnipresent analyte, by (i) improving the electrochemical properties of disposable screen-printed carbon electrodes, (ii) studying and selecting suitable modification (nano)materials, (iii) developing innovative sensing membranes, and (iv) establishing sensitive and selective quantification methodologies for convenient detection of low levels of gaseous H_2O_2. Through these advances, we successfully demonstrated that (v) the detection of gaseous H_2O_2 is possible in both simulated and real environments, even at its very low concentration levels (ppbv). Moreover, the presented overview has conclusively demonstrated that, in comparison to other reported research on the electrochemical H_2O_2 gas sensors, the sensors developed in this research project exhibit superior performance across nearly every aspect of their electroanalytical functionalities.

Table 4.1: Published data for detected concentrations of gaseous H_2O_2

Technique	Linear detection range	LOD	Interference	Response time [s]	Ref.
Amperometry	0.05–1.0 mg m^{-3}	0.01 ppmv	Not tested	< 90	[193]
Voltammetry	96–5400 ppbv	10.2 ppbv	Nitrogen oxides, sulfur dioxide	3600	[194]
Cyclic staircase Voltammetry	0–10 mmol dm^{-3}	3.49 $\cdot 10^{-2}$ µg dm^{-3}	Not tested	60	[154]
Pulse Amperometry	10–100 mg m^{-3}	0.53 mg m^{-3}	/	300	[195]
Phthalocyanine Chemiresistors	15–60 ppm	50 ppb	Not tested	600	[196]
Porphyrin Nanofiber Chemiresistors	0.1–10 ppm	2 ppb	CO, C_7H_8, NH_3, acetone, hexane, NO, NO_2	12–40 s	[197]
Chemiresistor	61.3 $\cdot 10^{-9}$–61.3 $\cdot 10^{-6}$ M	61.3 $\cdot 10^{-9}$ M	Not tested	3600	[142]
Chemiresistor	10.5–1.0 ppm	1 ppm	Not tested	840–1020	[198]
Cyclic voltammetry	15–121 mg m^{-3}	2, 3 µg m^{-3}	Sodium nitrite	720	Our sensors
Cyclic voltammetry	0.5–30 mg m^{-3}	4 µg m^{-3}	/	1200	Our sensor

References

[1] S. A. Penkett, B. J. Bandy, C. E. Reeves, D. Mckenna and P. Hignett, "Measurements of peroxides in the atmosphere and their relevance to the understanding of global tropospheric chemistry," *Faraday Discussions,* vol. 100, pp. 155-174, 1995.

[2] W. R. Stockwell, "On the HO_2 + HO_2 reaction: Its misapplication in atmospheric chemistry models," *Journal of Geophysical Research,* vol. 100, no. D6, pp. 11695-11698, 1995.

[3] P. J. Crutzen and M. G. Lawrence , "The Impact of Precipitation Scavenging on the Transport of Trace Gases: A 3-Dimensional Model Sensitivity Study," *Journal of Atmospheric Chemistry,* vol. 37, p. 81–112, 2000.

[4] M. G. Lawrence and P. J. Crutzen, "The impact of cloud particle gravitational settling on soluble trace gas distributions," *Tellus B: Chemical and Physical Meteorology,* vol. 50, no. 3, pp. 263-289, 1998.

[5] D. R. Hastie, P. B. Shepson, S. Sharma and H. I. Schiff, "The influence of the nocturnal boundary layer on secondary trace species in the atmosphere at Dorset, Ontario," *Atmospheric Environment. Part A. General Topics,* vol. 27, no. 4, pp. 533-541, 1993.

[6] W. J. Cooper and R. G. Zika, "Photochemical Formation of Hydrogen Peroxide in Surface and Ground Waters Exposed to Sunlight," *Science,* vol. 220, no. 4598, pp. 711-712, 1983.

[7] W. M. Draper and D. G. Crosby, "The photochemical generation of hydrogen peroxide in natural waters," *Archives of Environmental Contamination and Toxicology,* vol. 12, p. 121–126, 1983.

[8] T. E. Graedel and K. I. Goldberg, "Kinetic studies of raindrop chemistry: 1. Inorganic and organic processes," *Journal of Geophysical Research,* vol. 88, no. C15, pp. 10865-10882, 1983.

[9] M. D. Gurol and A. Akata, "Kinetics of ozone photolysis in aqueous solution," *An Official Publication of the American Institute of Chemical Engineers,* vol. 42, no. 11, pp. 3283-3292, 1996.

[10] C. Anastasio, B. C. Faust and J. C. Rao, "Aromatic carbonyl compounds as aqueous-phase photochemical sources of hydrogen peroxide in acidic sulfate aerosols, fogs and clouds: 1. non-phenolic methoxybenzaldehydes and methoxyacetophenones with reductants (phenols)," *Environmental Science and Technology,* vol. 31, pp. 218-232, 1996.

[11] W. B. Brown, I. H. Hillier, A. J. Masters, I. J. Palmer, D. H. V. Dos Santos, M. Stein and M. A. Vincent, "Modelling the photonucleation of water vapour by UV in the presence of oxygen and the absence of pollutants," *Faraday Discussions,* vol. 100, pp. 253-267, 1995.

[12] Y. Zuo and Y. Deng, "Evidence for the production of hydrogen peroxide in rainwater by lightning during thunderstorms," *Geochimica et Cosmochimica Acta,* vol. 63, no. 19–20, pp. 3451-3455, 1999.

[13] O. Legrini, E. Oliveros and A. M. Braun, "Photochemical processes for water treatment," *Chemical Reviews,* vol. 93, no. 2, p. 671–698, 1993.

[14] K. Stemmler and U. Von Gunten, "OH radical-initiated oxidation of organic compounds in atmospheric water phases: part 1. Reactions of peroxyl radicals derived from 2-butoxyethanol in water," *Atmospheric Environment,* vol. 34, no. 25, pp. 4241-4252, 2000.

[15] M. E. Lindsey and M. A. Tarr, "Quantitation of hydroxyl radical during Fenton oxidation following a single addition of iron and peroxide," *Chemosphere,* vol. 41, no. 3, pp. 409-417, 2000.

[16] A. Babuponnusami and K. Muthukumar, "A review on Fenton and improvements to the Fenton process for wastewater treatment," *Journal of Environmental Chemical Engineering,* vol. 2, no. 1, pp. 557-572, 2014.

[17] T. Javeed, R. Nawaz, S. A. Al-Hussain, A. Irfan, M. A. Irshad, S. Ahmad and M. E. A. Zaki, "Application of Advanced Oxidation Processes for the Treatment of Color and Chemical Oxygen Demand of Pulp and Paper Wastewater," *Water,* vol. 15, no. 7, p. 1347, 2023.

[18] A. O. Ayeni, F. K. Hymore, S. N. Mudliar, S. C. Deshmukh, D. B. Satpute, J. A. Omoleye and R. A. Pandey, "Hydrogen peroxide and lime based oxidative pretreatment of wood waste to enhance enzymatic hydrolysis for a biorefinery: Process parameters optimization using response surface methodology," *Fuel,* vol. 106, pp. 187-194, 2013.

[19] W. A. Rutala and D. J. Weber, "Disinfection and Sterilization in Health Care Facilities: What Clinicians Need to Know," *Clinical Infectious Diseases,* vol. 39, no. 5, p. 702–709, 2004.

[20] M. E. Falagas, P. C. Thomaidis, I. K. Kotsantis, K. Sgouros, G. Samonis and D. E. Karageorgopoulos, "Airborne hydrogen peroxide for disinfection of the hospital environment and infection control: a systematic review," *Journal of Hospital Infection,* vol. 78, no. 3, pp. 171-177, 2011.

[21] M. S. Noh, S. H. Jung, O. Kwon, S.-I. Lee, S.-J. Yang, E. Hahm and B.-H. Jun, "Evaluation of Sterilization Performance for Vaporized-Hydrogen-Peroxide-Based Sterilizer with Diverse Controlled Parameters," *ACS Omega,* vol. 5, no. 45, p. 29382–29387, 2020.

[22] G. McDonnell and D. A. Russell, "Antiseptics and Disinfectants: Activity, Action, and Resistance," *Clinical Microbiology Reviews,* vol. 12, no. 1, pp. 147-179, 1999.

[23] G. Rarata, K. Rokicka and P. Surmacz, "Hydrogen Peroxide as a High Energy Compound Optimal," *Central European Journal of Energetic Materials,* vol. 13, no. 3, pp. 778-790, 2016.

[24] P. Barbaccia, L. Lipocelli, G. Moschetti, N. Francesca, S. De Martino, V. Arrigo, R. Gaglio and L. Settanni, "Application of Hydrogen Peroxide to Improve the Microbiological Stability of Food Ice Produced in Industrial Facilities," *Applied Sciences,* vol. 12, no. 1, p. 210, 2022.

[25] A. M. Abdelshafy, Q. Hu, Z. Luo, Z. Ban and L. Li, "Hydrogen Peroxide from Traditional Sanitizer to Promising Disinfection Agent in Food Industry," *Food Reviews International,* 2023.

[26] J. Kaushal, S. Mehandia, G. Singh, A. Raina and S. K. Arya, "Catalase enzyme: Application in bioremediation and food industry," *Biocatalysis and Agricultural Biotechnology,* vol. 16, pp. 192-199, 2018.

[27] M. E. Quimbar, S. Q. Davis, S. T. Al-Farra, A. Hayes, V. Jovic, M. Masuda and A. R. Lippert, "Chemiluminescent Measurement of Hydrogen Peroxide in the Exhaled Breath Condensate of Healthy and Asthmatic Adults," *Analytical Chemistry,* vol. 92, no. 21, p. 14594–14600, 2020.

[28] E. Vidal, C. E. Domini, D. C. Whitehead and C. D. Garcia, "From glow-sticks to sensors: single-electrode electrochemical detection for paper-based devices," *Sensors & Diagnostics,* vol. 1, pp. 496-503, 2022.

[29] S. P. Bhattarai, N. Su and D. J. Midmore, "Oxygation Unlocks Yield Potentials of Crops in Oxygen-Limited Soil Environments," *Advances in Agronomy,* vol. 88, pp. 313-377, 2005.

[30] T. Lieke, T. Meinelt, S. H. Hoseinifar, B. Pan, D. L. Straus and C. E. W. Steinberg, "Sustainable aquaculture requires environmental-friendly treatment strategies for fish diseases," *Reviews in Aquaculture,* vol. 12, no. 2, pp. 943-965, 2020.

[31] W. J. Rogers, "7 - Sterilisation techniques for polymers," *Sterilisation of Biomaterials and Medical Devices,* pp. 151-211, 2012.

[32] H. Sies, "Role of Metabolic H2O2 Generation," *The Journal of Biological Chemistry,* vol. 289, no. 13, pp. 8735-8741, 2014.

[33] B. C. Dickinson and C. J. Chang, "Chemistry and biology of reactive oxygen species in signaling or stress responses," *Nature Chemical Biology,* vol. 7, p. 504–511, 2011.

[34] B. D'Autréaux and M. B. Toledano, "ROS as signalling molecules: mechanisms that generate specificity in ROS homeostasis," *Nature Reviews Molecular Cell Biology,* vol. 8, p. 813–824, 2007.

[35] H. Sies, "Hydrogen peroxide as a central redox signaling molecule in physiological oxidative stress: Oxidative eustress," *Redox Biology,* vol. 11, pp. 613-619, 2017.

[36] B. Halliwell and J. M. C. Gutteridge, Free Radicals in Biology and Medicine, Oxford: Oxford University Press, 2015.

[37] K. R. Messner and J. A. Imlay, "Mechanism of Superoxide and Hydrogen Peroxide Formation by Fumarate Reductase, Succinate Dehydrogenase, and Aspartate Oxidase," *The Journal of Biological Chemistry,* vol. 277, no. 45, p. 42563–42571, 2002.

[38] G.-Y. Liou and P. Storz, "Reactive oxygen species in cancer," *Free Radical Research ,* vol. 44, no. 5, p. 479–496, 2010.

[39] A. M. Day, J. D. Brown, S. R. Taylor, J. D. Rand, B. A. Morgan and E. A. Veal, "Inactivation of a Peroxiredoxin by Hydrogen Peroxide Is Critical for Thioredoxin-Mediated Repair of Oxidized Proteins and Cell Survival," *Molecular Cell,* vol. 45, no. 3, pp. 398-408, 2012.

[40] C. Wittmann, P. Chockley, S. K. Singh, L. Pase, G. J. Lieschke and C. Grabher, "Hydrogen peroxide in inflammation: messenger, guide, and assassin," *Advances in Hematology,* vol. 2012, 2012.

[41] Y. Lei, K. Wang, L. Deng, Y. Chen, E. C. Nice and C. Huang, "Redox regulation of inflammation: old elements, a new story," *Medicinal Research Reviews,* vol. 35, no. 2, pp. 306-340, 2014.

[42] R. M. Ransohoff, "How neuroinflammation contributes to neurodegeneration," *Science,* vol. 353, no. 6301, pp. 777-783, 2016.

[43] M. Hüll, M. Berger and M. Heneka , "Disease-Modifying Therapies in Alzheimer's Disease," *Drugs,* vol. 66, no. 16, p. 2075–2093, 2006.

[44] R. H. Burdon, V. Gill and C. Rice-Evans, "Oxidative Stress and Tumour Cell Proliferation," *Free Radical Research Communications,* vol. 11, no. 1-3, pp. 65-76, 1990.

[45] C. M. Doskey, V. Buranasudja, B. A. Wagner, J. G. Wilkes, J. Du, J. J. Cullen and G. R. Buettner, "Tumor cells have decreased ability to metabolize H_2O_2: Implications for pharmacological ascorbate in cancer therapy," *Redox Biology,* vol. 10, pp. 274-284, 2016.

[46] Y. Marincevic-Zuniga, J. Dahlberg, S. Nilsson, A. Raine, S. Nystedt, C. M. Lindqvist, E. C. Berglund, J. Abrahamsson, L. Cavelier, E. Forestier, M. Heyman, G. Lönnerholm, J. Nordlund and A.-C. Syvänen, "Transcriptome sequencing in pediatric acute lymphoblastic leukemia identifies fusion genes associated with distinct DNA methylation profiles," *Journal of Hematology & Oncology,* vol. 10, p. 1–14, 2017.

[47] D. L. Carden and N. D. Granger, "Pathophysiology of ischaemia–reperfusion injury," *The Journal of Pathology,* vol. 190, no. 3, pp. 255-266, 2000.

[48] N. D. Granger and P. R. Kvietys, "Reperfusion injury and reactive oxygen species: The evolution of a concept," *Redox Biology,* vol. 6, pp. 524-551, 2015.

[49] K. Tripathi and J. D. Feuerstein, "New developments in ulcerative colitis: latest evidence on management, treatment, and maintenance," *Drugs in Context,* vol. 8, no. 212572, 2019.

[50] S. Santhanam, A. Venkatraman and B. S. Ramakrishna, "Impairment of mitochondrial acetoacetyl CoA thiolase activity in the colonic mucosa of patients with ulcerative colitis," *Gut,* vol. 56, no. 11, p. 1543–1549, 2007.

[51] B. S. van Asbeck, R. Braams, J. M. Aarsman, R. C. Sprong and G. A. Groenewegen, "Hydrogen Peroxide in Blood of Patients with Sepsis Syndrome: A Realistic Phenomenon.," *Critical Care Medicine,* vol. 23, no. 1, p. A169, 1995.

[52] J. Pravda, "Hydrogen peroxide and disease: towards a unified system of pathogenesis and therapeutics," *Molecular Medicine,* vol. 26, 2020.

[53] J.-P. Bonnefont, D. Chretien, P. Rustin, B. Robinson, A. Vassault, J. Aupetit, C.

Charpentier, D. Rabier, J.-M. Saudubray and A. Munnich, "Alpha-ketoglutarate dehydrogenase deficiency presenting as congenital lactic acidosis," *The Journal of Pediatrics,* vol. 121, no. 2, pp. 255-258, 1992.

[54] W.-X. Wang, W.-L. Jiang, G.-J. Mao, M. Tan, J. Fei, Y. Li and C.-Y. Li, "Monitoring the Fluctuation of Hydrogen Peroxide in Diabetes and Its Complications with a Novel Near-Infrared Fluorescent Probe," *Analytical Chemistry,* vol. 93, no. 6, p. 3301–3307, 2021.

[55] Y. Tanaka, P. O. T. Tran, J. Harmon and P. R. Robertson, "A role for glutathione peroxidase in protecting pancreatic β cells against oxidative stress in a model of glucose toxicity," *Proceedings of the National Academy of Sciences USA,* vol. 99, no. 19, pp. 12363-12368, 2002.

[56] H. M. Kubisch, J. Wang, R. Luche, E. Carlson, T. M. Bray, C. J. Epstein and J. P. Phillips, "Transgenic copper/zinc superoxide dismutase modulates susceptibility to type I diabetes.," *Proceedings of the National Academy of Sciences USA,* vol. 91, no. 21, p. 9956–9959, 1994.

[57] F. Zhao and Q. Wang, "The protective effect of peroxiredoxin II on oxidative stress induced apoptosis in pancreatic β-cells," *Cell & Bioscience,* vol. 2, 2012.

[58] R. Hage and A. Lienke, "Applications of Transition-Metal Catalysts to Textile and Wood-Pulp Bleaching," *Angewandte Chemie,* vol. 45, no. 2, pp. 206-222, 2005.

[59] X. Liu, B. Zhang, Q. Hou, X. Wang, Y. Chen and Z. Tao, "H_2O_2 bleaching in mixed triploid poplar and acacia woodchips high-yield pulping process with substitution of 50 wt% NaOH by MgO and its kinetics study," *Industrial Crops and Products,* vol. 169, p. 113558, 2021.

[60] F. Liang, G. Fang, J. Jiao, Y. Deng, S. Han, H. Li, Q. Tian, A. Pan and B. Zhu, "Modified Hydrogen Peroxide Bleaching of Bamboo Chemo-mechanical Pulp Using Aqueous Alcohol Media," *BioResources,* vol. 14, no. 1, pp. 870-881, 2019.

[61] A. Rushdy, W. Noshy, A. Youssef and S. Kamel, "Influence of Bleaching Materials on Mechanical and Morphological Properties for Paper Conservation," *Egyptian Journal of Chemistry,* vol. 60, no. 5, pp. 893-903, 2017.

[62] F. A. P. Costa, E. M. dos Reis, J. C. R. Azevedo and J. Nozaki, "Bleaching and photodegradation of textile dyes by H_2O_2 and solar or ultraviolet radiation," *Solar Energy,* vol. 77, no. 1, pp. 29-35, 2004.

[63] P. Tang, B. Ji and G. Sun, "Whiteness improvement of citric acid crosslinked cotton fabrics: H_2O_2 bleaching under alkaline condition," *Carbohydrate Polymers,* vol. 147, pp. 139-145, 2016.

[64] S. N. Chattopadhyay, N. C. Pan, A. N. Roy, K. K. Samanta and A. Khan, "Hybrid bleaching of jute yarn using hydrogen peroxide and peracetic acid," *Indian Journal of Fibre & Textile Research,* vol. 46, pp. 78-82, 2021.

[65] C. W. Jones, Applications of Hydrogen Peroxide and Derivatives, Cambridge: The Royal Society of Chemistry, 1999.

[66] J. E. Dahl and U. Pallesen, "Tooth Bleaching—a Critical Review of the Biological Aspects," *Critical Reviews in Oral Biology & Medicine,* vol. 14, no. 4, pp. 292-304, 2003.

[67] A. J. McCaslin, V. B. Haywood, B. J. Potter, G. L. Dickinson and C. M. Russell, "Assessing dentin color changes from nightguard vital bleaching," *The Journal of the American Dental Association,* vol. 130, no. 10, pp. 1485-1490, 1999.

[68] A. Papathanasiou, D. Bardwell and G. Kugel, "A clinical study evaluating a new chairside and take-home whitening system," *Compendium of Continuing Education in Dentistry,* vol. 22, no. 4, pp. 289-294, 2001.

[69] M. A. M. Sulieman, "An overview of tooth-bleaching techniques: chemistry, safety and efficacy," *Periodontology 2000,* vol. 48, no. 1, pp. 148-169, 2008.

[70] R. W. Gerlach and X. Zhou, "Vital bleaching with whitening strips: summary of clinical research on effectiveness and tolerability.," *The Journal of Contemporary Dental Practice,* vol. 2, no. 3, pp. 1-16, 2001.

[71] M. Sulieman, M. Addy and J. S. Rees, "Development and evaluation of a method in vitro to study the effectiveness of tooth bleaching," *Journal of Dentistry,* vol. 31, no. 6, pp. 415-422, 2003.

[72] C. N. Satterfield, G. M. Kavanagh and H. Resnick, "Explosive Characteristics of Hydrogen Peroxide Vapor," *Industrial & Engineering Chemistry,* vol. 43, no. 11, p. 2507–2514, 1951.

[73] B. Greene, D. L. Baker and W. Frazier, "NASA Hydrogen Peroxide Propellant Hazards Technical Manual," in *28th Joint Army Navy NASA Air Force - JANNAF*, Charleston, 2005.

[74] E. F. C. Cain, Hydrogen Peroxide Handbook, Los Angeles: U.S. Air Force Rocket Propulsion Laboratory, 1967.

[75] J. E. Parmeter, "Historical Survey: German Research on Hydrogen Peroxide/Alcohol Explosives.," 01 01 2015. [Online]. Available: https://www.osti.gov/servlets/purl/1177376/.

[76] E. S. Shanley and F. P. Greenspan, "Highly Concentrated Hydrogen Peroxide," *Industrial and Engineering Chemistry,* vol. 39, no. 12, p. 1536–1543, 1947.

[77] M. Ventura, E. Wernimont, S. Heister and S. Yuan, "Rocket Grade Hydrogen Peroxide (RGHP) for use in Propulsion and Power Devices - Historical Discussion of Hazards," *Aerospace Research Central,* 2012.

[78] E. S. Shanley and H. O. Kauffmann, "Peroxide-glycerol explosive". United States Patent US2452074A, 26 10 1948.

[79] E. Bouillet, J.-C. Colery, C. Declerck and P. Ledoux, "Process for the Manufacture of Explosive Cartridges, and Explosive Cartridges Obtained Using the Said Process". United States Patent 4942800, 03 12 1987.

[80] M. Polis, K. Nikolczuk, A. Maranda, A. Stolarczyk and T. Jarosz, "Theft-Safe Explosive Mixtures Based on Hydrogen Peroxide: Study of Properties and Built-In Self-Deactivation Kinetics," *Materials,* vol. 14, no. 19, p. 5818, 2021.

[81] T. M. Klapötke and T. Wloka, "Peroxide explosives," *PATAI's Chemistry of Functional Groups,* pp. 1-28, 2014.

[82] P. Hou, P. Ju, L. Hao, C. Chen, F. Jiang, H. Ding and C. Sun, "Colorimetric determination of hydrogen peroxide based on the robust peroxidase-like activities of

flower-like YVO_4 microstructures," *Colloids and Surfaces A: Physicochemical and Engineering Aspects,* vol. 618, p. 126427, 2021.

[83] B. Zhou, J. Wang, Z. Guo, H. Tan and X. Zhu, "A simple colorimetric method for determination of hydrogen peroxide in plant tissues," *Plant Growth Regulation,* vol. 49, p. 113–118, 2006.

[84] N. A. Burmistrova , O. A. Kolontaeva and A. Duerkop, "New Nanomaterials and Luminescent Optical Sensors for Detection of Hydrogen Peroxide," *Chemosensors,* vol. 3, no. 4, pp. 253-273, 2015.

[85] Z. Wang, B. Dong, G. Feng, H. Shan, Y. Huan and Q. Fei, "Water-soluble Hemin-mPEG-enhanced Luminol Chemiluminescence for Sensitive Detection of Hydrogen Peroxide and Glucose," *Analytical Sciences,* vol. 35, p. 1135–1140, 2019.

[86] H. Guo, H. Aleyasin, B. C. Dickinson, R. E. Haskew-Layton and R. R. Ratan, "Recent advances in hydrogen peroxide imaging for biological applications," *Cell & Bioscience,* vol. 4, 2014.

[87] D.-J. Zheng, Y.-S. Yang and H.-L. Zhu, "Recent progress in the development of small-molecule fluorescent probes for the detection of hydrogen peroxide," *TrAC Trends in Analytical Chemistry,* vol. 118, pp. 625-651, 2019.

[88] K. Żamojć, M. Zdrowowicz, D. Jacewicz, D. Wyrzykowski and L. Chmurzyński, "Fluorescent Probes Used for Detection of Hydrogen Peroxide under Biological Conditions," *Critical Reviews in Analytical Chemistry,* vol. 46, no. 3, pp. 171-200, 2016.

[89] X. Zheng and Z. Guo, "Potentiometric determination of hydrogen peroxide at MnO_2-doped carbon paste electrode," *Talanta,* vol. 50, no. 6, pp. 1157-1162, 2000.

[90] J. F. Baez, M. Compton, S. Chahrati, R. Cánovas, P. Blondeau and F. J. Andrade, "Controlling the mixed potential of polyelectrolyte-coated platinum electrodes for the potentiometric detection of hydrogen peroxide," *Analytica Chimica Acta,* vol. 1097, pp. 204-213, 2020.

[91] V. S. Haritha, A. Vijayan, S. R. S. Kumar and R. B. Rakhi, "Voltammetric determination of hydrogen peroxide using MoS_2 modified glassy carbon electrodes," *Materials Letters,* vol. 301, p. 130258, 2021.

[92] A. L. Sanford, S. W. Morton, K. L. Whitehouse, H. M. Oara, L. Z. Lugo-Morales, J. G. Roberts and L. A. Sombers, "Voltammetric Detection of Hydrogen Peroxide at Carbon Fiber Microelectrodes," *Analytical Chemistry,* vol. 82, no. 12, p. 5205–5210, 2010.

[93] C. Wei, C. Shu, R. Qiong-Qiong, W. Wei and Z. Yuan-Di, "Recent advances in electrochemical sensing for hydrogen peroxide: a review," *Analyst,* vol. 137, pp. 49-58, 2012.

[94] H. Liu, L. Weng and C. Yang, "A review on nanomaterial-based electrochemical sensors for H_2O_2, H_2S and NO inside cells or released by cells," *Microchimica Acta,* vol. 184, p. 1267–1283, 2017.

[95] H. Shamkhalichenar and J.-W. Choi, "Review—Non-Enzymatic Hydrogen Peroxide Electrochemical Sensors Based on Reduced Graphene Oxide," *Journal of The Electrochemical Society,* vol. 167, p. 037531, 2020.

[96] M. S. P. Rao, A. R. M. Rao, K. V. Ramana and S. R. Sagi, "Thallimetric oxidations—V: Titrimetric and spectrophotometric determination of hydrogen peroxide," *Talanta,* vol. 37, no. 7, pp. 753-755, 1990.

[97] V. Gupta, P. Mahbub, P. N. Nesterenko and B. Paull, "A new 3D printed radial flow-cell for chemiluminescence detection: Application in ion chromatographic determination of hydrogen peroxide in urine and coffee extracts," *Analytica Chimica Acta,* vol. 1005, pp. 81-92, 2018.

[98] M. Song, J. Wang, B. Chen and L. Wang, "A Facile, Nonreactive Hydrogen Peroxide (H_2O_2) Detection Method Enabled by Ion Chromatography with UV Detector," *Analytical Chemistry,* vol. 89, no. 21, p. 11537–11544, 2017.

[99] H. A. Khorami, J. F. Botero-Cadavid, P. Wild and N. Djilali, "Spectroscopic detection of Hydrogen peroxide with an optical fiber probe using chemically deposited Prussian blue," *Electrochimica Acta,* vol. 115, pp. 416-424, 2014.

[100] Q. Zhang, S. Fu, H. Li and Y. Liu, "A Novel Method for the Determination of Hydrogen," *BioResources,* vol. 8, no. 3, pp. 3699-3705, 2013.

[101] P. Bollella, G. Fusco, C. Tortolini, G. Sanzò, G. Favero, L. Gorton and R. Antiochia, "Beyond graphene: Electrochemical sensors and biosensors for biomarkers detection," *Biosensors and Bioelectronics,* vol. 89, pp. 152-166, 2017.

[102] Y. Yu, M. Pan, J. Peng, D. Hu, Y. Hao and Z. Qian, "A review on recent advances in hydrogen peroxide electrochemical sensors for applications in cell detection," *Chinese Chemical Letters,* vol. 33, no. 9, pp. 4133-4145, 2022.

[103] M. Feng, H. Han, J. Zhang and H. Tachikawa, CHAPTER 15 - Electrochemical sensors based on carbon nanotubes, Cambridge: Academic Press, 2008.

[104] P. Murugan, R. D. Nagarajan, A. K. Sundramoorthy, D. Ganapathy, R. Atchudan, D. Nallaswamy and A. Khosla, "Electrochemical Detection of H_2O_2 Using an Activated Glassy Carbon Electrode," *ECS Sensors Plus,* vol. 1, p. 034401, 2022.

[105] T. Ahmad, A. Iqbal, S. A. Halim , J. Uddin, A. Khan, S. El Deeb and A. Al-Harrasi, "Recent Advances in Electrochemical Sensing of Hydrogen Peroxide (H_2O_2) Released from Cancer Cells," *Nanomaterials,* vol. 12, no. 9, p. 1475, 2022.

[106] G. Maduraiveeran, M. Kundu and M. Sasidharan, "Electrochemical detection of hydrogen peroxide based on silver nanoparticles via amplified electron transfer process," *Journal of Materials Science,* vol. 53, p. 8328–8338, 2018.

[107] N. Jaffrezic-Renault and S. V. Dzyadevych, "Conductometric Microbiosensors for Environmental Monitoring," *Sensors,* vol. 8, no. 4, pp. 2569-2588, 2008.

[108] N. B. Tanvir, O. Yurchenko, E. Laubender, R. Pohle, O. von Sicard and G. A. Urban, "Zinc peroxide combustion promoter in preparation of CuO layers for conductometric CO_2 sensing," *Sensors and Actuators B: Chemical,* vol. 257, pp. 1027-1034, 2018.

[109] L. Li, W. Guo, Y. Lin, D. Tang and J. Liu, "Facile and feasible conductometric immunoanalytical assay for alpha-fetoprotein using platinum-functionalized graphitic carbon nitride nanosheets," *Analytical Methods,* vol. 10, pp. 4886-4893, 2018.

[110] W. Nouira, A. Maaref, H. Elaissari, F. Vocanson, M. Siadat and N. Jaffrezic-

Renault, "Comparative study of conductometric glucose biosensor based on gold and on magnetic nanoparticles," *Materials Science and Engineering: C,* vol. 33, no. 1, pp. 298-303, 2013.

[111] A. A. Shul'ga and T. D. Gibson, "An alternative microbiosensor for hydrogen peroxide based on an enzyme field effect transistor with a fast response," *Analytica Chimica Acta,* vol. 296, no. 2, pp. 163-170, 1994.

[112] T. A. Sergeyeva, N. V. Lavrik, A. E. Rachkov, Z. I. Kazantseva, S. A. Piletsky and A. V. El'skaya, "Hydrogen peroxide – sensitive enzyme sensor based on phthalocyanine thin film," *Analytica Chimica Acta,* vol. 391, no. 3, pp. 289-297, 1999.

[113] J. Wang, Analytical Electrochemistry, Weinheim, Germany: Wiley-VCH, 1994.

[114] R. A. D. de Faria, L. G. D. Heneine, T. Matencio and Y. Messaddeq, "Faradaic and non-faradaic electrochemical impedance spectroscopy as transduction techniques for sensing applications," *International Journal of Biosensors & Bioelectronics,* vol. 5, no. 1, pp. 29-31, 2019.

[115] A. Lasia, Electrochemical Impedance Spectroscopy and its Applications, Sherbrooke, Canada: Springer New York, 2014.

[116] R. Raccichini, M. Amores and G. Hinds, "Critical Review of the Use of Reference Electrodes in Li-Ion Batteries: A Diagnostic Perspective," *Batteries,* vol. 5, no. 1, p. 12, 2019.

[117] T. Kim, W. Choi, H.-C. Shin, J.-Y. Choi, J. M. Kim, M.-S. Park and W.-S. Yoon, "Applications of Voltammetry in Lithium Ion Battery Research," *Journal of Electrochemical Science and Technology,* vol. 11, no. 1, pp. 14-25, 2020.

[118] D. Obrez, M. Kolar, N. Tasić and S. B. Hočevar, "Study of different types of copper electrodes for anodic stripping voltammetric detection of trace metal ions," *Electrochimica Acta,* vol. 457, p. 142480, 2023.

[119] J. Wang, J. Lu, S. B. Hočevar, P. A. M. Farias and B. Ogorevc, "Bismuth-Coated Carbon Electrodes for Anodic Stripping Voltammetry," *Analytical Chemistry,* vol. 72, no. 14, p. 3218–3222, 2000.

[120] S. B. Hočevar, I. Švancara, B. Ogorevc and K. Vytřas, "Antimony Film Electrode for Electrochemical Stripping Analysis," *Analytical Chemistry,* vol. 79, no. 22, p. 8639–8643, 2007.

[121] D. Harvey, Modern Analytical Chemistry, Greencastle, Indiana: James M. Smith, 2000.

[122] A. Hayat and J. L. Marty, "Disposable Screen Printed Electrochemical Sensors: Tools for Environmental Monitoring," *Sensors,* vol. 14, no. 6, pp. 10432-10453, 2014.

[123] R. W. Murray, A. G. Ewing and R. A. Durst, "Chemically modified electrodes. Molecular design for electroanalysis," *Analytical Chemistry,* vol. 59, no. 5, pp. 379A-390A, 1987.

[124] A. Hayat, C. Yang, A. Rhouati and J. L. Marty, "Recent Advances and Achievements in Nanomaterial-Based, and Structure Switchable Aptasensing Platforms for Ochratoxin A Detection," *Sensors,* vol. 13, no. 11, pp. 15187-15208,

2013.

[125] A. Hayat, S. Andreescu and J.-L. Marty, "Design of PEG-aptamer two piece macromolecules as convenient and integrated sensing platform: application to the label free detection of small size molecules," *Biosensors and Bioelectronics,* vol. 45, pp. 168-173, 2013.

[126] A. Hayat, W. Haider, M. Rolland and J.-L. Marty, "Electrochemical grafting of long spacer arms of hexamethyldiamine on a screen printed carbon electrode surface: application in target induced ochratoxin A electrochemical aptasensor," *Analyst,* vol. 138, pp. 2951-2957, 2013.

[127] A. Heller and B. Feldman, "Electrochemical Glucose Sensors and Their Applications in Diabetes Management," *Chemical Reviews,* vol. 108, no. 7, p. 2482–2505, 2008.

[128] J. D. Newman and A. P. F. Turner, "Home blood glucose biosensors: a commercial perspective," *Biosensors and Bioelectronics,* vol. 20, no. 12, pp. 2435-2453, 2005.

[129] J. P. Hart and S. A. Wring, "Recent developments in the design and application of screen-printed electrochemical sensors for biomedical, environmental and industrial analyses," *TrAC Trends in Analytical Chemistry,* vol. 16, no. 2, pp. 89-103, 1997.

[130] T. N. Murakami, N. Kawashima and T. Miyasaka, "A high-voltage dye-sensitized photocapacitor of a three-electrode system," *Chemical Communications,* pp. 3346-3348, 2005.

[131] G. J. Moody, G. S. Sanghera and J. D. R. Thomas, "Amperometric enzyme electrode system for the flow injection analysis of glucose," *Analyst,* vol. 111, pp. 605-609, 1986.

[132] N. Thiyagarajan, J.-L. Chang, K. Senthilkumar and J.-M. Zen, "Disposable electrochemical sensors: A mini review," *Electrochemistry Communications,* vol. 38, pp. 86-90, 2014.

[133] K. C. Honeychurch and J. P. Hart, "Screen-printed electrochemical sensors for monitoring metal pollutants," *TrAC - Trends in Analytical Chemistry,* vol. 22, no. 7, pp. 456-469, 2003.

[134] "Metrohm DropSens," DropSens, 2022. [Online]. Available: https://www.dropsens.com/en/screen_printed_electrodes_pag.html.

[135] M. Khairy, R. O. Kadara and C. E. Banks, "Electroanalytical sensing of nitrite at shallow recessed screen printed microelectrode arrays," *Analytical Methods,* vol. 2, pp. 851-854, 2010.

[136] R. O. Kadara, N. Jenkinson and C. E. Banks, "Screen printed recessed microelectrode arrays," *Sensors and Actuators B: Chemical,* vol. 142, no. 1, pp. 342-346, 2009.

[137] P. Fanjul-Bolado, D. Hernández-Santos, P. J. Lamas-Ardisana, A. Martín-Pernía and A. Costa-García, "Electrochemical characterization of screen-printed and conventional carbon paste electrodes," *Electrochimica Acta,* vol. 53, no. 10, pp. 3635-3642, 2008.

[138] T. Romih , I. Konjević, L. Žibret , I. Fazarinc, A. Beltram, D. Majer, M. Finšgar and S. B. Hočevar, "The Effect of Preconditioning Strategies on the Adsorption of Model Proteins onto Screen-Printed Carbon Electrodes," *Sensors,* vol. 22, no. 11, p.

4186, 2022.

[139] A. Lobato, M. Šubic, T. Romih, L. Žibret, D. Metarapi, M. Benčina, R. Jerala, K. Vidović, S. B. Hočevar and N. Tasić, "Development of a simple gelatin-based sensing platform for the sensitive label-free impedimetric detection of SARS-CoV-2," *Electrochimica Acta,* vol. 463, p. 142823, 2023.

[140] F. V. Lovecchio, E. S. Gore and D. H. Busch, "Oxidation and reduction behavior of macrocyclic complexes of nickel. Electrochemical and electron spin resonance studies," *Journal of the American Chemical Society,* vol. 69, no. 10, p. 3109–3118, 1974.

[141] R. A. Marcus, "On the Theory of Oxidation-Reduction Reactions Involving Electron Transfer.," *The Journal of Chemical Physics,* vol. 24, no. 5, pp. 966-978, 1956.

[142] J. E. Giaretta, F. Oveissi, F. Dehghani and S. Naficy, "Paper-Based, Chemiresistive Sensor for Hydrogen Peroxide Detection," *Advanced Materials Technologies,* vol. 6, no. 4, p. 2001148, 2021.

[143] S.-W. Chiu and K.-T. Tang, "Towards a Chemiresistive Sensor-Integrated Electronic Nose: A Review," *Sensors,* vol. 13, no. 10, pp. 14214-14247, 2013.

[144] B. Williamson and V. K. La Mer, "The Kinetics of Activation—Diffusion Controlled Reactions in Solution. The Temperature Dependence of the Quenching of Fluorescence," *Journal of the American Chemical Society,* vol. 70, no. 2, p. 717–721, 1948.

[145] R. A. Durst, "Chemically modified electrodes: Recommended terminology and definitions," *Pure and Applied Chemistry,* vol. 69, no. 6, pp. 1317-1324, 1997.

[146] W. Kutner, J. Wang , M. L'her and R. P. Buck, "Analytical aspects of chemically modified electrodes: Classification, critical evaluation and recommendations (IUPAC Recommendations 1998)," *Pure and Applied Chemistry,* vol. 70, no. 6, pp. 1301-1318, 1998.

[147] R. Gulaboski, V. Mirčeski, R. Kappl, M. Hoth and M. Bozem, "Review—Quantification of Hydrogen Peroxide by Electrochemical Methods and Electron Spin Resonance Spectroscopy," *Journal of The Electrochemical Society,* vol. 166, no. 8, pp. G82-G101, 2019.

[148] S. Chen, R. Yuan, Y. Chai and F. Hu , "Electrochemical sensing of hydrogen peroxide using metal nanoparticles: a review," *Microchimica Acta,* vol. 180, p. 15–32, 2013.

[149] D. W. Kimmel, G. LeBlanc, M. E. Meschievitz and D. E. Cliffel, "Electrochemical Sensors and Biosensors," *Analytical Chemistry,* vol. 84, no. 2, p. 685–707, 2012.

[150] N. S. Sangeetha and S. S. Narayanan, "Amperometric H_2O_2 sensor based on gold nanoparticles/poly (celestine blue) nanohybrid film," *SN Applied Sciences,* vol. 1, 2019.

[151] A. Sukeri, A. S. Lima and M. Bertotti, "Development of non-enzymatic and highly selective hydrogen peroxide sensor based on nanoporous gold prepared by a simple unusual electrochemical approach," *Microchemical Journal,* vol. 133, pp. 149-154, 2017.

[152] N. Tujunen, E. Kaivosoja, V. Protopopova, J. J. Valle-Delgado, M. Österberg, J.

Koskinen and T. Laurila, "Electrochemical detection of hydrogen peroxide on platinum-containing tetrahedral amorphous carbon sensors and evaluation of their biofouling properties," *Materials Science and Engineering: C,* vol. 55, pp. 70-78, 2015.

[153] L. Han, L. Tang, D. Deng, H. He, M. Zhou and L. Luo, "A novel hydrogen peroxide sensor based on electrodeposited copper/cuprous oxide nanocomposites," *Analyst,* vol. 144, pp. 685-690, 2019.

[154] L. Stojanov, A. Rafailovska, V. Jovanovski and V. Mirceski, "Electrochemistry of Copper in Polyacrylic Acid: The Electrode Mechanism and Analytical Application for Gaseous Hydrogen Peroxide Detection," *The Journal of Physical Chemistry C,* vol. 126, no. 43, p. 18313–18322, 2022.

[155] K. Wang, Y. Sun, W. Xu, W. Zhang, F. Zhang, Y. Qi, Y. Zhang, Q. Zhou, B. Dong, C. Li, L. Wang and L. Xu, "Non-enzymatic electrochemical detection of H_2O_2 by assembly of CuO nanoparticles and black phosphorus nanosheets for early diagnosis of periodontitis," *Sensors and Actuators B: Chemical,* vol. 355, p. 131298, 2022.

[156] L. Agüí, P. Yáñez-Sedeño and J. M. Pingarrón, "Role of carbon nanotubes in electroanalytical chemistry: a review," *Analytica Chimica Acta,* vol. 622, no. 1-2, pp. 11-47, 2008.

[157] G. W. Hance and T. Kuwana, "Effect of Glassy Carbon Pretreatment on Background Double-Layer Capacitance and Adsorption of Neutral Organic Molecules," *Analytical Chemistry,* vol. 59, pp. 131-134, 1987.

[158] J. F. Evans and T. Kuwana, "Introduction of Functional Groups onto Carbon Electrodes via Treatment with Radio-Frequency Plasmas," *Analytical Chemistry,* vol. 51, pp. 358-365, 1979.

[159] Y. Zhou, G. Yu, F. Chang, B. Hu and C.-J. Zhong, "Gold–platinum alloy nanowires as highly sensitive materials for electrochemical detection of hydrogen peroxide," *Analytica Chimica Acta,* vol. 757, pp. 56-62, 2012.

[160] Y. Liu, G. Sun, C. Jiang, X. T. Zheng, L. Zheng and C. M. Li, "Highly sensitive detection of hydrogen peroxide at a carbon nanotube fiber microelectrode coated with palladium nanoparticles," *Microchimica Acta,* vol. 181, p. 63–70, 2014.

[161] P. Jakubec, V. Urbanová, Z. Marková and R. Zbořil, "Novel Fe@Fe-O@Ag nanocomposite for efficient non-enzymatic sensing of hydrogen peroxide," *Electrochimica Acta,* vol. 153, pp. 62-67, 2015.

[162] A. Uzunoglu, A. D. Scherbarth and L. A. Stanciu, "Bimetallic PdCu/SPCE non-enzymatic hydrogen peroxide sensors," *Sensors and Actuators B: Chemical,* vol. 220, pp. 968-976, 2015.

[163] D. Chirizzi, M. R. Guascito, E. Filippo, C. Malitesta and A. Tepore, "A novel nonenzymatic amperometric hydrogen peroxide sensor based on CuO@Cu_2O nanowires embedded into poly(vinyl alcohol)," *Talanta,* vol. 147, pp. 124-131, 2016.

[164] M. Lian, X. Chen, Y. Lu and W. Yang, "Self-Assembled Peptide Hydrogel as a Smart Biointerface for Enzyme-Based Electrochemical Biosensing and Cell Monitoring," *ACS Applied Materials & Interfaces,* vol. 8, no. 38, p. 25036–25042, 2016.

[165] A. L. Eckermann, D. J. Feld, J. A. Shaw and T. J. Meade, "Electrochemistry of redox-active self-assembled monolayers," *Coordination Chemistry Reviews,* vol. 254, no. 15-16, pp. 1769-1802, 2010.

[166] R. Thangamuthu, Y.-C. Pan and S.-M. Chen, "Electrocatalytic reduction of hydrogen peroxide and its determination in antiseptic and soft-glass cleaning solutions at phosphotungstate-doped-glutaraldehyde-cross-linked poly-l-lysine film electrodes," *Sensors and Actuators B: Chemical,* vol. 151, no. 2, pp. 377-383, 2011.

[167] M.-Y. Hua, H.-C. Chen, R.-Y. Tsai, Y.-C. Lin and L. Wang, "A novel biosensing mechanism based on a poly(N-butyl benzimidazole)-modified gold electrode for the detection of hydrogen peroxide," *Analytica Chimica Acta,* vol. 693, no. 1-2, pp. 114-120, 2011.

[168] F.-Y. Kong, W.-W. Li, J.-Y. Wang, H.-L. Fang, D.-H. Fan and W. Wang, "Direct electrolytic exfoliation of graphite with hemin and single-walled carbon nanotube: Creating functional hybrid nanomaterial for hydrogen peroxide detection," *Analytica Chimica Acta,* vol. 884, pp. 37-43, 2015.

[169] M. Baghayeri and H. Veisi, "Fabrication of a facile electrochemical biosensor for hydrogen peroxide using efficient catalysis of hemoglobin on the porous Pd@Fe_3O_4-MWCNT nanocomposite," *Biosensors and Bioelectronics,* vol. 74, pp. 190-198, 2015.

[170] Y. Sun, M. Luo, X. Meng, J. Xiang, L. Wang, Q. Ren and S. Guo, "Graphene/Intermetallic PtPb Nanoplates Composites for Boosting Electrochemical Detection of H2O2 Released from Cells," *Analytical Chemistry,* vol. 89, no. 6, p. 3761–3767, 2017.

[171] W. Wang, L. Kong, J. Zhu and L. Tan, "One-pot preparation of conductive composite containing boronic acid derivative for non-enzymatic glucose detection," *Journal of Colloid and Interface Science,* vol. 498, pp. 1-8, 2017.

[172] X. Li, F. Ran, F. Yang, J. Long and L. Shao, "Advances in MXene Films: Synthesis, Assembly, and Applications," *Transactions of Tianjin University,* vol. 27, p. 217–247, 2021.

[173] Y. Gogotsi and B. Anasori, "The Rise of MXenes," *ACS Nano,* vol. 13, no. 8, p. 8491–8494, 2019.

[174] Y. R. Kumar, K. Deshmukh, L. J. Kennedy, R. Keçili, C. M. Hussain, M. K. Kesarla and S. K. K. Pasha, "Chapter 7 - MXenes and their composites: emerging materials for gas sensing and biosensing," in *Mxenes and their Composites*, Elsevier, 2022, pp. 241-279.

[175] V. S. Tripathi, V. B. Kandimalla and H. Ju, "Amperometric biosensor for hydrogen peroxide based on ferrocene-bovine serum albumin and multiwall carbon nanotube modified ormosil composite," *Biosensors and Bioelectronics,* vol. 21, no. 8, pp. 1529-1535, 2006.

[176] M. A. Komkova, E. E. Karyakina, F. Marken and A. A. Karyakin, "Hydrogen Peroxide Detection in Wet Air with a Prussian Blue Based Solid Salt Bridged Three Electrode System," *Analytical Chemistry,* vol. 85, no. 5, p. 2574–2577, 2013.

[177] M. S. Lin and H. J. Leu, "A Fe3O4-Based Chemical Sensor for Cathodic Determination of Hydrogen Peroxide," *Electroanalysis,* vol. 17, no. 22, pp. 2068-

2073, 2005.

[178] S. K. Pandey, S. Sachan and S. K. Singh, "Electrochemically reduced graphene oxide modified with electrodeposited thionine and horseradish peroxidase for hydrogen peroxide sensing and inhibitive measurement of chromium," *Materials Science for Energy Technologies,* vol. 2, no. 3, pp. 676-686, 2019.

[179] Y. Xiong, C. Wang, Y. Wu, C. Luo, D. Zhan and S. Wang, "Electrochemical Enzyme Sensor Based on the Two-Dimensional Metal–Organic Layers Supported Horseradish Peroxidase," *Molecules,* vol. 27, p. 8599, 2022.

[180] S. Singh, M. Singh, K. Mitra, R. Singh, S. K. Sen Gupta, I. Tiwari and B. Ray, "Electrochemical sensing of hydrogen peroxide using brominated graphene as mimetic catalase," *Electrochimica Acta,* vol. 258, pp. 1435-1444, 2017.

[181] H. Qi, C. Zhang and X. Li, "Amperometric third-generation hydrogen peroxide biosensor incorporating multiwall carbon nanotubes and hemoglobin," *Sensors and Actuators B: Chemical,* vol. 114, no. 1, pp. 364-370, 2006.

[182] E. Canbay, B. Şahin, M. Kıran and E. Akyilmaz, "MWCNT–cysteamine–Nafion modified gold electrode based on myoglobin for determination of hydrogen peroxide and nitrite," *Bioelectrochemistry,* vol. 101, pp. 126-131, 2015.

[183] B. Dinesh, V. Mani, R. Saraswathi and S.-M. Chen, "Direct electrochemistry of cytochrome c immobilized on a graphene oxide–carbon nanotube composite for picomolar detection of hydrogen peroxide," *RSC Advances,* vol. 4, pp. 28229-28237, 2014.

[184] M. A. Komkova, A. Holzinger, A. Hartmann, A. R. Khokhlov, C. Kranz, A. A. Karyakin and O. G. Voronin, "Ultramicrosensors based on transition metal hexacyanoferrates for scanning electrochemical microscopy," *Beilstein Journal of Nanotechnology,* vol. 4, p. 649–654, 2013.

[185] L. Xia, L. Yu, D. Hu and G. Z. Chen, "Electrolytes for electrochemical energy storage," *Materials Chemistry Frontiers,* vol. 1, pp. 584-618, 2017.

[186] K. Perzyna, R. Borkowska, J. Syzdek, A. Zalewska and W. Wieczorek, "The effect of additive of Lewis acid type on lithium–gel electrolyte characteristics," *Electrochimica Acta,* vol. 57, pp. 58-65, 2011.

[187] J. Syzdek, M. B. Armand, M. Gizowska, M. Marcinek, E. Sasim, M. Szafran and W. Wieczorek, "Ceramic-in-polymer versus polymer-in-ceramic polymeric electrolytes—A novel approach," *Journal of Power Sources,* vol. 194, no. 1, pp. 66-72, 2009.

[188] J. Syzdek, R. Borkowska, K. Perzyna, J. M. Tarascon and W. Wieczorek, "Novel composite polymeric electrolytes with surface-modified inorganic fillers," *Journal of Power Sources,* vol. 173, no. 2, pp. 712-720, 2007.

[189] J. Luo, A. H. Jensen, N. R. Brooks, J. Sniekers, M. Knipper, D. Aili, Q. Li, B. Vanroy, M. Wübbenhorst, F. Yan, L. Van Meervelt, Z. Shao, J. Fang, Z.-H. Luo, D. E. De Vos, K. Binnemans and J. Fransaer, "1,2,4-Triazolium perfluorobutanesulfonate as an archetypal pure protic organic ionic plastic crystal electrolyte for all-solid-state fuel cells," *Energy & Environmental Science,* vol. 8, pp. 1276-1291, 2015.

[190] Y. Zhang, C. Li, X. Cai, J. Yao, M. Li, X. Zhang and Q. Liu, "High alkaline tolerant electrolyte membrane with improved conductivity and mechanical strength via lithium chloride/dimethylacetamide dissolved microcrystalline cellulose for Zn-Air batteries," *Electrochimica Acta,* vol. 220, pp. 635-642, 2016.

[191] J. You, S. Xie, J. Cao, H. Ge, M. Xu, L. Zhang and J. Zhou, "Quaternized Chitosan/Poly(acrylic acid) Polyelectrolyte Complex Hydrogels with Tough, Self-Recovery, and Tunable Mechanical Properties," *Macromolecules,* vol. 49, p. 1049−1059, 2016.

[192] T. A. Zawodzinski and R. A. Osteryoung, "1 -Methyl-3-ethylimidazolium Hydrogen Dichloride: Synthesis and Application to the Study of Protons in Ambient-Temperature Chloroaluminate Ionic Liquids," *Inorganic Chemistry,* vol. 27, pp. 4383-4384, 1988.

[193] J. Kulys, "Flow-through amperometric sensor for hydrogen peroxide monitoring in gaseous media," *Sensors and Actuators B: Chemical,* vol. 9, pp. 143-147, 1992.

[194] S. D. Holmstrom and J. A. Cox, "Solid-State Voltammetric Determination of Gaseous Hydrogen Peroxide Using Nanostructured Silica as the Electrolyte," *Electroanalysis,* vol. 10, no. 9, pp. 597-601, 1998.

[195] U. Klun, D. Zorko, L. Stojanov, V. Mirčeski and V. Jovanovski, "Amperometric sensor for gaseous H_2O_2 based on copper redox mediator incorporated electrolyte," *Sensors and Actuators Reports,* vol. 5, p. 100144, 2023.

[196] F. I. Bohrer, C. N. Colesniuc, J. Park, I. K. Schuller, A. C. Kummel and W. C. Trogler, "Selective Detection of Vapor Phase Hydrogen Peroxide with Phthalocyanine Chemiresistors," *Journal of the American Chemical Society,* vol. 130, no. 12, p. 3712–3713, 2008.

[197] J.-S. Lee, D.-W. Jeong and Y. T. Byun, "Porphyrin nanofiber/single-walled carbon nanotube nanocomposite-based sensors for monitoring hydrogen peroxide vapor," *Sensors and Actuators B: Chemical,* vol. 306, p. 127518, 2020.

[198] X. Xie, N. Gao, M. Hunter, L. Zhu, X. Yang, S. Chen and L. Zang, "PEDOT Films Doped with Titanyl Oxalate as Chemiresistive and Colorimetric Dual-Mode Sensors for the Detection of Hydrogen Peroxide Vapor," *Sensors,* vol. 23, no. 6, p. 3120, 2023.

Bibliography

Publications Related to the Thesis

Journal Articles

J. Isailović, K. Vidović, S. B. Hočevar, "Simple electrochemical sensors for highly sensitive detection of gaseous hydrogen peroxide using polyacrylic-acid-based sensing membrane, " *Sensors and Actuators B: Chemical*, vol. 352, no. 131053, p. 1–7, 2022. doi: 10.1016/j.snb.2021.131053

J. Isailović, A. Oberlintner, U. Novak, M. Finšgar, F. M. Oliveira, J. Paštika, Z. Sofer, N. Tasić, R. Gusmão, S. B. Hočevar, "Study of Chitosan-Stabilized $Ti_3C_2T_x$ MXene for Ultrasensitive and Interference-Free Detection of Gaseous H_2O_2, " *ACS Applied Materials & Interfaces*, vol. 15, iss. 26, p. 31643–31651, 2023. doi: 10.1021/acsami.3c05314

Conference Paper

J. Isailović, V. Jovanovski, P. Jovanovič (2019). Development of hydrogen peroxide gas sensor for security applications. In *Book of abstracts*. 7th Regional Symposium on Electrochemistry South-East Europe & 8th Kurt Schwabe Symposium. Split, Croatia.

J. Isailović, P. Jovanovič, V. Jovanovski (2019). Development of hydrogen peroxide gas sensor for security applications. In *Book of Abstracts - Proceedings 2019 : IPSSC + CMBE*.

J. Isailović, K. Vidović, S. B. Hočevar (2021). Electrochemical sensors for gaseous hydrogen peroxide. In *27th Croatian Meeting of Chemists and Chemical Engineers with international participation [and] 5th Symposium Vladimir Prelog : book of abstracts*. Veli Lošinj, Croatia.

J. Isailović, S. B. Hočevar, N. Tasić (2022).Development and comparison of hydrogen peroxide electrochemical gas sensors. In: *Mátrafüred 2022 : International Conference on Chemical Sensors*. Visegrád, Hungary.

J. Isailović, N. Tasić, S. B. Hočevar (2023). Development of novel highly sensitive hydrogen peroxide electrochemical gas sensor. In *Program of the 34th Topical Meeting of the International Society of Electrochemistry : Electrochemistry: Reaching out to society*. Mar del Plata, Argentina.

J. Isailović, S. B. Hočevar, N. Tasić (2023). Incorporation and stabilization of $Ti_3C_2T_x$ MXene into the sensitive H_2O_2 gas sensing platform. In *Programme and the Book of abstracts, 7CSCS-2023 : 7th Conference of the Serbian Society for Ceramic Materials*. Belgrade, Serbia.

Other Publications

J. Isailović (2019). Electrochemical sensors for security and environmental applications. In: *9th ISE Satellite Student Regional Symposium on Electrochemistry*. Ruđer Bošković Institute Zagreb, Croatia.

Biography

Doctoral candidate Jelena Isailović was born on January 19th, 1994, in Novi Sad, Serbia. She attended the "Dositej Obradović" Primary School in Novi Sad, Serbia, from 2001 to 2009. In 2013, she graduated from the Medical High School "7. April", Novi Sad, Serbia. In 2017, she obtained her BSc degree in Chemistry, at the Faculty of Sciences at the University of Novi Sad, Serbia (Department of Chemical Technology and Environmental Protection), with an average grade point of 9.52 on 33 curriculum subjects. During her Bachelor studies, she completed a 2-month laboratory internship at the Institute for Public Health of Vojvodina, Novi Sad, Serbia, addressing analytical investigations on multiple toxins from the Danube River and tap water. In 2017, she enrolled in the MSc program in Analytical Chemistry at the Faculty of Sciences, University of Novi Sad, Serbia, where she completed the winter semester. As part of the Erasmus+ exchange program in Advanced Spectroscopy in Chemistry, she completed the summer semester at the Faculty of Science and Technology, University of Lille, France. She successfully defended her MSc thesis in 2018, with an average grade point of 9.5 on 6 curriculum subjects. In October 2018, she enrolled in Ph.D. studies at the Jožef Stefan International Postgraduate School, Ljubljana, Slovenia (Program: Sensor Technologies). Since January 2019, she has been employed as a Young Researcher (YR) at the National Institute of Chemistry, Ljubljana, Slovenia, under the supervision and academic guidance of Dr. Samo B. Hočevar, Head of the Department of Analytical Chemistry (D04).

Her main research interests include the conceptualization and development of novel sensing architectures applicable to electrochemical gas sensing and biosensing. She has published two articles in peer-reviewed renowned international journals: Sensors and Actuators B: Chemical (IF=8.4) and ACS Applied Materials and Interfaces (IF=9.5).